PEPTIDE NANOVESICLES: SUPRAMOLECULAR ASSEMBLY OF BRANCHED AMPHIPHILIC PEPTIDES

by

SUSHANTH GUDLUR

M.S., University of Pune, India, 2003

AN ABSTRACT OF A DISSERTATION

submitted in partial fulfillment of the requirements for the degree

DOCTOR OF PHILOSOPHY

Department of Biochemistry
College of Arts and Sciences

KANSAS STATE UNIVERSITY
Manhattan, Kansas

2012

Abstract

Peptide-based delivery systems show great potential as safer drug delivery vehicles. They overcome problems associated with lipid-based or viral delivery systems, vis-a-vis stability, specificity, inflammation, antigenicity, and tune-ability. We have designed and synthesized a set of 15 and 23-residue branched, amphiphilic peptides that mimic phosphoglycerides in molecular architecture. They undergo supramolecular self-assembly and form solvent-filled, bilayer delineated spheres with 50-150 nm diameters (confirmed by TEM and DLS). Whereas weak hydrophobic forces drive and sustain lipid bilayer assemblies, these structures are further stabilized by β-sheet hydrogen bonding and are stable at very low concentrations and even in the presence of SDS, urea and trypsin as confirmed by circular dichroism spectroscopy. Given sufficient time, they fuse together to form larger assemblies and trap compounds of different sizes within the enclosed space. They are prepared using a protocol that is similar to preparing lipid vesicles. We have shown that different concentrations of the fluorescent dye, 5(6)-Carboxyfluorescein can be encapsulated in these assemblies and delivered into human lens epithelial cells and MCF-7 cells grown on coverslips. Besides fluorescent dyes, we have delivered the plasmid (EGFP-N3, 4.7kb) into N/N 1003A lens epithelial cells and observed expression of EGFP (in the presence and absence of a selection media). In the case of large molecules like DNA, these assemblies act as nanoparticles and offer some protection to DNA against certain nucleases. Linear peptides that lacked a branching point and other branched peptides with their sequences randomized did not show any of the lipid-like properties exhibited by the branched peptides. The peptides can be chemically decorated with target specific sequences for use as DDS for targeted delivery.

PEPTIDE NANOVESICLES: SUPRAMOLECULAR ASSEMBLY OF BRANCHED AMPHIPHILIC PEPTIDES

by

SUSHANTH GUDLUR

M.S., University of Pune, India, 2003

A DISSERTATION

submitted in partial fulfillment of the requirements for the degree

DOCTOR OF PHILOSOPHY

Department of Biochemistry
College of Arts and Sciences

KANSAS STATE UNIVERSITY
Manhattan, Kansas

2012

Approved by:

Major Professor
John M. Tomich

Copyright

Abstract

Peptide-based delivery systems show great potential as safer drug delivery vehicles. They overcome problems associated with lipid-based or viral delivery systems, vis-a-vis stability, specificity, inflammation, antigenicity, and tune-ability. We have designed and synthesized a set of 15 and 23-residue branched, amphiphilic peptides that mimic phosphoglycerides in molecular architecture. They undergo supramolecular self-assembly and form solvent-filled, bilayer delineated spheres with 50-150 nm diameters (confirmed by TEM and DLS). Whereas weak hydrophobic forces drive and sustain lipid bilayer assemblies, these structures are further stabilized by β-sheet hydrogen bonding and are stable at very low concentrations and even in the presence of SDS, urea and trypsin as confirmed by circular dichroism spectroscopy. Given sufficient time, they fuse together to form larger assemblies and trap compounds of different sizes within the enclosed space. They are prepared using a protocol that is similar to preparing lipid vesicles. We have shown that different concentrations of the fluorescent dye, 5(6)-Carboxyfluorescein can be encapsulated in these assemblies and delivered into human lens epithelial cells and MCF-7 cells grown on coverslips. Besides fluorescent dyes, we have delivered the plasmid (EGFP-N3, 4.7kb) into N/N 1003A lens epithelial cells and observed expression of EGFP (in the presence and absence of a selection media). In the case of large molecules like DNA, these assemblies act as nanoparticles and offer some protection to DNA against certain nucleases. Linear peptides that lacked a branching point and other branched peptides with their sequences randomized did not show any of the lipid-like properties exhibited by the branched peptides. The peptides can be chemically decorated with target specific sequences for use as DDS for targeted delivery.

Table of Contents

List of Figures

List of Tables

Acknowledgements

This work would not have been possible without the help, guidance and support of my advisor, Prof. John M. Tomich, to whom I am very grateful. His enthusiasm for science and his ability to generate new ideas at the drop of a hat are highly contagious and I hope I have been infected with them. Best of all, I thank him for the freedom he has given me in the lab to pursue this work in the direction I was interested in.

I thank my committee members Dr. Michael Zolkiewski, Dr. Lawrence Davis and Dr. Ruth Welti for giving me useful insights, suggestions, and for their constructive criticism. In particular, I would like to thank Dr. Zolkiewski for all his help with the AUC experiments.

It has been a great pleasure working with Dr. Yasuaki Hiromasa and I am indebted to him for all his help especially with the AUC experiments. His humor and pep talks have helped me smile even on days when none of my experiments worked. I would like to extend my gratitude to Dr. Takeo Iwamoto for teaching me to use some of the instruments in the lab, which I have relied upon for this work.

I thank Dr. Dolores Takemoto and her lab members, especially Sam Molina, Dr. Satyabrata Das and Dr. Debarshi Banerjee for their help with the cell culture experiments. I am lucky to have a friend like Dr. Satyabrata Das who has helped me with my initial cell culture experiments and continued to provide me with technical assistance over the phone after moving out of K-State. I am grateful to Dr. Gerald Reeck for letting me use his lab to carry out some of my experiments. In this regard, I appreciate the help extended to me by Matthew Heerman.

Burt Hall, specifically the Tomich lab, is a fun place to do research, thanks to the amazing researchers who occupy this building. I am thankful to all the members of the Tomich lab (past and present) for their help. I have had the opportunity to make some wonderful friends

in the lab during the course of my research. Xiao Yao and Adriana Avila have been awesome lab mates and absolutely fun to work with. I thank them for all their help and friendship. In particular, I thank Adriana Avila for taking care of my cell culture experiments while I was away from lab or was just plain lazy. Special thanks to Pinakin Sukthankar, who has been my go-to-guy for chemical synthesis or whenever I needed help understanding a chemical process. I owe it to Ben Katz, who constantly stole my pipettes and markers, for cultivating the habit of labeling my lab supplies. Thanks to Deane Lehmann for making my office desk a food-station, I never had to run my experiments on an empty stomach.

I thank Dr. Christopher Sorensen and Dr. Louis Nemzer for teaching me to use the DLS setup in their lab and help analyze, and understand the DLS data. After meeting Dr. Sorensen, I will now concede that not all physicists are boring. Thanks to Lloyd Willard for the excellent TEM images I have used in this dissertation.

It has been a long journey for me and I have had the good fortune to cross paths with some interesting, sincere and reliable friends who have supported, criticized and made fun of my work, life and everything about me while still motivating me to carry on. The ones who did this best and whom I would love to thank are, Harsh Shah, Narasimhan Krishnan, Prasanna Ayyaru, Jose Abraham, Pradeep Malreddy, Amita Joshi and Stacy Littlechild.

Last but not the least, I thank Google Inc., for saving me a lot of time and effort by making it easier for me to search for information online using their search engine.

Dedication

To my parents (Suguna Chander Swamy and Vani Swamy) and my brother (Suman Swamy), for their patience, continuous moral and financial support, and for believing in me.

Chapter 1 - Introduction

Self-assembly is a common phenomenon in nature. The self-complementarity of the two DNA strands drives their assembly into a double helical structure, protein assemblies are required for cellular functions, and lipid assembly is involved in cell membranes. In the context of lipids and peptides, the self-assembling molecule is usually amphiphilic with a hydrophobic and hydrophilic domain. These domains can be spatially separated either along the length of the molecule or along a defined section of the molecule[1]. The hydrophilic segments can either be charged (cationic, anionic or zwitterionic) or uncharged[2,3,4]. While such segments are spatially segregated in lipids, it may not seem so evident in peptides and proteins where the primary sequence may contain alternating or random segments of hydrophobic and hydrophilic regions. Upon folding, the final, functional structure could have continuous faces of hydrophobic or hydrophilic regions that allow them to interact with solvent, a ligand or an adjacent molecule.

Self-assembly in biomacromolecules is usually facilitated by weak non-covalent interactions that can be any one or mixture of hydrogen bonding, Van der Waal forces, ionic, and electrostatic interactions. When such amphiphilic molecules are introduced into an aqueous environment, the hydrophobic segments tend to come together to exclude water thereby providing the driving force for assembly aided by intermolecular associations.The hydrophilic segments of the molecule remain exposed to the aqueous solvent. Much of our understanding of self-assembly of amphiphiles comes from studies with lipids. Attempts to mimic lipid amphiphiles have led to the design and development of many different types of molecules that retain the amphiphilicity and relatively short length of lipids.

1.1. Various morphologies of self-assembling molecules

Amphiphiles, when exposed to an aqueous solution self-assemble into a variety of nano and micro structures such as micelles, vesicles or molecular gels composed of tubules, fibrils and fibres. Such amphiphiles tend to assemble into ordered structures that have the least free energy. Micelles can be polymeric or non polymeric and adopt structures that are spherical, worm like or disk shaped. Vesicles when composed entirely of lipids are called liposomes but other non-lipid vesicle types exist, like, niosomes, proniosomes, polyhedral niosomes, polymersomes and vesicles formed by the self-assembly of peptide amphiphiles (peptosomes). Finally, structures that do not fall into either of these common categories can be as diverse as rods, bipyramids, liquid crystalline structures[5], lamellar, hexagonal phase, cubic phase, icosahedral, cage like, high axial ratio microstructures (HARM)[6], fibres, cochleates and myelin figures[2]. The energetics, geometric constraints and the strength of the interacting forces (between the monomers) of the individual amphiphilic molecules determine the architecture of the final assembly. Other factors influencing the final assembly are pH, temperature, ionic strength of the solvent, as well as the concentration of the monomer. Using the packing parameter of the monomer one can predict the favored structure of the assembly[7]. The packing parameter depends on the area of the head group a_0, volume of the hydrocarbon chain or chains v, and the extended chain length l_0 of the monomer:

$$\text{Packing number} = \frac{v}{a_0 l_0}$$

While the head group of the amphiphiles plays a critical role in predicting the overall shape and size of the assemblies, the tail regions play an important role too, especially in the formation of spherical micelles, rod like micelles and spherical bilayer vesicles.

Fig. 1.1, illustrates some of the morphologies exhibited by self-assembling molecules. There are many review articles (cited when relevant) that deal with the various morphologies adopted by self-assembling molecules. This introduction deals exclusively with research related to spherical aggregates especially micelles and vesicles.

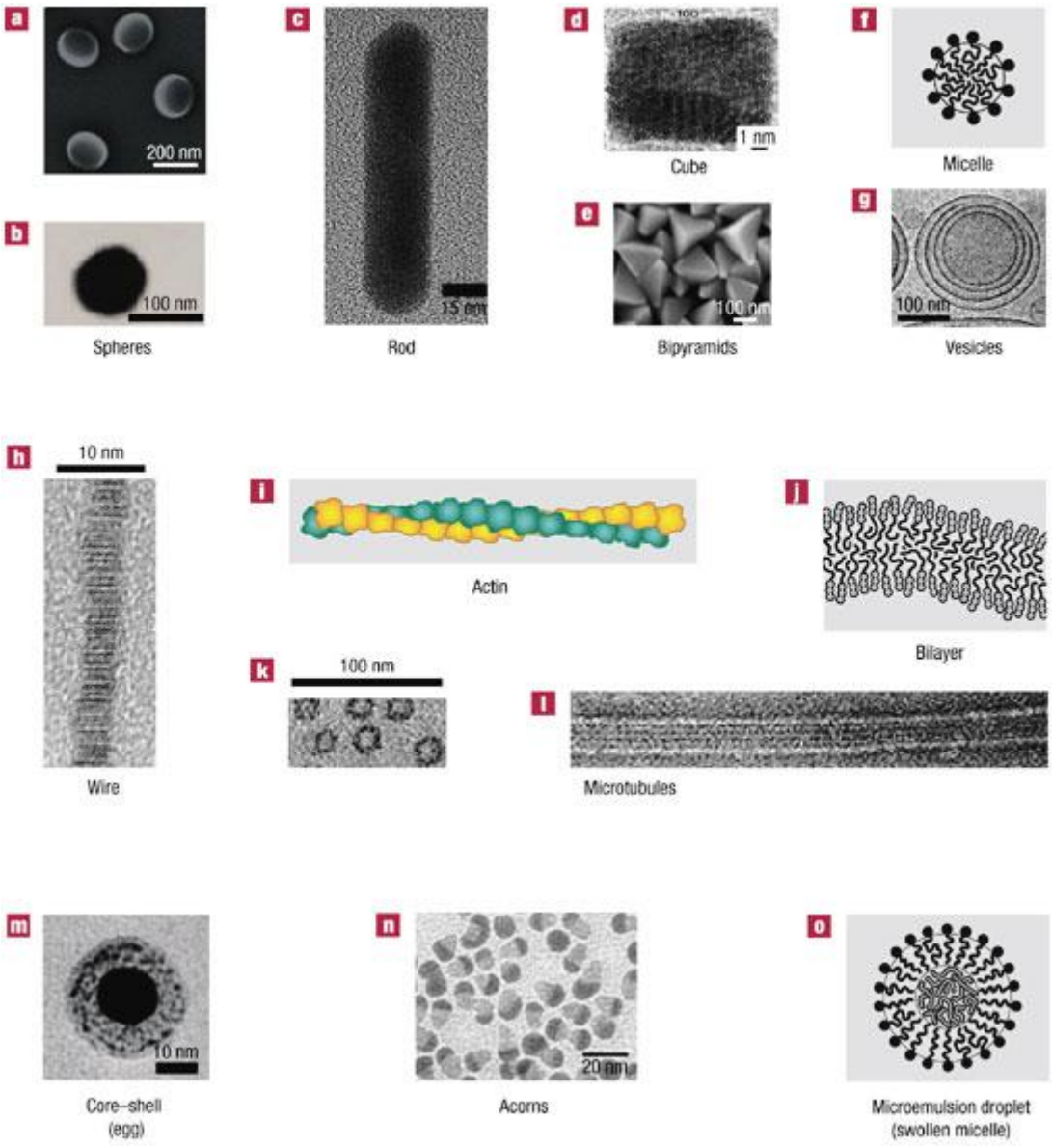

Figure 1.1. Various morphologies exhibited by self-assembling amphiphiles.

"(a); TEM image of 60-nm gold nanosphere (b); TEM image of Au nanorod (c); HRTEM image of cubic Pt nanocrystal oriented along [001] (d); SEM image of Ag bipyramids approximately 150 nm in edge length (e); a schematic micelle (f) and a cryo-TEM image of evolving vesicles

(g). h–l, One-component nanoparticles with at least one dimension in the nanoregime. HRTEM image of PbSe nanowire14 formed in the presence of oleic acid and n-tetradecylphosphonic acid (h); schematics of actin (i) and surfactant or lipid bilayer (j); TEM images of microtubules98 (k,l; scale bar refers to both). m–o, Two or more components (core–shell structures and so on). TEM image of Au colloid99 stabilized by sodium citrate and 19 layers of polyelectrolyte (m); HRTEM image of CoPd 'acorns'100 (n); microemulsion droplet (o).” [Reproduced with permission from Macmillan Publishers Ltd; Min *et al*. (2008) [8], *Nat Mater*, **7**(7), 527-538., © 2008]

1.1.1. Micelles

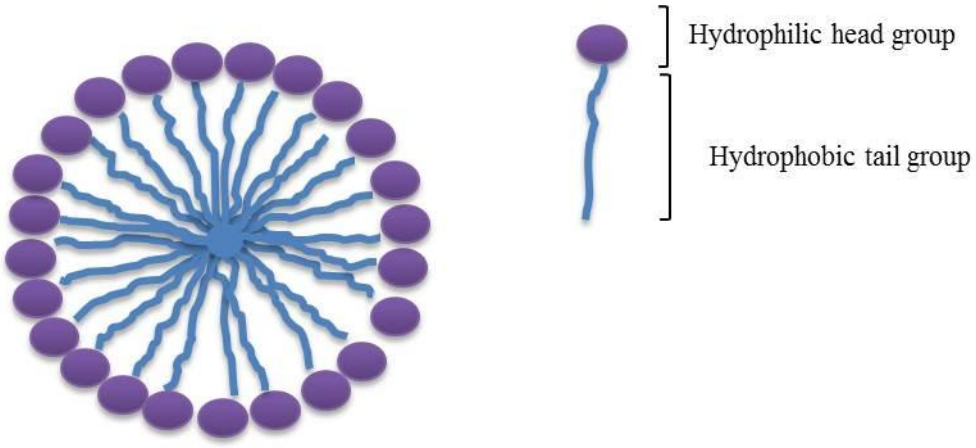

Figure 1.2. Illustration of a micelle.

They are the simplest form of amphiphilic aggregation/assembly and are useful in their ability to encapsulate water insoluble molecules within their hydrophobic core (Fig. 1.2). At a concentration below their assembly point, called the Critical Micellar Concentration (CMC), the amphiphiles exist as monomers but when the monomer concentration exceeds the CMC, they tend to aggregate/assemble into stable structures. These structures are in a dynamic equilibrium with the monomers present in solution. Further increase in concentration could lead to a change in the overall shape (discoidal, rod like or liquid crystalline phase). Thus, giving one the ability to tune the overall shape and size of the final assembly.

Non-polymeric micelles like SDS and Tween 80 (Polysorbate 80) have been well studied but polymeric micelles on the other hand are a relatively new concept and include biodegradable polymers prepared from block copolymers. Block copolymers are linear blocks or repeat units of hydrophobic and hydrophilic residues covalently linked to impart amphilicity to the molecule. $K_{60}L_{60}$ is one such example of a diblock copolymer where a polypeptide of 60 lysine residues is covalently linked to a polypeptide composed of 60 leucine residues. The block of leucine resides form the hydrophobic segment of the block copolymer while the positively charged lysine residues form the more hydrophilic segment. Triblock copolymers are similar to diblock copolymers but differ in having an extra hydrophobic or hydrophilic segment that can be fused to either of the existing segments. In general, a polymeric micelle consists of two parts, a core shell composed of insoluble hydrophobic segments and the outer corona composed of the soluble hydrophilic segments (Fig. 1.3). While simple spherical micelles with a core particle and corona are common, it gets more complex with structures like onion type micelles[9], shell cross linked micelles[10], Janus micelles[11,12,13], schizophrenic diblock copolymer micelles[14], multicompartmental hamburger micelles[15], which have been recently reported.

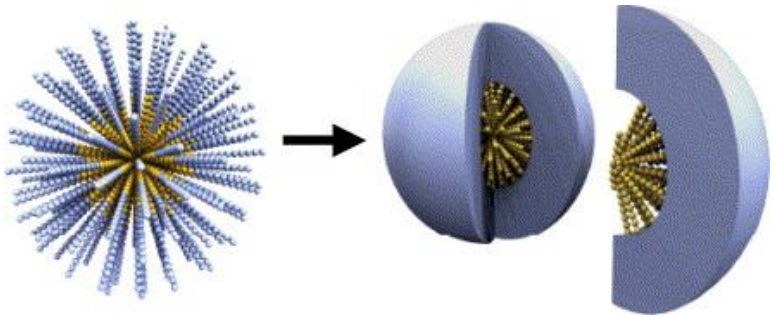

Figure 1.3. Polymer micelle.

Self-assembly and polymerization of a block copolymer yields a Shell-crosslinked knedel polymer assemblies, where the crosslinked shell can be decorated with biologically relevant ligands [Reproduced with permission from Elsevier; Tu *et al*. (2004) ***16***, *Adv Drug Deliv Rev,* **56**(11), 1537-63., © 2004].

1.1.2. Polymer Vesicles

Among the different structures discussed in *section 1.1.* vesicles show considerable utility in that they have the ability to encapsulate cargo (both hydrophobic and hydrophilic) thus giving them the potential to act as drug delivering vehicles. Lipid based vesicles and micelles are the first and most extensively studied drug carriers so far. Hence, it is no surprise that currently most, if not all commercially available drug carriers are lipid based.

Vesicles are colloidal aggregates that are mostly spherical in shape. In biology, vesicles are envisioned as small bilayer delimited chambers that entrap solvent. The solvent can in turn contain dissolved solutes (water soluble compounds) that can range from peptides, proteins, genetic material to bioactive compounds like anticancer drugs. It can also trap non-polar or hydrophobic substances within their membrane thus making them a versatile structure that allows them to take part in many diverse biological functions. Such versatility has made them the most attractive choice for use in cell mimetic systems in biology. Apart from its biological uses, vesicles have found application in pharmacology to deliver drugs, genetic materials and vaccines, in the cosmetic industry, micro-reactor chemistry, food industry and more[17] .

At one point, lipids were the only choice for making vesicles artificially but with the explosion of the field of self-assembling molecules, we now have a variety of molecules to choose from. Fig. 1.4, is an attempt at classifying the various polymeric vesicles described so far. It is difficult to strictly classify the various polymeric vesicles due to the issue of multi-functionality. This is particularly true with the advent of hybrid polymers, where two or more different materials are utilized to make an amphiphile. For example, vesicles formed from the self-assembly of an amphiphile that combines a synthetic polymer like polyethylene oxide (PEO) to a polypeptide (poly(L-Lysine) or a lipid offer more solubility, longer half-lives (in the blood stream) and the option of functionalizing the molecule with desired ligands. Such a molecule could fit into a

block copolymer, a lipid vesicle or a peptide vesicle depending on the fraction of the individual component or the fraction that drives the assembly.

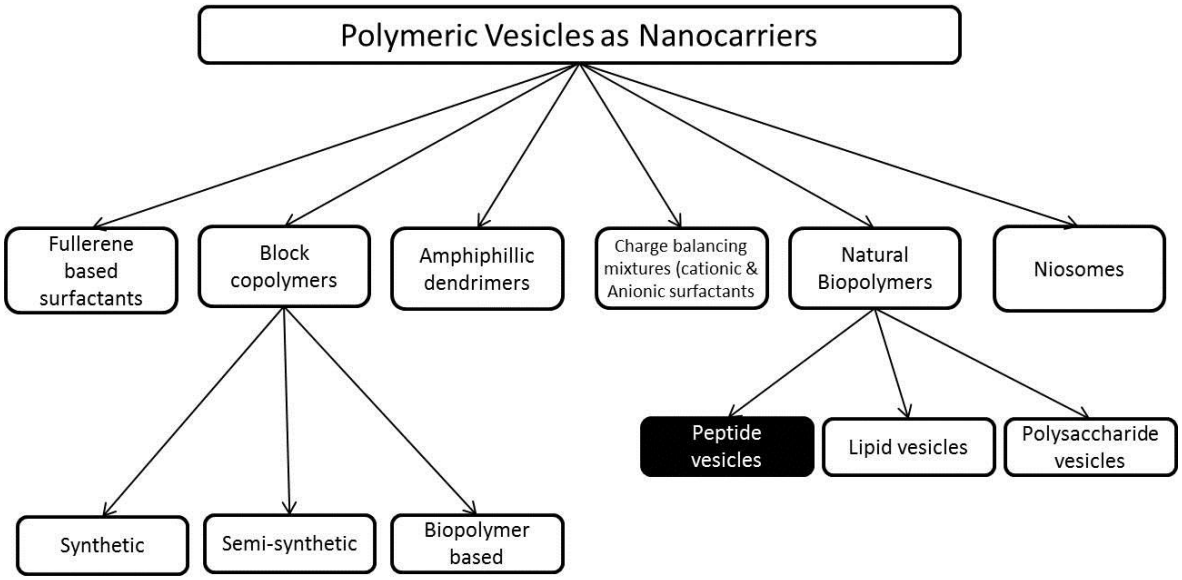

Figure 1.4. Classification of polymeric vesicles that undergo self-directed assembly to form vesicles.

1.1.2.1. Block copolymers

Block copolymers are blocks of hydrophobic and hydrophilic polymeric units that are linked together covalently to impart amphilicity to the molecule. Like phospholipids, these amphiphiles self-assemble into various ordered structures[18,19,20]. Vesicles formed from block copolymers are commonly referred to as polymersomes. Among the various polymeric vesicles being researched, polymersomes, are by far the best characterized. Many variants of these block polymers have been reported and tested in vitro for their ability to encapsulate and deliver cargo. The blocks of such block copolymer can be entirely synthetic, semi-synthetic or composed of biopolymers like polypeptides. Fig. 1.6 lists some of the common polymers used in designing

block copolymers. Table 1.1, lists some of the polypeptide based block copolymers that self-assemble into vesicles.

By controlling the molecular weight of the monomers, one can control the properties of the polymersomes such as elasticity, permeability and mechanical stability[21]. Moreover, polymeric building blocks allow for greater chemical diversity than lipids[22]. Due to their higher molecular weight, polymersomes are inherently thicker, tougher and more stable than conventional liposomes. It has been shown that polymersome membranes sustain dilational strains up to 40-50 % when compared with ~5 % or less for lipid membranes[21,23,24]. A coarse grain molecular dynamics simulation supports the experimental observation that while lipid membranes require only about ~ 5 % strain rate for rupture, it takes 20 % or higher strain to rupture the thicker copolymer membranes[25]. These polymersomes can be designed to be responsive to stimuli such as pH, temperature, redox potential, magnetic field, light and ultrasound[22].

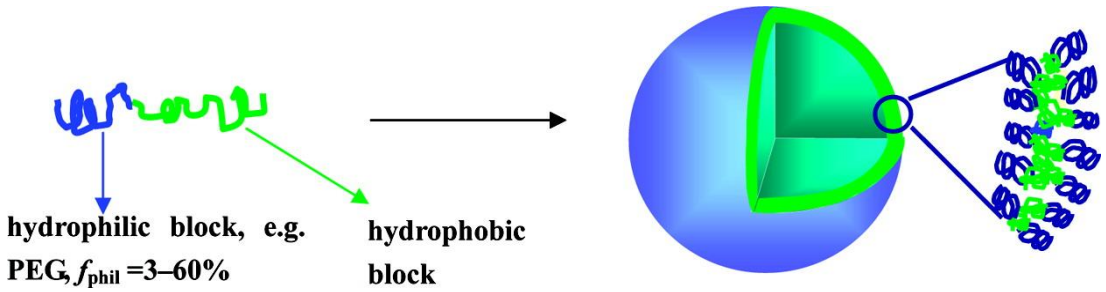

Figure 1.5. Polymersomes derived from asymmetric block copolymers.

[Reproduced with permission from American Chemical Society; Meng *et al*. (2009)[22], *Biomacromolecules*, **10**(2), 197-209., © 2009]

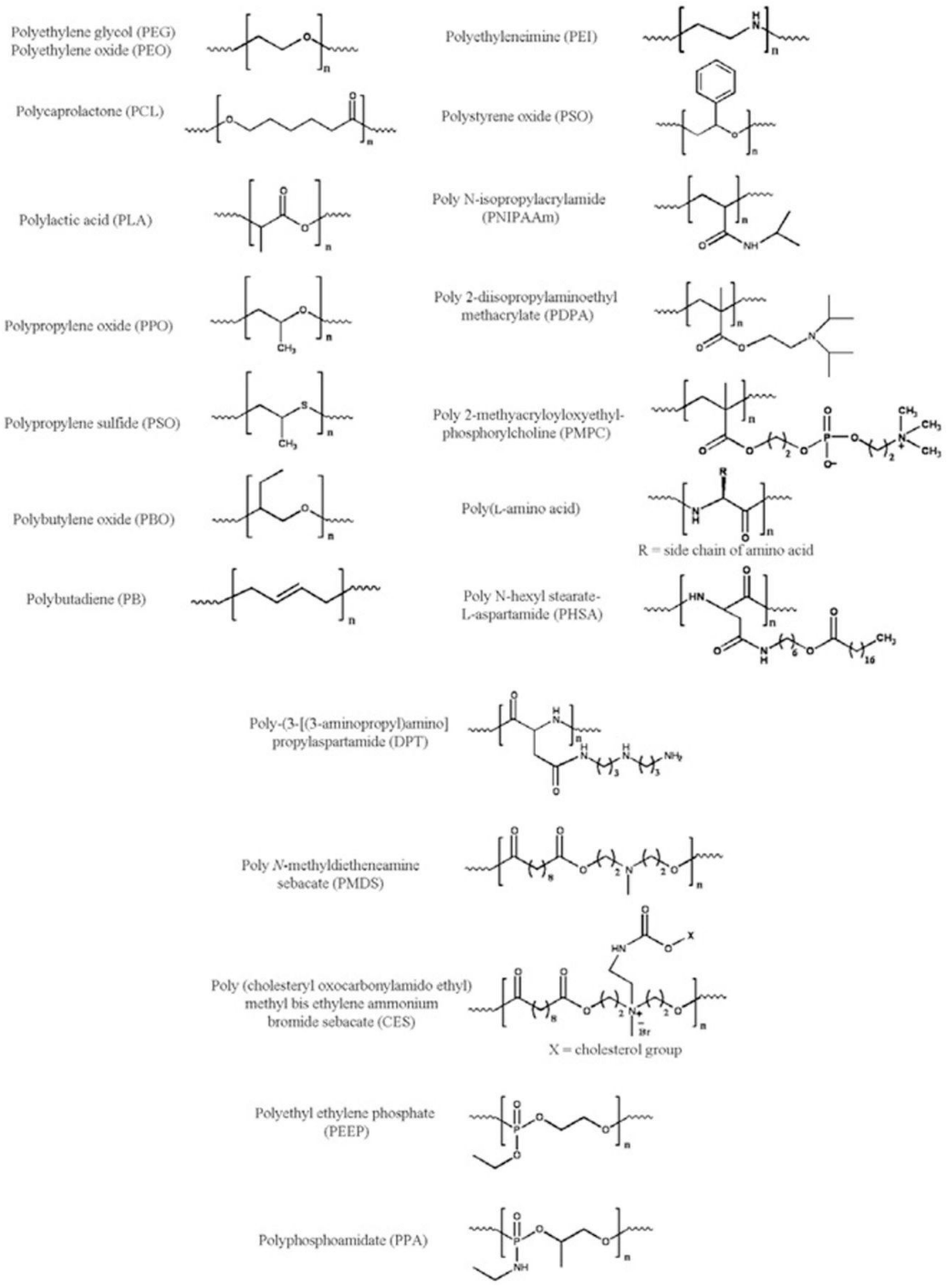

Figure 1.6. Common polymers used for self-assembled delivery vehicles.

[Reproduced with permission from Elsevier; Branco *et al*. (2009)[26], *Acta Biomaterialia*, **5**(3), 817-31., © 2009]

Table 1-1. Polypeptide based block copolymers that self-assemble into vesicles.

[Reproduced with permission from Elsevier; Carlsen *et al*. (2009)[27], *Curr Opin Colloid Interface Sci.*, 14(5), 329-339., © 2009]

Polypeptide-based vesicles in aqueous solution		
	Material	Key features
Polypeptide hybrid	PB-*b*-PLGA	pH responsive, cross-linking
	PLGA-*b*-PPO-*b*-PLGA	Size change with temperature; structure change with pH
	PNIPAM-*b*-PZLLys	Temperature responsive
	PB-*b*-PLLys	Temperature and pH responsive; β-sheet cross-linking
	PZLLys-*b*-DGBE-*b*-PZLLys	Vesicles and large compound micelles
	PEG-*b*-PAsp/PEG-*b*-P(Asp-AP)	PICsomes, semi-permeable vesicles
	Dextran-*b*-PBLG	Polypeptide-*b*-polysaccharide vesicles, glycoprotein-mimic
Copolypeptide	PMLG–phosphate	Globular structures and fibrous aggregates
	PLGA-*b*-PLLys	Schizophrenic vesicles
	PLLeu-*b*-PELLys	Micron-sized sheets and vesicles
	PLLeu-*b*-PLGA	Large range of morphologies
	PLLys-*b*-PLLeu	Vesicle loading, water permeability
	PLArg-*b*-PLLeu	Vesicles with protein-transduction domains
	PLLys-*b*-PBLG-*b*-PLLys	Size change with temperature
	PLLys-*b*-PLPhe	Size change with pH

1.1.2.2. Niosomes

These are non-ionic surfactant vesicles that are capable of entrapping hydrophobic and hydrophilic solutes[28]. They can be unilamellar or multilamellar depending on the method of preparation. They are usually mixed with an additive like cholesterol to give rigidity to the vesicle membranes. They were first reported in the 1970s as a feature of the cosmetic industry[29,30]. (Niosomes were developed and patented by L'Oreal in the 1970s and 80s). The first product, Niosome, was introduced in 1987 by Lancome[31,32]. Examples of non-ionic surfactants used to make niosomes include, C_{16} monoalkyl glycerol ether, sorbitan esters, and others.

1.1.2.3. Amphiphilic Dendrimers

Dendrimers are synthetic, hyperbranched spherical molecules that are capable of trapping small molecules within their structure. Amphiphilic dendrimers (Janus dendrimers) are capable of self-assembling into stable bilayer vesicles, referred to as dendrimersomes[33]. A Janus dendrimer is formed by covalently linking two distinct dendritic building blocks. They can be made

amphiphilic by attaching a non-polar block (e.g. alkoxy gallate ether[34] to a polar block (e.g. aliphatic arborol). A review by Rosen *et al*. (2009)[35] details the self-assembly and disassembly of dendrons. Fig. 1.7, is an illustration from the above review.

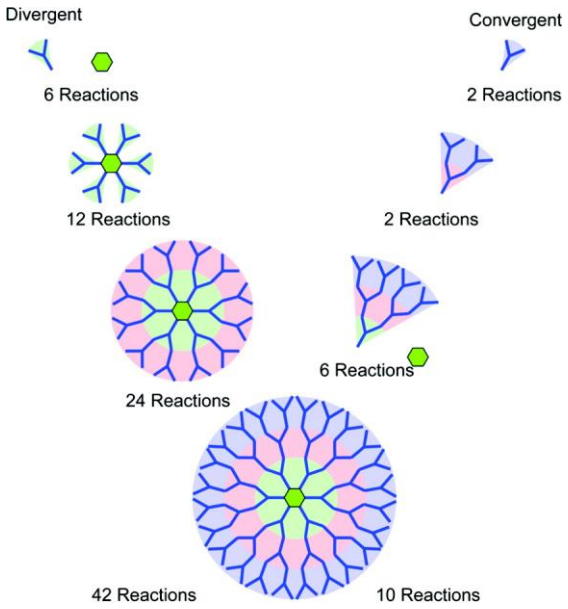

Figure 1.7. Convergent and divergent synthesis of dendrimers and dendrons.
[Reproduced with permission from American Chemical Society; Rosen *et al*. (2009)[35], *Chem Rev.*, **109**(11), 6275-6540., © 2009]

1.1.2.4. Fullerene based surfactants

A hollow sphere, ellipsoid or tube composed entirely of carbon is a fullerene. Because of their extremely hydrophobic nature, fullerenes are insoluble in aqueous solvents. Some ways to make them amphiphilic include adding polar functional groups such as carboxylic acids and amines, starlike fullerene derivatives, pure hydrocarbon penta-substituitions stabilizing the cyclopentadienide anion[36]. Such molecules are capable of self-assembling into bilayer vesicles and in the process, entrap solutes[37] (Fig.1.9).

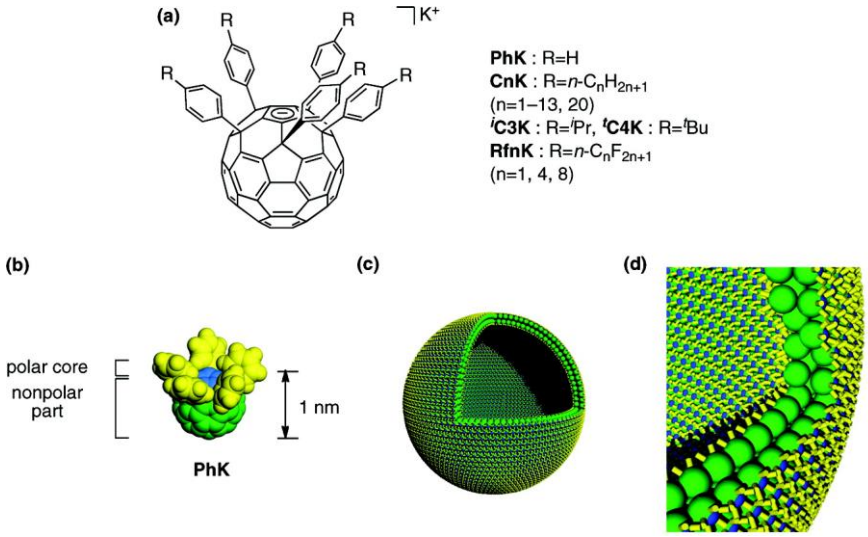

Figure 1.8. Fullerene bilayer vesicles.

"Schematic images of vesicles made of fullerene anions. (a) Chemical structures of potassium complexes of fullerene anions. (b) CPK drawing of PhK. (c) Schematic model of bilayer vesicle of PhK. (d) A magnified image of the bilayer PhK vesicle." [Reproduced with permission from American Chemical Society; Homma, T. *et al*. (2011)[38], *J. Am. Chem. Soc.*, **133** (16), 6364–6370, © 2011]

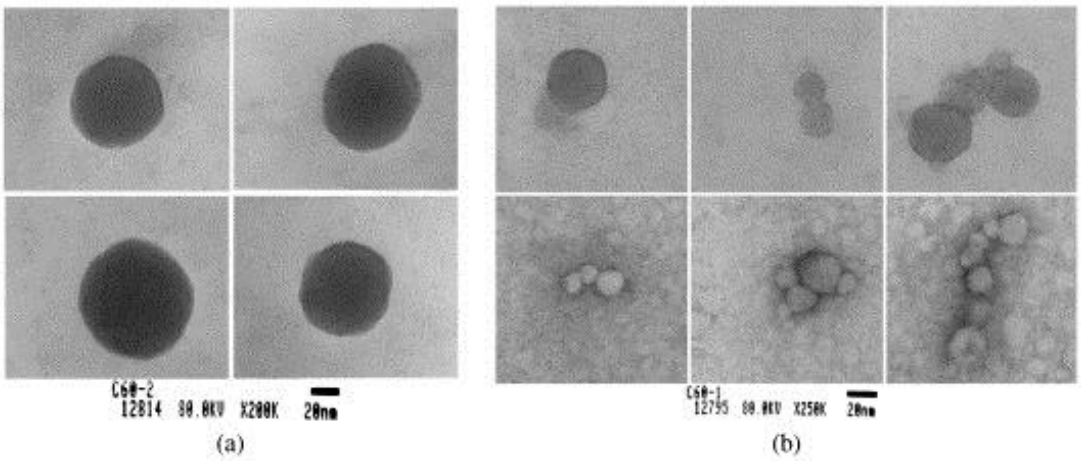

Figure 1.9. TEM micrographs of isolated vesicles and clusters (of fullerene vesicles).

"(a) spherical vesicles with diameters 2R of 61 to 78 nm at c=4.17×10−6 g ml−1; (b) various cluster geometries at c=4.17×10−4 g ml−1." [Reproduced with permission from Elsevier; Burger *et al*. (2004)[37], *J. Colloid Interface Sci.*, **275**(2), 632-41., © 2004]

1.1.2.5. Charge balancing mixtures of cationic and anionic surfactants

Mixing certain oppositely charged (anionic and cationic) surfactants can lead to the spontaneous formation of single walled equilibrium vesicles[39]. The size, charge and permeability of such equilibrium vesicles can be controlled by adjusting the molar ratios of the two surfactants. One example of such a charge balancing mixture is cetyl trimethylammonium tosylate (CTAT) and sodium dodecylbenzene sulfonate (SDBS).

1.1.2.6. Natural biopolymers

One of the main advantages of employing natural biopolymer vesicles as drug carriers is that they are relatively more biocompatible and biodegradable than other synthetic and semi-synthetic polymer vesicles. Lipids, polysaccharides and peptides are all capable of self-assembling into vesicles and other nano and micro structures.

1.1.2.6.1. Lipid vesicles

Liposomes are lipid vesicles that are usually formed from the self-assembly of phospholipids which are amphiphilic in nature (Fig. 10). The membranes of these vesicles can be unilamellar or multilamellar depending on the method of preparation. Liposomes can be prepared from a variety of lipids like 1,2-Dimyristoyl-*sn*-Glycero-3-Phosphocholine (DMPC), Dipalmitoylphosphatidylcholine (DPPC), 1-palmitoyl-2-oleoyl-sn-glycero-3-phosphocholine (POPC) to name just a few. Most of our knowledge on vesicle assembly, dynamics and properties come from studies on liposomes. The first lipid vesicle, formed by the dispersion of phospholipids in water was reported by Bangham and coworkers[40] in 1964 and since then, many different and diverse vesicles have been designed and developed. There are a number of reviews published on liposomes. Strictly speaking, unlike poly-peptides, poly-saccharides and poly-nucleotides, lipids are not polymers by definition but they most readily self-assemble into macromolecular aggregates. Liposomes have found uses in many biological and pharmaceutical

applications. They are employed in studies related to cell physiology, as model cell membranes, diagnostic agents, drug delivery vehicles, in cosmetics and textiles.

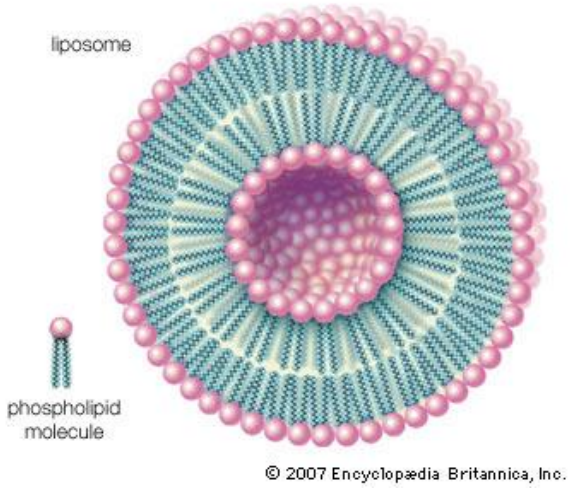

Figure 1.10. Illustration of a Liposome.

[liposome. [Art]. In Encyclopædia Britannica. Retrieved from http://www.britannica.com/EBchecked/media/92244/Phospholipids-can-be-used-to-form-artificial-structures-called-liposomes]

1.1.2.6.2. Polysaccharide vesicles

These are relatively less common. Chitin, chitosan and their derivatives have been investigated for their use as drug carriers. Although most of the vesicles in this category are a combination of lipids and polysaccharides, it is the polysaccharide part that drives the vesicle formation. Chitosan derived polymer vesicles are the most studied in this category. Due to their membrane-penetrating ability, these vesicles, palmitoyl glycol chitosan vesicles, are a good choice for intranasal, or oral administration of gut-labile molecules[41].

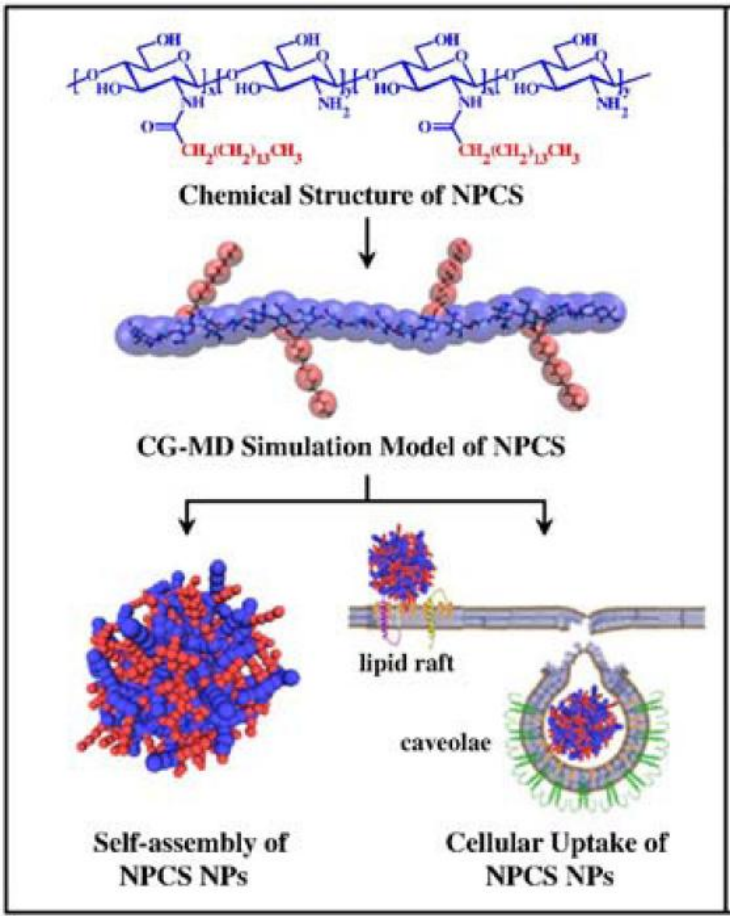

Figure 1.11. Polysaccharide vesicles.

"Schematic illustrations showing the self-assembly of N-palmitoyl chitosan (NPCS) polymers into nanoparticles (NPs) via the coarse-grained (CG) molecular dynamic (MD) simulations".

[Reproduced with permission from Elsevier; Chiu *et al*. (2010)[42], *J. Controlled Release*, **146**(1), 152-9., © 2010]

1.1.2.6.3. Peptide vesicles

Peptide derivatives or peptides linked to synthetic molecule have been shown to form many different nanostructures like tubes, fibers, rods, micelles, vesicles, doughnuts, bilayers and more[43,44,45,46,47,48]. On the other hand, vesicles, whose monomers are composed entirely of peptides, are relatively rare. While block copolymer monomers composed entirely of polypeptides, and polypeptides like Ac-V_mK_n-NH_2, Ac-G_mD_n-OH, Ac-V_6D-OH, Ac-KA_6-OH have been reported to form vesicles, these examples are only a few when compared to the many

synthetic polymers that are capable of self-assembling into vesicles. The field of peptide vesicles is still in its infancy but growing at a rapid pace. Vauthey *et al.* (2002)[49] were the first to show that a simple 7-8 residue amphiphilic peptide is capable of self-assembling into nanotubes and nanovesicles. They called these peptides, "Surfactant-Like Peptide". Santos *et al*. (2002)[50], designed similar peptides as the ones by Vauthey *et al.* (2002)[49] with glycine and aspartic acid that were capable of self-assembling into nanotubes and naovesicles. van Hell *et al*. (2007)[51], have shown the self-assembly of an amphiphilic oligopeptide SA2 into a nanosized vesicle. These vesicles not only carry the advantage of being relatively more biocompatible and biodegradable than other synthetic and semi-synthetic polymer vesicles but also are more stable than lipid and polysaccharide vesicles[21].

Peptide amphiphiles that are capable of self-assembling into nanovesicles can be as simple as a short polypeptide sequence, or can be a more complex molecule that is characterized by the presence of an alkyl chain (mostly synthetic) with a hydrophobic tail composed of amino acids and with an epitope head. Fig. 12, is an example of a peptide amphiphile.

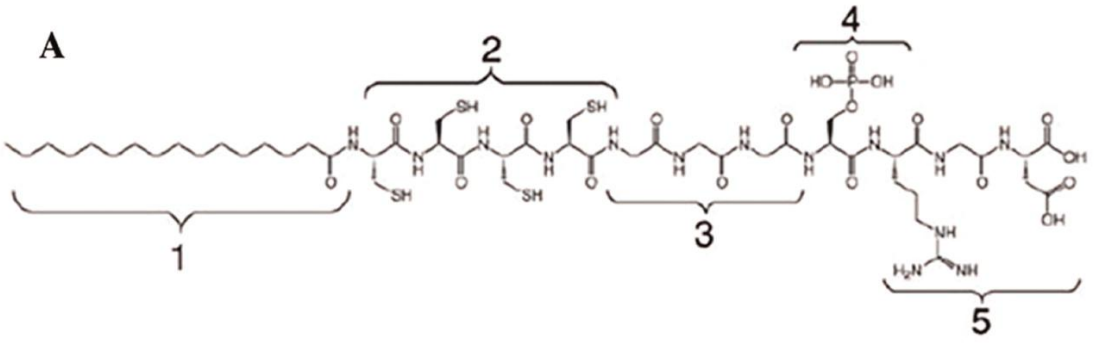

Figure 1.12. Peptide amphiphile structure.

"Peptide molecule and its 5 basic structural sequential features: (1) a hydrophobic alkyl chain, (2) 4 cysteine residues, (3) 3 glycines, (4) a phosphoserine group, and (5) an integrin-binding motif, RGD". (Reproduced with permission from Sage Publications; Semino C. E. (2008). *J. Dent Res.*, **87**(7), 606-16. © 2008, International & American Associations for Dental Research]

The forces that dictate vesicle formation in lipids and other polymeric vesicles apply to peptide amphiphiles too (peptide sequence, length and the overall geometry of the individual peptide molecule). Some examples of designer peptide amphiphiles that form nano structures include G_nD_2, A_6D, V_6D, V_6D_2, A_6K, I_3K, A_6K_2, GAVILRR, $A_2V_2L_3WE_{2or7}$ and similar peptides. Excellent reviews by Zhao *et al*. (2010)[52] and Zhang, S (2002)[53] summarize the various peptide amphiphiles that form nano structures and discusses a more exhaustive list of the various peptide amphiphiles. Some interesting results from the studies involving peptide amphiphiles are the use of isoleucines to promote interdigitation, mixing of oppositely charged peptides to reduce the CACs of the assemblies, peptides with their hydrophobic sequences containing alanine and valine form more homogeneous and stable nanostructures than those with glycine, isoleucine or leucine[54]. The hydrophobic chain length plays a critical role in the final assembly. Typically, the size of the hydrophobic tail in such peptide amphiphiles is about 3-9 hydrophobic residues. The length of the hydrophobic tail can determine the thickness of the outer layer of such nano structures but with longer chain lengths comes the issue of solubility and conversely, shorter chain lengths decrease the propensity of aggregation. Hence a balance of chain length is desired and is usually achieved by increasing or decreasing the hydrophilic head portion of the molecule.

1.2. Mechanism of vesicle formation

At its simplicity, any amphiphile that has a geometric packing parameter close to unity will tend to form a bilayer that can then be made to form vesicles under the appropriate conditions. When phospholipids aggregate into vesicular structures (from a hydrated precipitate) they form either multilamellar vesicles (MLVs), large unilamellar vesicles (LUVs) or small unilamellar vesicles (SUVs). The free energy of the hydrated precipitate is lowest while energy must be dissipated into the system for MLV, LUV and SUV[55]. The mechanism of vesicle formation in lipids has been well studied and the principle may be extended to other non-lipid based systems. From a drug delivery point of view, it might be most useful to prepare LUVs or SUVs that can encapsulate bioactive compounds. The starting point for such structures could usually be MLVs. Traditionally, MLVs were prepared by drying a film of phospholipids in a round bottom flask and adding water while gently or vigorously shaking. The process of vesicle formation (MLVs from hydrated precipitates) involves hydration of the different layers of the film. One can visualize the hydrated precipitate to be a layer composed of many thin layers of phospholipid film. When water is added, the top layer is hydrated leading to the formation of a convex bump. As more water is added, it seeps into the other layers, hydrating them and forming bilayers that eventually form tubular fibrils that increase the contact area with water. Upon agitation, these tubules break off and seal off the exposed areas immediately to take the shape of vesicles[55]. On the other hand, unilamellar vesicle formation involves a planar bilayer fragment as an intermediate structure[56]. These intermediate structures are unstable since their edges are exposed to the solvent. Micelles and vesicles are closely related especially when micelles can be induced to transition into vesicles upon certain stimuli like pH, temperature or composition.

The vesicles formed by the hydration of phospholipid films are metastable structures and are not in their lowest free energy equilibrium state. That state belongs to the spontaneously forming flat bilayer and it requires energy input to destabilize them into small dispersions. This energy input can be classified broadly into two mechanisms[57].

- Mechanical fragmentation of pre-formed bilayer structures
- Induction of bilayer curvature by breaking the symmetry of the flat bilayer

Since these vesicles do not form spontaneously, the characteristics of vesicles formed is largely dependent on procedural differences. Common parameters involved include[55, 58]:

- rate of surfactant depletion
- intensity of vortexing
- time and intensity of sonication.

There are two main energy components involved in the formation of a vesicle from a bilayer, the curvature free energy required to bend the bilayer into forming vesicles (f_c) and translational entropy. Entropy increases as the flat bilayer disperses into smaller aggregates. Thus, it's favorable for the formation of numerous vesicles. Since larger vesicles have lower curvature energy, they are more stable than smaller ones. The curvature free energy required to bend the bilayer into forming vesicles (f_c) for a single vesicle is in the order of 50-300k_BT[59](curvature moduli is expressed in terms of k_BT, where k_B is the Boltzmann constant), the contribution from entropy is only a few k_BT. Hence vesiculation is overall an unfavorable process. But, when the mean curvature modulus of the bilayer is low or when the concentration of the monomer is low, entropy factor dominates and vesicles now predominate. There is also the possibility of the bilayer having a non-zero spontaneous curvature, leading to vesicle formation. A number of spontaneously forming vesicles have been reported yet these vesicles may or may not be in their

equilibrium state[60]. In principle, thermodynamically stable vesicles should possess the following properties: [61,58]

- are generated spontaneously
- are stable with time with respect to size and shape
- have size distributions and stability independent of preparation methods
- are found in equilibrium with other phases.

It would be difficult to follow all these factors experimentally but vesicles that show most of these features are thought to be in an equilibrium state. Equilibrium vesicles of different mixtures in aqueous medium have been reported. Excellent reviews by Antunnes *et al*. (2009)[17] and Lasic, D. D., (1988)[55], discuss the dynamics of vesicle formation and stability in lipids and other polymeric vesicles and summarizes the equilibrium vesicles reported so far. Although, the principles and energy constraints described here are with respect to lipids and surfactant polymers, they hold true to a large extent for other polymer vesicles too, since the forces driving vesicle formation are similar.

Polymersomes

The polymers that constitute such polymersomes (block copolymer vesicles) are usually synthetic polymers but can also be composed of natural polymers. They have been compared to lipid vesicles although their properties more closely mimic viral capsids[62]. The property of polymersomes that stands out in comparison to lipid vesicles is their size. Polymersomes are usually large molecular weight aggregates that can be orders of magnitude greater than that observed for natural surfactants. The factors that dictate vesicle formation for lipids can be extended to polymersomes (and other amphiphiles that self-assemble into vesicles). Just like the packing parameter in lipids, the hydrophilic fraction f, along with the molecular weight and the effective interaction parameter of its hydrophobic block with water can be used to predict the

final structure an amphiphile would take. Among these, the hydrophilic fraction *f* plays a critical role in determining the final morphology. When an amphiphile takes the shape of a cylinder, wedge or a cone based on its time averaged molecular shape, it assumes a membrane, cylindrical or spherical morphology (Fig 1.13).

As a general rule monomer with a $f \approx 35\ \% \pm 10\ \%$, forms polymersomes whereas a monomer with a $f > 45\ \%$ will be expected to form micelles. Inverted microstructures are formed from monomers whose $f < 25\ \%$[62]. While the hydrophilic fraction *f* determines the morphology of the structure formed, the molecular weight of the monomer influences the thickness of the polymersome. Low glass transition temperature (T_g) on the other hand of the hydrophobic fraction

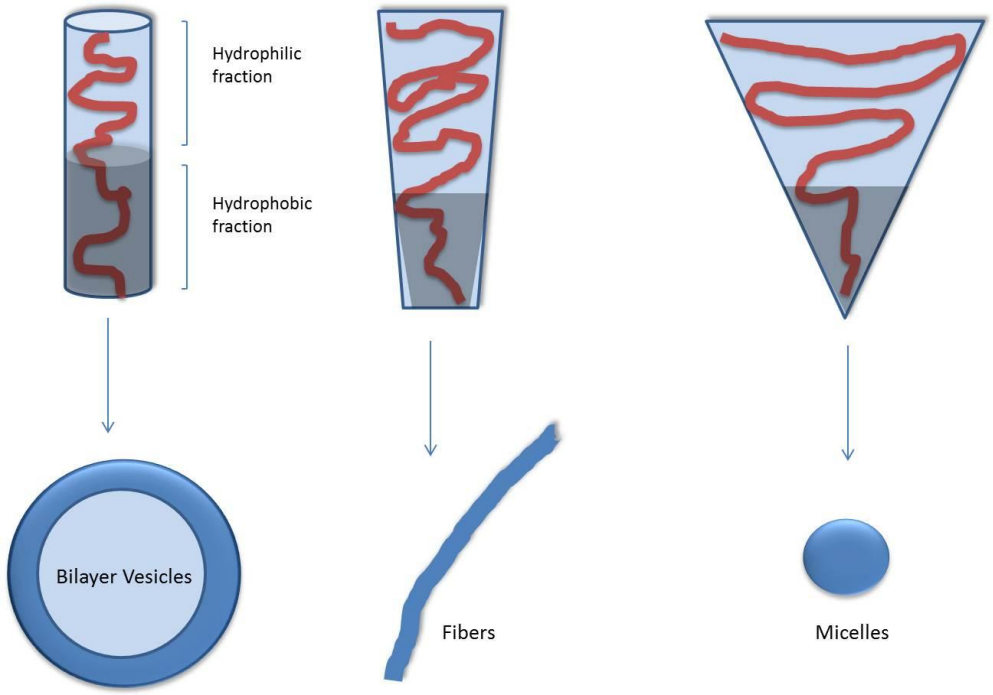

Figure 1.13. Monomer shape and hydrophilic fraction dictates assembly.

[Illustration based on Fig.2 of Discher, D. E., and Ahmed, F. (2006)[62]]

could help directly form polymersomes in water like the block copolymers of PBD- or PEE-PEG. Copolymers whose hydrophobic blocks have a high T_g require an organic solvent to first lower the T_g to provide chain mobility and hence cannot form polymersomes in pure water. Hence, apart from the factors mentioned above that influence polymersome formation, in certain cases, the concentration of the polymer solution as well as the percentage of water in the final mixture can be detrimental to polymersome formation[63]. As for the thickness of the polymersome membrane, a scaling of the copolymer membrane thickness with copolymer molecular weight was experimentally documented and confirmed by molecular dynamics (MD) simulations[25], a correlation could be achieved with:

$$d \sim MW_h^{\,b} \; (b = \sim 0.55)$$

where, d: membrane thickness; MW: molecular weight of the hydrophobic moiety(h). Not only is the membrane thickness affected by the molecular weight of the copolymer but so is its permeability. Based on coarse grain-MD simulations, higher molecular weight copolymers with longer chain lengths exhibit reduced area elastic modulus and chain entanglement (interdigitation) in its membrane region which eventually decreases lateral mobility of the copolymer in the membrane and hence permeability of solutes across the membrane[25].

1.3. Vesicles stabilized by β-Sheet secondary structures

The self-assembling molecules in most peptide based polymeric vesicles either lack a defined secondary structure or adopt a helical conformation when in their final assembled structure. Recently, however, vesicular[64,65,66,67] and micellar[68,69,70] assemblies stabilized by β-sheets have been reported. Gebhardt *et al*. (2007)[67] in their work with poly(butadiene)$_{107}$-poly(L-lysine)$_{27}$ coblock polymers elucidated the effects of secondary structure on the morphology of vesicles. In

the case of poly(butadiene)$_{107}$-poly(L-lysine)$_{27}$ coblock polymers, transition from α-helix to β-sheet takes place at a pH above the pKa of the lysine side chains. This transition resulted in a slight increase in the hydrodynamic radii of the vesicles and the overall assembly was still intact as determined by dynamic light scattering (DLS) and static light scattering (SLS). The formation of parallel β-sheets between the corona chains at the vesicular interface served to release interfacial curvature by creating a flatter interface. A molecular simulation study on the self-assembly of peptide amphiphiles[71] shows the interplay between hydrophobic interaction between the alkyl chains and hydrogen bonding between the peptide blocks resulting in assemblies like spherical β-sheets, micelles with β-sheets in the corona, and long cylindrical fibers (Fig.14). Similarly, PEO-b-Poly(V_1) and PEO-b-Poly(V_2) block copolymers self-assemble in water to form a mixture of vesicles and toroids (Fig. 16) and are stabilized by inter- and intrachain β-sheets, confirmed by circular dichroism spectroscopy (Fig. 15)[64].

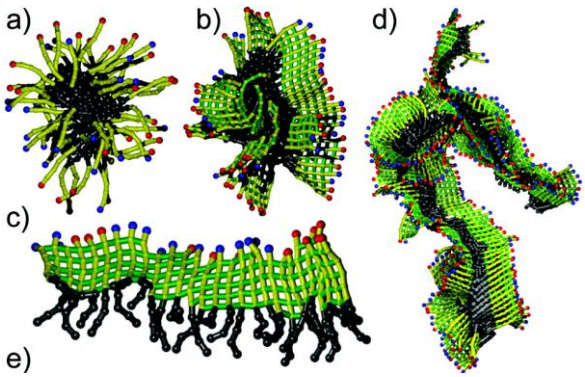

Figure 1.14. Snapshots from molecular simulations of peptide amphiphiles.

"(a) The spherical micelle, (b) the micelle with β-sheets on the outside forming the corona, (c) the β-sheets, and (d) the fiber aggregate". [Reproduced with permission from American Chemical Society; Velichko *et al*. (2008)[71], *J. Phys Chem B.*, **112**(8), 2326-34. © 2008, American Chemical Society]

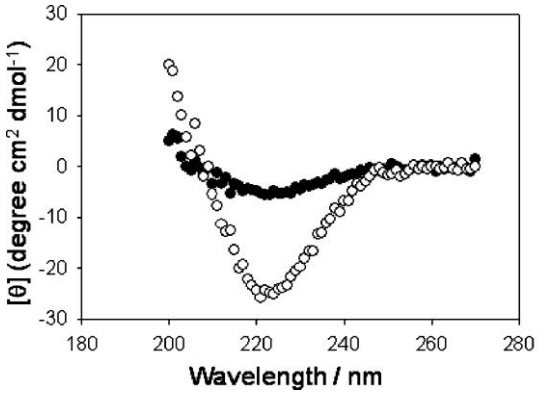

Figure 1.15. Example of CD spectra showing secondary structuring from the peptidic component of the PEO-b-poly(side-chain peptide) copolymers.

●, PEO-*b*-poly(V1); ○, PEO-*b*-poly(V2). [Reproduced with permission from American Chemical Society; Adams *et al*. (2008)[64], *Biomacromolecules*, **9**(11), 2997-3003. © 2008, American Chemical Society]

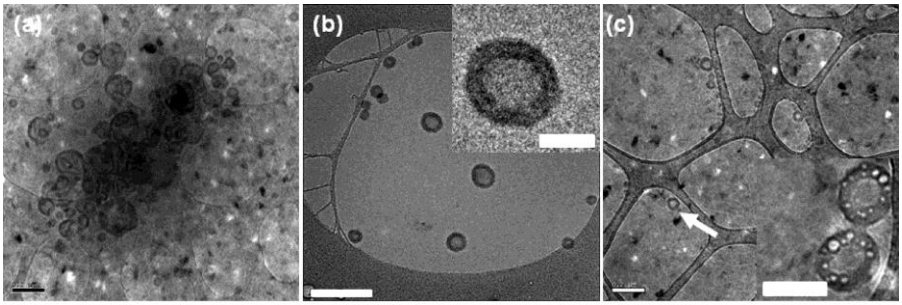

Figure 1.16. Cryo-TEM micrographs showing the self-assembled structures prepared from PEO-*b*-poly(graft-peptide) copolymers.

"(a) PEO-b-poly(V1), (b) PEO-b-poly(V2), (c) PEO-b-poly(V2) showing toroid-like structures, an example of which is highlighted by the arrow (scale bars = 200 nm (a and c) and = 100 nm (b)). Insets to (b), (c), show high magnification cryo-TEM micrographs showing a single vesicle or toroids (scale bars represent 50 nm)". [Reproduced with permission from American Chemical Society; Adams *et al*. (2008)[64], *Biomacromolecules*, **9**(11), 2997-3003. © 2008, American Chemical Society]

1.4. Characterization techniques - vesicles and micelles

Common techniques employed in characterizing polymer nanovesicles and micelles include the following types of analyses.

Table 1-2. Characterization techniques.

Structural Analyses	
Microscopy	Transmission Electron Microscopy (TEM) Scanning electron microscopy (SEM) Freeze fracture TEM, CryoTEM Atomic force microscopy (AFM)
Scattering techniques	Dynamic light scattering (DLS) Static light scattering (SLS) Small angle neutron scattering (SANS) Small angle X-ray scattering (SAXS)
Determination of CMC	1,6-diphenyl-1,3,5-hexatriene Benzoylacetone Pyrene
Encapsulation/Leakage Studies	Sodium fluorescein Carboxyfluorescein Calcein Rhodamine B and many other fluorescent dyes

To differentiate between micelles and vesicles, SANS is probably the best technique. Combination of DLS and SLS can also be used. For micelles, the ratio of the radius of gyration (from SLS) to hydrodynamic radius (R_g/R_h) is ~0.8 while that for a vesicle is 1. For CMC determination, pyrene preferentially partitions into the hydrophobic core region of the micelles and this partitioning leads to a change in its vibrational band intensities that can be followed in a fluorescence spectrophotometer.

1.5. Therapeutic applications of nanovesicles

A few decades ago, the most common way to administer a drug was to administer the free drug orally, intravenously or nasally. Unless the desired action of the drug is systemic, the obvious problem with such an approach is the exposure of the drug to cells that do not require the drug. Added to that, the dilution of the drug once administered into the body requires it to be administered in high enough doses for it to remain effective. This type of an approach could have some serious drawbacks of side effects such as cell toxicity. Thus, the method in which a drug is delivered can have a significant effect on its efficacy and the quality of life of the recipient. It may be administered as a free drug or packaged into a carrier molecule and then delivered. These carrier molecules are commonly referred to as drug delivery systems (DDS). Using drugs by DDS, can improve the biodistribution and pharmacokinetics of the drug molecule. Different drug molecules present different types of problems, related to their solubility, toxicity and instability. DDS can help attenuate some or most of these problems. The other advantages of using a DDS to deliver drugs include sustained and controlled release of the drug molecules. Most drug molecules are quickly cleared by the reticuloendothelial system and DDS can be designed to release the drug molecules over a period of time instead of all at once. This helps keep the drug molecules in the system long enough for the drug to be effective. An excellent review by Allen *et al*. (2004)[72] summarizes the advantages and limitations of lipid and polymer-based nanoparticle DDS.

Polymeric Nanovesicles show promise as delivery vehicles. Various drugs (hydrophobic and hydrophilic), proteins, nucleic acids and small molecules can be encapsulated within the large compartment of these vesicles and administered in vitro or in vivo. Polymeric vesicles offer superior advantages over their lipid counterparts (Liposomes) in terms of stability, storage and

tunability. Drug delivery through polymeric vesicles increases the stability of the drug, extends the circulation time in the blood and can be designed for controlled release. Most polymersomes and peptide amphiphiles have a very low critical aggregation concentration (CAC) in the range of 10^{-6} – 10^{-7} M, which is 1000 times lesser than most surfactants (10^{-3}–10^{-4}M) [73,74] on a molar basis. This allows for retention of payloads for a longer period as well as delivery to more distal areas of the body. A review of the literature reveals a plethora of compounds encapsulated and successfully delivered in vitro and in vivo using polymeric vesicles. These include various anti-cancer drugs like Doxorubicin and Paclitaxil, proteins like myoglobin, hemoglobin and albumin, fluorescent molecules, plasmids and siRNA. A review by Levine *et al*. (2008)[75] summarizing the literature of polymersome research related to cancer diagnosis and therapeutics, gives a more detailed account of the type of polymersomes and cargo that have been developed so far.

Polymeric vesicles are also useful as diagnostic tools and in optical imaging when they can encapsulate fluorescent agents. One example of such a use would be the encapsulation of a porphyrin-based near infrared (NIR) fluorophore that is able to generate a signal even through a 1 cm solid tumor[76]. When such nanovesicles are injected into an animal, their biodistribution can be monitored using non-invasive optical methods eliminating the need to sacrifice the animal.

The surface of these nanovesicles can be functionalized with various ligand molecules that are specific for up-regulated receptors or molecules on disease cells. This site-specific delivery further reduces the potential side-effects due to systemic delivery. The various ligand molecules that have been attempted include (but are not limited to) various antibodies, transactivator of transcription (TAT) peptide and anti-HER-2/neu *peptide* mimetic (AHNP) peptides.

1.6. References

[1] Rughani, R. V. and Schneider, J. P. (2008). Molecular design of beta-hairpin peptides for material construction. *MRS Bulletin / Materials Research Society, 33*(5), 530-535.

[2] Giddi, H. S., Arunagirinathan, M. A., and Bellare, J. R. (2007). Self-assembled surfactant nano-structures important in drug delivery: A review. *Indian Journal of Experimental Biology, 45*(2), 133-159.

[3] Rajagopal, K., and Schneider, J. P. (2004). Self-assembling peptides and proteins for nanotechnological applications. *Current Opinion in Structural Biology, 14*(4), 480-486.

[4] Tu, R. S., and Tirrell, M. (2004). Bottom-up design of biomimetic assemblies. *Advanced Drug Delivery Reviews, 56*(11), 1537-1563.

[5] Drummond, C. J., and Fong, C. (1999). Surfactant self-assembly objects as novel drug delivery vehicles. *Current Opinion in Colloid and Interface Science, 4*(6), 449-456.

[6] Goldstein, A. S., Lukyanov, A. N., Carlson, P. A., Paul Yager, and Gelb, M. H. (1997). Formation of high-axial-ratio-microstructures from natural and synthetic sphingolipids. *Chemistry and Physics of Lipids, 88*(1), 21-36.

[7] Israelchvili, J. (1985). *Intermolecular and surface forces*. Academic, New York.

[8] Min, Y., Akbulut, M., Kristiansen, K., Golan, Y., and Israelachvili, J. (2008). The role of interparticle and external forces in nanoparticle assembly. *Nature Materials, 7*(7), 527-538.

[9] Procházka, K., Martin, T. J., Webber, S. E., and Munk, P. (1996). Onion-type micelles in aqueous media. *Macromolecules, 29*(20), 6526-6530.

[10] Read, E. S., and Armes, S. P. (2007). Recent advances in shell cross-linked micelles. *Chemical Communications (Cambridge, England), (29)*(29), 3021-3035.

[11] Erhardt, R., Böker, A., Zettl, H., Kaya, H., Pyckhout-Hintzen, W., Krausch, G., et al. (2001). Janus micelles . *Macromolecules, 34*(4), 1069-1075.

[12] Erhardt, R., Zhang, M., Böker, A., Zettl, H., Abetz, C., Frederik, P., et al. (2003). Amphiphilic janus micelles with polystyrene and poly(methacrylic acid) hemispheres. *Journal of the American Chemical Society, 125*(11), 3260-3267.

[13] Voets, I. K., de Keizer, A., de Waard, P., Frederik, P. M., Bomans, P. H., Schmalz, H., et al. (2006). Double-faced micelles from water-soluble polymers. *Angewandte Chemie (International Ed.in English), 45*(40), 6673-6676.

[14] Bütün, V., Liu, S., Weaver, J. V. M., Bories-Azeau, X., Cai, Y., and Armes, S. P. (2006). A brief review of 'schizophrenic' block copolymers. *Reactive and Functional Polymers, 66*(1), 157-165.

[15] Li, Z., Hillmyer, M. A., and Lodge, T. P. (2006). Control of structure in multicompartment micelles by blending μ-ABC star terpolymers with AB diblock copolymers. *Macromolecules, 39*(2), 765-771.

[16] Tu, R. S., and Tirrell, M. (2004). Bottom-up design of biomimetic assemblies. *Advanced Drug Delivery Reviews, 56*(11), 1537-1563.

[17] Antunes, F. E., Marques, E. F., Miguel, M. G., and Lindman, B. (2009). Polymer-vesicle association. *Advances in Colloid and Interface Science, 147-148*, 18-35.

[18] Hajduk, D. A., Kossuth, M. B., Hillmyer, M. A., and Bates, F. S. (1998). Complex phase behavior in aqueous solutions of poly(ethylene oxide)-Poly(ethylethylene) block copolymers. *The Journal of Physical Chemistry B, 102*(22), 4269-4276.

[19] Warriner, H. E., Idziak, S. H., Slack, N. L., Davidson, P., and Safinya, C. R. (1996). Lamellar biogels: Fluid-membrane-based hydrogels containing polymer lipids. *Science (New York, N.Y.), 271*(5251), 969-973.

[20] Yu, K., and Eisenberg, A. (1998). Bilayer morphologies of self-assembled crew-cut aggregates of amphiphilic PS-b-PEO diblock copolymers in solution. *Macromolecules, 31*(11), 3509-3518.

[21] Discher, B. M., Won, Y. Y., Ege, D. S., Lee, J. C., Bates, F. S., Discher, D. E., et al. (1999). Polymersomes: Tough vesicles made from diblock copolymers. *Science (New York, N.Y.), 284*(5417), 1143-1146.

[22] Meng, F., Zhong, Z., and Feijen, J. (2009). Stimuli-responsive polymersomes for programmed drug delivery. *Biomacromolecules, 10*(2), 197-209.

[23] Cornelissen, J. J. L. M., Fischer, M., Sommerdijk, N. A. J. M., and Nolte, R. J. M. (1998). Helical superstructures from charged poly(styrene)-poly(isocyanodipeptide) block copolymers. *Science (New York, N.Y.), 280*(5368), 1427-1430.

[24] Needham,D. and Zhelev,D.V.(2000). *The Mechanochemistry of Lipid Vesicles Examined by Micropipette Manipulation Techniques in Vesicles* (ed Rosoff, M.) Ch. 9 (Marcel Dekker,New York, 2000).

[25] Srinivas, G., Discher, D. E., and Klein, M. L. (2004). Self-assembly and properties of diblock copolymers by coarse-grain molecular dynamics. *Nature Materials, 3*(9), 638-644.

[26] Branco, M. C., and Schneider, J. P. (2009). Self-assembling materials for therapeutic delivery. *Acta Biomaterialia, 5*(3), 817-831.

[27] Carlsen, A., and Lecommandoux, S. (2009). Self-assembly of polypeptide-based block copolymer amphiphiles. *Current Opinion in Colloid and Interface Science, 14*(5), 329-339.

[28] Yoshioka, T., Sternberg, B., and Florence, A. T. (1994). Preparation and properties of vesicles (niosomes) of sorbitan monoesters (span 20, 40, 60 and 80) and a sorbitan triester (span 85). *International Journal of Pharmaceutics, 105*(1), 1-6.

[29] Vanlerberghe, G., R. M. Handjani-Vila, and A. Ribier. 1978. Les niosomes, une nouvelle famille de vesicules a` base d'amphiphiles non ioniques. *In* Physicochimie des compose´s amphiphiles. Coll. Nat. CNRS. Editions du CNRS. Paris. 303–311.

[30] Handjani-Vila, R. M., Ribier, A., Rondot, B., and Vanlerberghie, G. (1979). Dispersions of lamellar phases of non-ionic lipids in cosmetic products. *International Journal of Cosmetic Science, 1*(5), 303-314.

[31] Procédé de fabrication de dispersions aqueuses de spérules lipidiques et nouvelles compositions correspondantes, L'Oréal, French Patent 2315991, 1975

[32] Cosmetic and pharmaceutical compositions containing niosomes and a water-soluble polyamide, and a process for preparing these compositions, L'Oréal, US Patent 4830857, 1989

[33] Percec, V., Wilson, D. A., Leowanawat, P., Wilson, C. J., Hughes, A. D., Kaucher, M. S., et al. (2010). Self-assembly of janus dendrimers into uniform dendrimersomes and other complex architectures. *Science (New York, N.Y.), 328*(5981), 1009-1014.

[34] Ropponen, J., Nummelin, S., and Rissanen, K. (2004). Bisfunctionalized janus molecules. *Organic Letters, 6*(15), 2495-2497.

[35] Rosen, B. M., Wilson, C. J., Wilson, D. A., Peterca, M., Imam, M. R., and Percec, V. (2009). Dendron-mediated self-assembly, disassembly, and self-organization of complex systems. *Chemical Reviews, 109*(11), 6275-6540.

[36] Sawamura, M., Toganoh, M., Suzuki, K., Hirai, A., Iikura, H., and Nakamura, E. (2000). Stepwise synthesis of fullerene cyclopentadienide R(5)C(60)(-) and indenide R(3)C(60)(-). an approach to fully unsymmetrically substituted derivatives. *Organic Letters, 2*(13), 1919-1921.

[37] Burger, C., Hao, J., Ying, Q., Isobe, H., Sawamura, M., Nakamura, E., et al. (2004). Multilayer vesicles and vesicle clusters formed by the fullerene-based surfactant C60(CH3)5K. *Journal of Colloid and Interface Science, 275*(2), 632-641.

[38] Homma, T., Harano, K., Isobe, H., & Nakamura, E. (2011). Preparation and properties of vesicles made of Nonpolar/Polar/Nonpolar fullerene amphiphiles. *Journal of the American Chemical Society, 133*(16), 6364-6370.

[39] Kaler, E. W., Murthy, A. K., Rodriguez, B. E., and Zasadzinski, J. A. (1989). Spontaneous vesicle formation in aqueous mixtures of single-tailed surfactants. *Science (New York, N.Y.), 245*(4924), 1371-1374.

[40] Bangham, A. D., and Horne, R.W. (1964) Negative staining of phospholipids and their structural modification by surface active agents as observed in the electron microscope. J. Mol. Biol. 8, 660 – 66.

[41] Uchegbu, I. F., Schatzlein, A. G., Tetley, L., Gray, A. I., Sludden, J., Siddique, S., et al. (1998). Polymeric chitosan-based vesicles for drug delivery. *The Journal of Pharmacy and Pharmacology, 50*(5), 453-458

[42] Chiu, Y. L., Ho, Y. C., Chen, Y. M., Peng, S. F., Ke, C. J., Chen, K. J., et al. (2010). The characteristics, cellular uptake and intracellular trafficking of nanoparticles made of hydrophobically-modified chitosan. *Journal of Controlled Release : Official Journal of the Controlled Release Society, 146*(1), 152-159.

[43] Nagai, A., Nagai, Y., Qu, H., and Zhang, S. (2007). Dynamic behaviors of lipid-like self-assembling peptide A6D and A6K nanotubes. *Journal of Nanoscience and Nanotechnology, 7*(7), 2246-2252.

[44] Santoso, S., Hwang, W., Hartman, H., and Zhang, S. (2002). Self-assembly of surfactant-like peptides with variable glycine tails to form nanotubes and nanovesicles. *Nano Letters, 2*(7), 687-691.

[45] von Maltzahn, G., Vauthey, S., Santoso, S., and Zhang, S. (2003). Positively charged surfactant-like peptides self-assemble into nanostructures. *Langmuir, 19*(10), 4332-4337.

[46] Xu, H., Wang, J., Han, S., Wang, J., Yu, D., Zhang, H., Xia, D, Zhao, X., Waigh, T. A., Lu, J. R. (2009). Hydrophobic-region-induced transitions in self-assembled peptide nanostructures. *Langmuir, 25*(7), 4115-4123.

[47] Yang, S. J., and Zhang, S. (2006). Self-assembling behavior of designer lipid-like peptides. *Supramolecular Chemistry, 18*(5), 389-396.

[48] Zhao, X., Pan, F., Perumal, S., Xu, H., Lu, J. R., and Webster, J. R. P. (2009). Interfacial assembly of cationic peptide surfactants. *Soft Matter, 5*(8), 1630-1638.

[49] Vauthey, S., Santoso, S., Gong, H., Watson, N., Zhang, S. Molecular self-assembly of surfactant-like peptides to form nanotubes and nanovesicles. *Proc. Natl. Acad. Sci.* 99, 5355-5360 (2002).

[50] Santoso, S., Hwang, W., Hartman, H., Zhang, S. Self-assembly of surfactant-like peptides with variable glycine tails to form nanotubes and nanovesicles. *Nano Lett.* 2, 687-691 (2002).

[51] van Hell, A. J., Costa, C. I., Flesch, F. M., Sutter, M., Jiskoot, W., Crommelin, D. J., et al. (2007). Self-assembly of recombinant amphiphilic oligopeptides into vesicles. *Biomacromolecules, 8*(9), 2753-2761.

[52] Zhao, X., Pan, F., Xu, H., Yaseen, M., Shan, H., Hauser, C. A., et al. (2010). Molecular self-assembly and applications of designer peptide amphiphiles. *Chemical Society Reviews, 39*(9), 3480-3498.

[53] Zhang, S. (2002). Emerging biological materials through molecular self-assembly. *Biotechnology Advances, 20*(5-6), 321-339.

[54] Zhao, X., and Zhang, S. (2006). Molecular designer self-assembling peptides. *Chemical Society Reviews, 35*(11), 1105-1110.

[55] Lasic, D. D. (1988). The mechanism of vesicle formation. *The Biochemical Journal, 256*(1), 1-11.

[56] Hernandez-Zapata, E., Martinez-Balbuena, L., and Santamaria-Holek, I. (2009). Thermodynamics and dynamics of the formation of spherical lipid vesicles. *Journal of Biological Physics, 35*(3), 297-308.

[57] Winterhalter, M., and Lasic, D. D. (1993). Liposome stability and formation: Experimental parameters and theories on the size distribution. *Chemistry and Physics of Lipids, 64*(1-3), 35-43.

[58] Marques, E. F. (2000). Size and stability of catanionic vesicles: effects of formation path, sonication, and aging. *Langmuir, 16*(11), 4798-4807

[59] Antunes, F. E., Marques, E. F., Miguel, M. G., and Lindman, B. (2009). Polymer-vesicle association. *Advances in Colloid and Interface Science, 147-148*, 18-35.

[60] Lasic, D. D., Joannic, R., Keller, B. C., Frederik, P. M., and Auvray, L. (2001). Spontaneous vesiculation. *Advances in Colloid and Interface Science, 89-90*, 337-349.

[61] Kaler, E. W., Herrington, K. L., Murthy, A. K., and Zasadzinski, J. A. N. (1992). Phase behavior and structures of mixtures of anionic and cationic surfactants. *The Journal of Physical Chemistry, 96*(16), 6698-6707.

[62] Discher, D. E., and Ahmed, F. (2006). Polymersomes. *Annual Review of Biomedical Engineering, 8*, 323-341.

[63] Shen, H., and Eisenberg, A. (2000). Block length dependence of morphological phase diagrams of the ternary system of PS-b-PAA/Dioxane/H2O. *Macromolecules, 33*(7), 2561-2572.

[64] Adams, D. J., Atkins, D., Cooper, A. I., Furzeland, S., Trewin, A., and Young, I. (2008). Vesicles from peptidic side-chain polymers synthesized by atom transfer radical polymerization. *Biomacromolecules, 9*(11), 2997-3003.

[65] Iatrou, H., Frielinghaus, H., Hanski, S., Ferderigos, N., Ruokolainen, J., Ikkala, O., et al. (2007). Architecturally induced multiresponsive vesicles from well-defined polypeptides: Formation of gene vehicles. *Biomacromolecules, 8*(7), 2173-2181.

[66] Kar, S., Drew, M. G., and Pramanik, A. (2011). Formation of vesicles through solvent assisted self-assembly of hydrophobic pentapeptides: Encapsulation and pH responsive release of dyes by the vesicles. *Protein and Peptide Letters, 18*(9), 886-897.

[67] Gebhardt, K. E., Ahn, S., Venkatachalam, G., and Savin, D. A. (2008). Role of secondary structure changes on the morphology of polypeptide-based block copolymer vesicles. *Journal of Colloid and Interface Science, 317*(1), 70-76.

[68] Sun, J., Chen, X., Lu, T., Liu, S., Tian, H., Guo, Z., et al. (2008). Formation of reversible shell cross-linked micelles from the biodegradable amphiphilic diblock copolymer poly(L-cysteine)-block-poly(L-lactide). *Langmuir : The ACS Journal of Surfaces and Colloids, 24*(18), 10099-10106.

[69] Sallach, R. E., Wei, M., Biswas, N., Conticello, V. P., Lecommandoux, S., Dluhy, R. A., et al. (2006). Micelle density regulated by a reversible switch of protein secondary structure. *Journal of the American Chemical Society, 128*(36), 12014-12019.

[70] Sinaga, A., Hatton, T. A., and Tam, K. C. (2007). Poly(acrylic acid)-block-poly(L-valine): Evaluation of beta-sheet formation and its stability using circular dichroism technique. *Biomacromolecules, 8*(9), 2801-2808.

[71] Velichko, Y. S., Stupp, S. I., and de la Cruz, M. O. (2008). Molecular simulation study of peptide amphiphile self-assembly. *The Journal of Physical Chemistry.B, 112*(8), 2326-2334.

[72] Allen, T. M. and Cullis, P. R. Drug Delivery Systems: Entering the Mainstream. *Science*, 303, 1818-1822 (2004).

[73] Wang, L., Zeng, R., Li, C., and Qiao, R. (2009). Self-assembled polypeptide-block-poly(vinylpyrrolidone) as prospective drug-delivery systems. *Colloids and Surfaces.B, Biointerfaces, 74*(1), 284-292.

[74] Lin, J., Zhu, J., Chen, T., Lin, S., Cai, C., Zhang, L., et al. (2009). Drug releasing behavior of hybrid micelles containing polypeptide triblock copolymer. *Biomaterials, 30*(1), 108-117.

[75] Levine, D. H., Ghoroghchian, P. P., Freudenberg, J., Zhang, G., Therien, M. J., Greene, M. I., et al. (2008). Polymersomes: A new multi-functional tool for cancer diagnosis and therapy. *Methods (San Diego, Calif.), 46*(1), 25-32.

[76] Tanisaka, H., Kizaka-Kondoh, S., Makino, A., Tanaka, S., Hiraoka, M., and Kimura, S. (2008). Near-infrared fluorescent labeled peptosome for application to cancer imaging. *Bioconjugate Chemistry, 19*(1), 109-117.

Chapter 2 - Branched Amphiphilic Peptides, bis(h_n)-K-K_n Self-Assemble into Nanovesicles

2.1. Introduction

Lipid-based carriers have traditionally been the method of choice for delivering bioactive compounds into living systems[1]. However, despite certain advantages, lipid-based vesicles possess a number of shortcomings, especially with regard to stability, bioreactivity and toxicity[2]. Cationic liposomes especially, are known to trigger specific signaling pathways which involve protein kinase C (PKC)[3], stimulate toll-like receptor 4 (TLR4) in dendritic cells[4] or directly bind to membrane lipids and modulate the activity of membrane proteins[5,6]. Virus mediated delivery of genetic material has made much progress but still suffers from many serious drawbacks, which include immunogenicity[7,8,9], lack of specificity[10] and insertional mutagenesis[11] leading to such adverse effects as the development of cancer. Recent research on non lipid-based carriers shows promise in replacing liposomes and other lipid-based delivery systems as a means for targeting cells or tissues[12]. Non lipid-based systems have shown improved stability, specificity and tune-ability over lipid-based vesicles[13]. Linear blocks of amphiphilic peptides have been shown to undergo self-assembly into various supramolecular assemblies like macroscopic hydrogels[14,15,16], nanotubes[17,18], fibers[19], β-sheet tapes[20] and nanovesicles[21]. Peptide vesicles are one such example of non lipid-based carriers, with most of the research centered on di- or tri-block copolymers[22,23,24,25,26]. These relatively high molecular weight, linear covalently linked polymers are composed of repeating hydrophobic and hydrophilic segments and mostly adopt a helical secondary structure. β-sheet stabilized spherical assemblies are a relatively new field of research and there are few examples in literature of such peptides or proteins adopting this morphology (e.g., spherulites[27] and amylospheroids[28]).

2.2. Materials and Methods

2.2.1. Materials

Dichloromethane, Dimethylformamide, Piperidine and n-Methylpyrrolidone, Trifluoroacetic acid, Acetonitrile were purchased from American Bioanalytical (Natick, MA), Diethyl ether, and 2,2,2-Trifluoroethanol, were purchased from Fisher Scientific (Fairlawn, NJ), all F-moc protected amino acids were purchased from Anapsec, Inc. (Fremont, CA), CLEAR-amide resin was purchased from Applied Biosystems (Foster City, CA), 5(6)-Carboxyfluorescein was purchased from Fluka (Sigma-Aldrich, St. Louis, MO), 200 proof ethanol was purchased from Decon Laboratories, Inc.(King of Prussia, PA), Amicon ultra-0.5 mL, 30K MWCO Centrifugal units with regenerated cellulose filters were purchased from Millipore (Billerica, MA)

2.2.2. Peptide Synthesis

Peptides were synthesized using standard solid phase chemistries and 9-fluorenylmethoxycarbonyl (Fmoc)-protected amino acids on CLEAR-amide resin on a model No. 431 peptide synthesizer (Applied Biosystems; Foster City, CA). This resin generates a C-terminus with a Carboxyamide moiety. The synthesis of the peptide begins with the first amino acid, lysine (with its α-amino group blocked with Fmoc and its ε-amine group blocked with t-Boc) attached covalently to the resin. The t-Boc at the ε-amine group allows for linear extension of the peptide while preventing any side reactions at the side-chain amino group. Three more lysines are added in in a likewise fashion to produce the tetra-lysine C-terminal segment. After the fourth Fmoc/*t*-Boc lysine is attached, a fifth lysine with both the α- and ε-amine groups blocked with Fmoc groups [$N^{\alpha,\varepsilon}$ di-Fmoc-L-Lysine] $C_{36}H_{34}N_2O_6$, is added. This amino acid allows for the introduction of a branch point. The release of the two Fmoc protecting groups allows for the simultaneous addition of two identical amino acids to the now bifurcated

sequence. Upon the addition of new Fmoc-protected amino acids, extension occurs at both sites, thereby permitting the synthesis of the two (bis) hydrophobic tails attached to the common C-terminal oligo-lysine segment: FLIVIGSII (h_9) or FLIVI (h_5) (Fig. 2.1). The N-termini are blocked with acetyl capping. The stepwise addition of amino acids to both the α- and ε-amine of a lysine was previously described by Iwamoto *et al*. (1994)[37].–The completed peptides, are cleaved with simultaneous side-chain deprotection by treatment with water in 95 % trifluoroacetic acid for 2 h at room temperature. The cleaved peptides are then washed four times with diethyl ether and dissolved in water, and then lyophilized (Fig. 2.2).

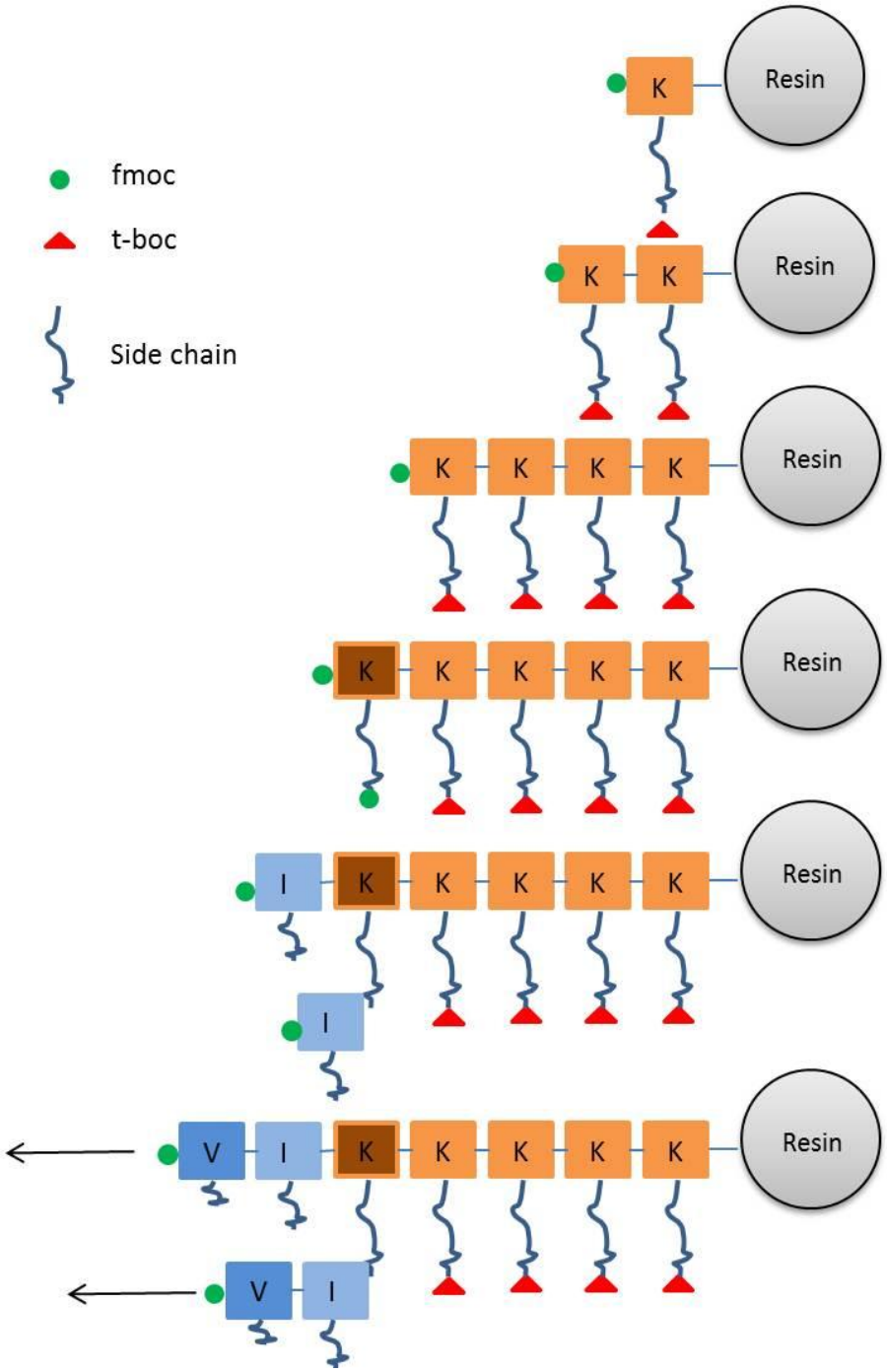

Figure 2.1. Illustration of the steps involved in synthesizing a branched peptide.

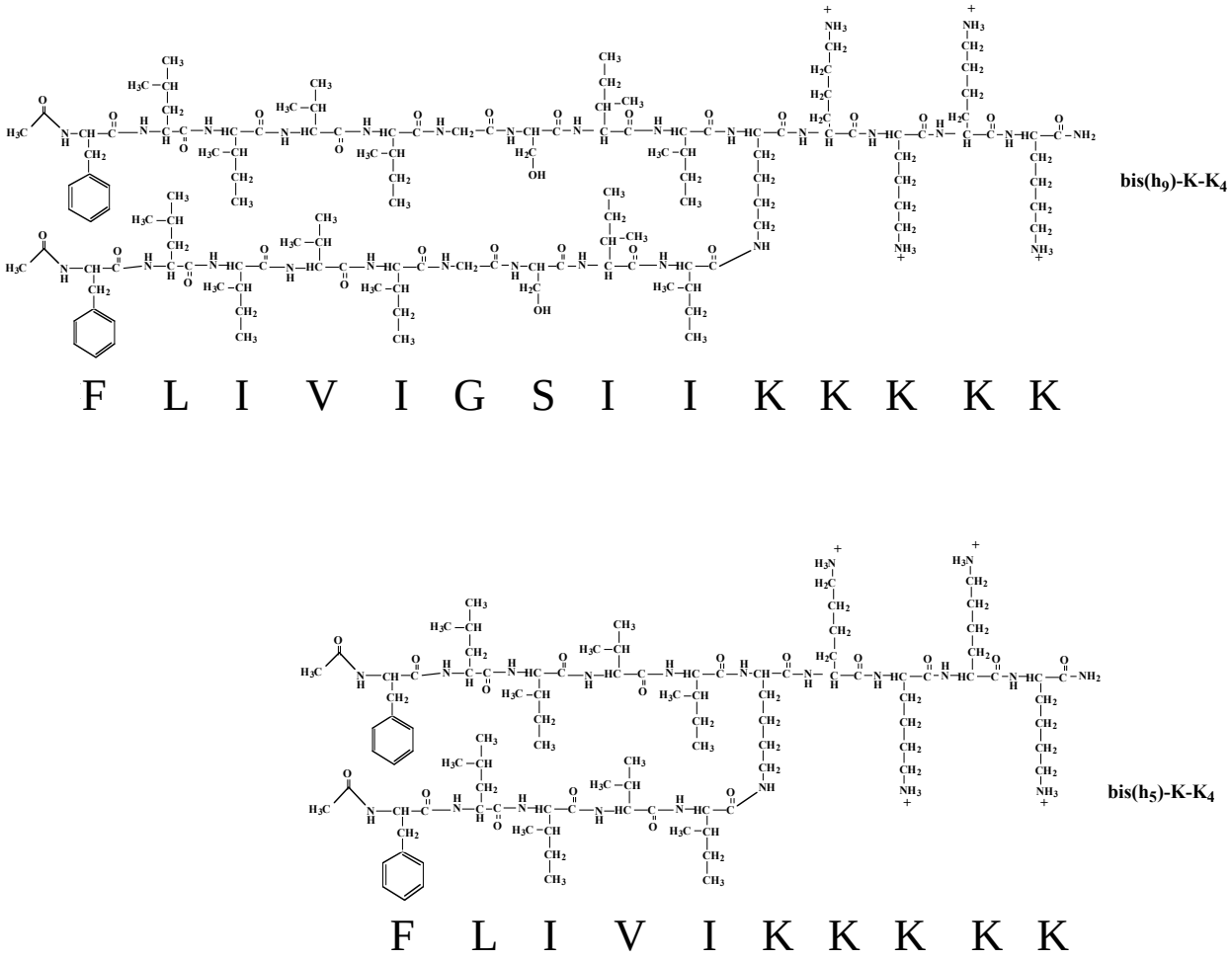

Figure 2.2. Chemical structure of vesicle forming sequences.

These sequences are acetyl capped at the N-termini and Carboxyamide blocked at the C-terminal. At neutral pH the lysine side chains are positively charged.

2.2.3. Vesicle Preparation

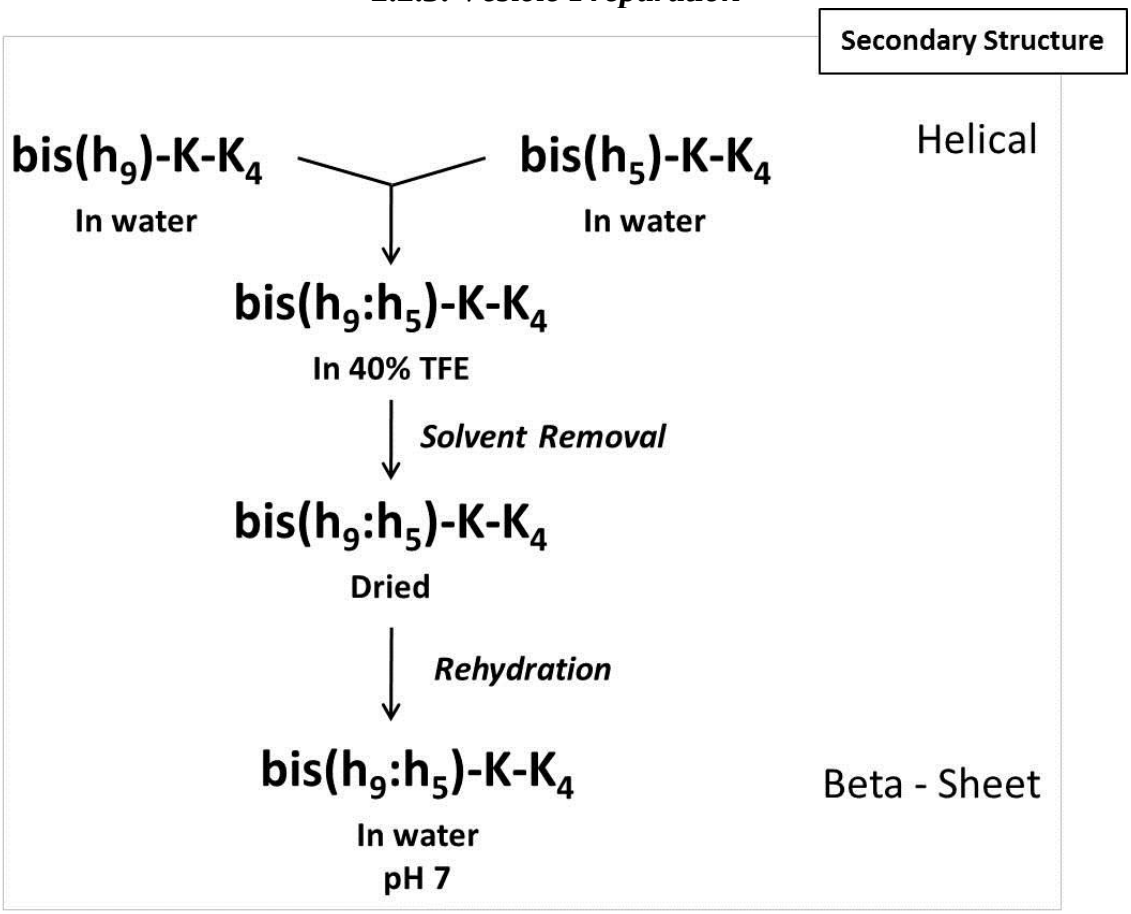

Figure 2.3. A general protocol for preparation of bilayer assemblies

The general method of vesicle preparation is described using N-acetyl capped peptides. It should be noted the same procedure can be carried out using uncapped peptides. Each of the N-acetyl capped lyophilized peptide samples are individually dissolved in DDI water and their absorbance read in a spectrophotometer. Peptide concentrations are calculated using the molar absorptivity (ε) of Phe in water at 257.5 nm (195 cm^{-1} M^{-1}). The two peptides (bis(h_9)-K-K_4 and bis(h_5)-K-K_4) are then mixed together in an equimolar ratio in a 40 % Trifluoroethanol solution and vortexed briefly and allowed to stand for a few hours before removing the solvent under vacuum. In one experiment, the peptides were mixed to a final concentration of 1.6 mM of each peptide,

followed by solvent removal. The dried samples are then redissolved in DDI water by the dropwise addition of the water. The rehydrated samples are then vortexed briefly and allowed to stand at least 2 h before any measurements are made.

2.2.4. Molecular modeling

All Molecular dynamics (MD) simulations were carried out by Dr. Jian Gao under the supervision of Dr. Jianhan Chen (Biochemistry Department, Kansas State University, Manhattan, KS). The MD simulation of peptide and DPPC bilayers were carried out in CHARMM[29,30] using the MARTINI coarse-grained (CG) force field[31,32]. The model bilayers contain 128 peptide or Dipalmitoylphosphatidylcholine (DPPC) molecules, solvated in about 5000 CG waters. The equilibrium properties of the bilayers were calculated from 100 ns MD simulations at 320 K. Additional 100 ns MD simulations were performed at elevated temperatures from 350 K up to 1000 K (every 50 K) to investigate the thermo-stability of these model bilayers. Peptide or lipid diffusion constants and order parameters were monitored to infer bilayer integrity. The self-assembly simulations were initiated from homogeneously dispersed systems that contain about 10000 CG waters and 128 branched peptide or DPPC molecules. The simulations were carried out at 500 K until self-assembly occurred, which took up to 200 ns for both sequences. The final state often contains small aggregates besides the bilayer. While a single bilayer is expected for the most stable state, these final states are kinetically stable and much longer simulations would be required to observe full incorporation of all peptides into a single bilayer.

2.2.5. Transmission Electron Microscopy

All Transmission Electron Micrographs (TEM) were taken with the help of Lloyd Willard at the Department Diagnostic Medicine and Pathobiology, College of Veterinary Medicine, Kansas State University.

For phosphotungstic acid (PTA) staining, bis(h_9)-K-K_4 was co-dissolved in DDI water at a 1:1 molar ratio with bis(h_5)-K-K_4 for a final concentration of 1.6 mM of each peptide. Next, 15 µL of the peptide vesicle solution was placed on a copper grid (which in turn was placed on a piece of parafilm that was placed in a Petri dish) and allowed to stand for 3 min. Excess peptide solution was wicked off by lightly touching the edge of a filter paper to the grid, followed by the addition of 15 µL of 10 % PTA to the grid, which was allowed to stand for about 5 min. Excess PTA solution was wicked off by lightly touching the edge of a filter paper to the grid, and the grid was washed lightly with DDI water using a syringe which was fitted with a hypodermic needle. Excess water was wicked off by lightly touching the edge of a filter paper to the grid and the grid was allowed to dry for at least 30 min before the TEM images were taken.

For osmium tetraoxide (OsO_4) staining, bis(h_9)-K-K_4 was co-dissolved in DDI water at a 1:1 molar ratio with bis(h_5)-K-K_4 for a final concentration of 25 µM of each peptide. Next, 7 µL of the peptide vesicle solution was placed on a copper grid (which in turn was placed on a piece of parafilm that was placed in a Petri dish) and allowed to stand for about 10 min. A drop of OsO_4 was placed on the parafilm, a few inches away from the copper grid containing the peptide sample. The Petri dish was covered to allow the OsO_4 vapors to deposit on the peptide sample for a period of about 5 min. These grids were then allowed to dry for at least 15-20 min before the TEM photos were taken.

2.2.6. Confocal Microscopy

Confocal microscopy was performed using a Nikon C1 scanning confocal microscope with a 2-laser units system: air-cooled argon laser (454 nm) and He–Ne laser (543 nm). Optical sections (images) of the vesicles were taken using a Nikon Plan Fluor 100×/1.3/WD 0.20/oil objective, standardized pinhole (30 µm) and appropriate gain settings. Images were processed using Nikon EZ-C1 Viewer software. Stock solutions of bis(h_9)-K-K_4 and bis(h_5)-K-K_4 in DDI water were co-

dissolved at a 1:1 molar in a 5(6)-Carboxyfluorescein solution for a final peptide concentration of 1.6 mM each. About 25 µL of the sample was then mounted on a glass slide and covered with a coverslip and sealed with nail polish. The slides were allowed to sit for 48-72 hours before pictures were taken. In a separate experiment, the bis(h_9)-K-K_4 and bis(h_5)-K-K_4 peptides (1:1) where allowed to sit for three days (72 h) in an unbuffered 5(6)-Carboxyfluorescein solution before pictures were taken.

2.2.7. Analytical Ultracentrifugation

Sedimentation velocity experiments were conducted using an Optima XL-1 analytical ultracentrifuge (Beckman Coulter, Fullerton, CA) with a An-60 Ti rotor. Sedimentation was monitored by both absorbance (at 257 nm and 5 min interval) and interference optics with 30 s interval. 350 µL of each sample was loaded into a double sector filled epon centerpiece with sapphire windows. Sedimentation was carried out at 40,000 rpm for 3 h at 20°C . The raw scans were then processed using DCDT+ 2.2.1 software to obtain g(s*) distribution. Theoretical distribution (sum of individual peptide distribution) was obtained using OriginLab v. 7.0 software.

N-acetyl capped peptides for AUC were prepared using the protocol described above. Three different samples were prepared from bis(h_5)-K-K_4 alone, bis(h_9)-K-K_4 alone, and a 1:1 molar ratio mixture of the two peptides, each with a final peptide concentration of 1 mM dissolved in DDI water and pH adjusted to 7 using a dilute solution of NaOH.

2.2.8. Circular Dichroism

Circular Dichroism (CD) Spectroscopy was used to analyze the secondary structures formed by the individual peptides and the peptide mixture formed by the above process. All Spectra were collected in a Jasco J-815 CD spectrophotometer using a circular quartz cuvette. The pathlength of the cuvette used for all scans was 0.1 mm unless noted. All spectra were scanned from 260 nm

to 190 nm at room temperature. The final spectrum is an average of five scans recorded at a scan rate of 50 nm/min with a 1 nm step interval and measured in mdeg. Raw scans were processed (subtracted from blank and smoothed) using Spectra Analysis (registered software from Jasco). Peptide concentrations were determined as previously described measuring the absorbance of stock solutions at 257.5 nm and diluting the samples to the final concentrations.

For experiments related to the study of secondary structure in increasing ethanol-water concentrations, 400 µM of the individual peptide (bis(h_9)-K-K_4 and bis(h_5)-K-K_4 were prepared in different ethanol concentrations (70 % - 10 %) using water as a diluent. Spectra were collected in a 1 mm quartz cuvette (Starna cells, Inc., Atascadero, CA). All other parameters were kept consistent to the method described above.

2.2.9. Attenuated Total Reflectance-Fourier Transform Infra-Red Spectroscopy (ATR-FTIR)

The IR spectra were generated using a lyophilized equimolar mixture of bis(h_9)-K-K_4 and bis(h_5)-K-K_4. A Nicolet 380 (Thermo Scientific, FL), ATR-FTIR fitted with a ZnSe crystal was used to collect the spectra of the sample. Spectra were collected at a resolution of 1 cm^{-1} and averaged 64 times. The collected spectra were plotted using SigmaPlot (ver.9.01, Systat Software, Inc., Chicago, IL)

2.2.10. Dynamic Light Scattering (DLS)

Bis(h_5:h_9)-K-K_4 samples were prepared using the protocol described in section 2.2.3. The concentration of the peptide sample used was 1 mM each. The rehydrated samples were allowed to stand at room temperature for 2 h before filtering through a 0.22 µ filter to remove any dust particles that might be present. 5 mL of the sample was filtered directly into a clean glass tube. The light scattering setup consisted of an argon ion laser operating at 488 nm (blue light). The vertically polarized incident beam was focused onto the sample using a lens while the scattered

light was collected using a second lens and imaged onto a 300 µm pinhole. All experiments were performed at room temperature. The scattered light was collected at four different angles; the data shown here is that for 30º. The diffracted light from the pinhole was collected using a photomultiplier tube. A commercial correlator was used to calculate the scattered-light intensity autocorrelation function. The Mean correlation time τ, was obtained by plotting the collected intensity trace using Dynals v2.0 (Photocor Instruments, Inc., College Park, MD), a commercially available software. Using τ, the diffusion coefficient was calculated using the equation $\tau = \frac{1}{2Dq^2}$, where τ is the correlation time and q is the wave vector:

$$q = \frac{4\pi n_{liquid}}{\lambda_o} \sin\left(\frac{\theta}{2}\right)$$

Where n_{liquid} is the refractive index of the solution (1.33); λ_0 wavelength of light (488 x 10^{-9} m); θ is the angle at which the detector was located with respect to the sample (30º).

The hydrodynamic radius was calculated using the Stokes-Einstein equation:

$$D = \frac{k_B T}{6\pi\eta R_H}$$

Where K_B is the Boltzmann's constant (1.38 x 10^{-23} J K^{-1}); T is temperature in Kelvin (300 K); η is viscosity (0.7978 x 10^{-3} Pa.s); R_H is the hydrodynamic radius in meters.

2.2.11. 5(6)-Carboxyfluorescein Encapsulation

Stock solutions of the individual peptides were prepared by dissolving the lyophilized peptides in water and their absorbance was recorded in a CARY 50 UV/Vis spectrophotometer (Varian Inc., Palo Alto, CA) using a 3 mm path length quartz cuvette (Starna Cells Inc., Atascadero, CA). The peptide concentration was determined using the molar extinction coefficient of phenylalanine at 257.5 nm (as described in section 2.2.3). Peptide stock solutions were 4.8 mM for bis(h_5)-K-K_4

and 4.7 mM for bis(h_9)-K-K_4. For all experiments the final working concentration of the peptide was 100 µM.

Stock solution of 5(6)-Carboxyfluorescein was prepared by weighing out 10mg of the dry powder and dissolved in 10 mL of water. The resulting solution was briefly vortexed followed by sonication for 15 min and was filtered through a 0.22 µm syringe driven filter unit (Millipore). This stock solution was wrapped in aluminum foil and stored at 4ºC until further use. All peptide samples were prepared in 1.5 mL Eppendorf tubes. Preparation of peptide samples in various ethanol concentrations proceeded with the addition of 5(6)-Carboxyfluorescein followed by the addition of peptide into a solution of 200 proof ethanol (Decon Laboratories Inc., King of Prussia, PA). This mixture was then diluted to a final volume of 200 µL by the dropwise (~100 µL per minute) addition of water. The final concentration of the peptide was always 100 µM and that of 5(6)-Carboxyfluorescein was kept to 132.5 µM These samples were allowed to sit at room temperature for 2 h before spinning them through a 30,000 Da molecular weight cut-off (MWCO) filter unit (Millipore) at 14,000 g for 10 min in a benchtop centrifuge. At the end of the spin, the retentate in the removable-filter unit was inverted and placed in a fresh tube and spun at 2000 g for 5 min. The filtrate and retentate were then dried in a speed-vac for 3 h. The dried samples were brought up in a solution of 50 % ethanol-water to a final volume of 200 µL. The samples were immediately sealed with parafilm and vortexed. The resulting samples were allowed to sit for 2 h at room temperature before their fluorescence intensities were collected in a CARY Eclipse fluorescence spectrophotometer (Varian Inc., Palo Alto, CA). Fluorescence intensities were collected after transferring the rehydrated samples into a 3 mm pathlength quartz cuvette (Starna Cells, Inc., Atascadero, CA) and sealing the top of the cuvette with parafilm. Fluorescence intensities were collected with the following parameters: For 5(6)-

Carboxyfluorescein detection: excitation wavelength: 493 nm; emission scan: 500-650 nm; Scan rate: 50 nm/min; PMT detector voltage: 480 v. For peptide detection: excitation wavelength: 259 nm; emission scan: 265-400 nm; scan rate: 50 nm/min; PMT detector voltage: 800 v.

For studies involving the encapsulation of increasing amounts of 5(6)-Carboxyfluorescein, peptide samples were prepared with slight modification to the method previously described in Section 2.2.3. Two sets of samples were prepared until the drying step of the protocol described in section 2.2.3 (Fig. 2.4). For the first set of samples, the dried peptide samples containing bis(h_5)-K-K_4 and bis(h_9)-K-K_4 in an equimolar ratio were rehydrated with increasing amounts of 5(6)-Carboxyfluorescein dissolved in 100 % ethanol (20 µL). After allowing these samples to sit at RT for 1 h, they were diluted with drop wise addition of water until the final ethanol concentration was 10 %. These samples were allowed to stand at RT for 2 h before centrifuging them through a 30,000 Da (MWCO) filter (Millipore) at 14,000 g for 10 min. The second set, where the peptide vesicles are allowed to be formed before the addition of 5(6)-Carboxyfluorescein were initially rehydrated with 200 proof ethanol (10 µL) and diluted to 10 % ethanol by the dropwise addition of water (180 µL). 5(6)-Carboxyfluorescein dissolved in 100 % ethanol (10 µL) was added to this sample just before spinning them as described above. The MWCO filters

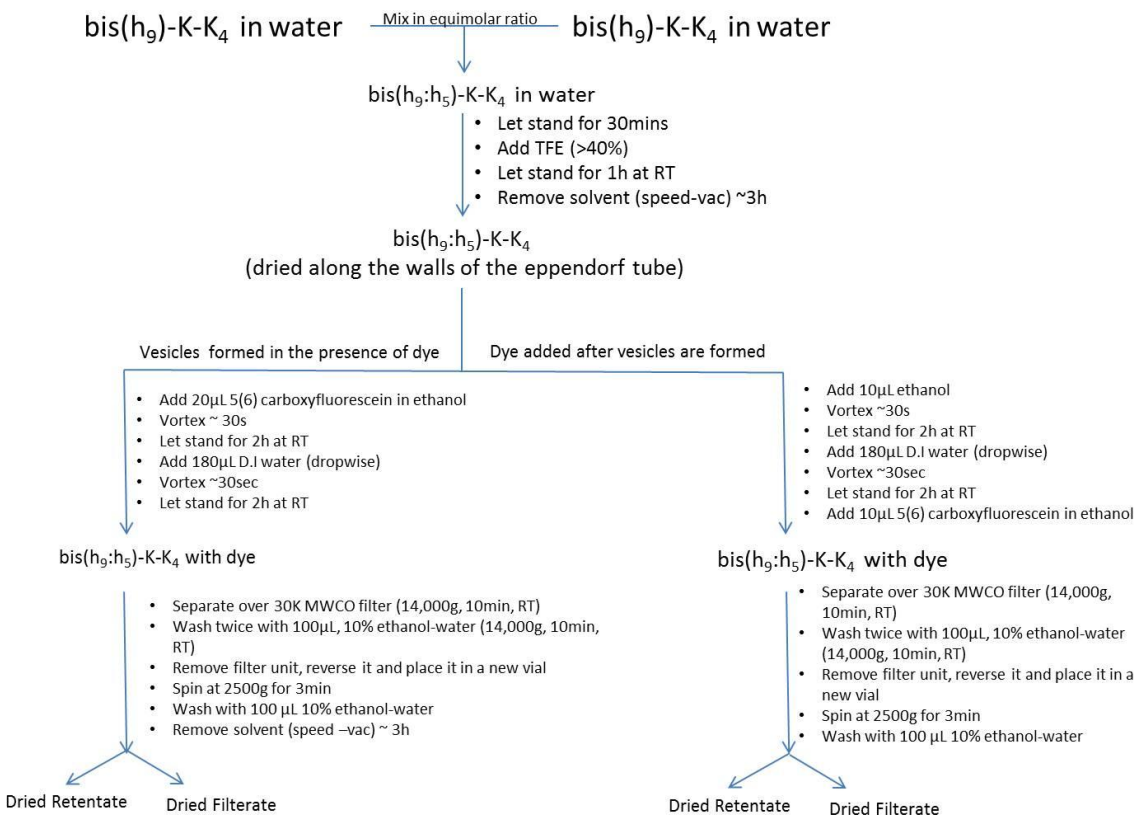

Figure 2.4. Protocol for sample preparation in studies involving 5(6)-Carboxyfluorescein encapsulation.

were initially prewetted with 10 % ethanol-water (50 µL) and spun at 14,000g for 5 min. After the peptide samples were spun down for the first time, they were washed three times with 10 % ethanol-water (80 µL each time) at 14,000 g for 5 min. This step was necessary to minimize sample retention in the filter dead space. Controls with 5(6)-Carboxyfluorescein without any peptide were prepared in parallel. The retentate and filtrate were dried under vacuum and brought up in a solution of 100 % trifluoroethanol (TFE). These samples were immediately sealed with parafilm, vortexed and allowed to sit at room temperature for 2 h before their fluorescence intensities were collected as described above.

5(6)-Carboxyfluorescein was prepared by drying increasing (25 μL-200 μL) amounts of stock solutions of 5(6)-Carboxyfluorescein under vacuum. The dried samples were dissolved in either 20 μL or 10 μL of ethanol. These samples were sealed with parafilm, vortexed and allowed to sit at RT for 1h before adding them to the appropriate peptide samples.

2.3. Results and Discussion

While all previously reported peptides involved in vesicle formation are linear, the peptides described herein are unique in that they are branched and mimic bilayer-forming phosphoglycerides in architecture. These peptides are relatively short, extremely stable, and easy to modify chemically. These sequences evolved from earlier studies on several adhesive peptides[33,34]. Previously, we identified several peptide constructs that produced nano-fibrils, which displayed mechanical adhesive properties due to entanglement[33]. The hydrophobic core sequence used in the adhesives occurs in nature as an internal fragment of the human dihydropyridine sensitive L-type calcium channel segment, CaIVS3 (DPWNVFDFLIVIGSIIDVILSE). The underlined segment is a portion of a transmembrane helix that contributes to the central water-filled pore of this channel[35,36]. Lyophilization of the CaIVS3 peptide resulted in insoluble clumps resistant to mechanical disruption. This property suggested that strong cohesive forces were driving this association. In this report, the adhesive sequences were redesigned to be amphiphilic with a single cationic oligopeptide at the C-terminus containing a branch-point for the attachment of two hydrophobic adhesive sequences FLIVIGSII and FLIVI in a parallel array (Fig. 2.5). The incorporated oligo peptides, termed bis(h_9)-K-K_4 and bis(h_5)-K-K_4, are unique, having previously proven to be strong β-structure formers in water, assembling into large β-sheet assemblies as judged by analytical ultracentrifugation studies[34].

2.3.1. Design and synthesis of bilayer-forming and control peptides

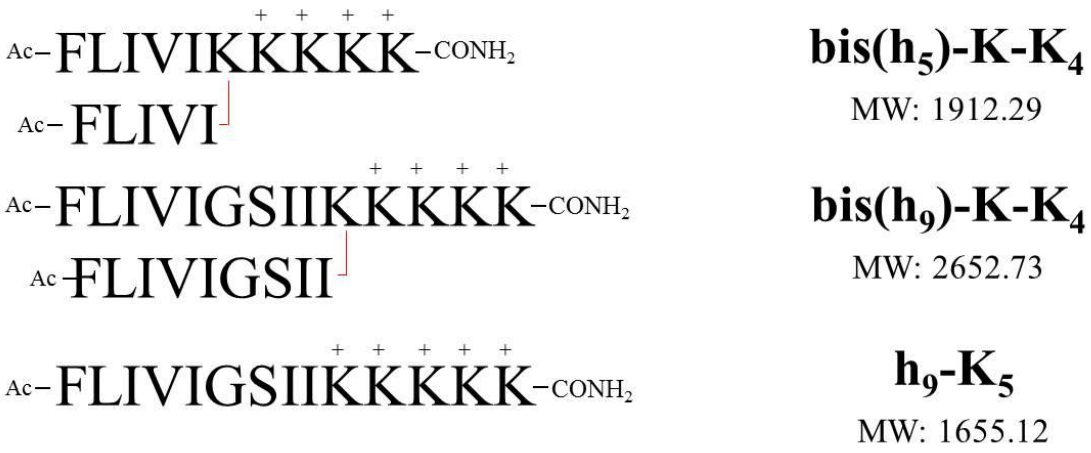

Figure 2.5. Branched bilayer-forming sequences.

The peptide assemblies are an equimolar mixture of the acetylated bis(h_9)-K-K_4 and bis(h_5)-K-K_4 sequences unless otherwise stated. The linear h_9-K_5 control sequence does not associate to give any type of structure.

The amphiphilic peptides employ an oligo-lysine (K=5) segment with the α- and ε-amino groups of the N-terminal lysyl-residue acting as the branch point for the addition of a pair of nine- (FLIVIGSII) or five- (FLIVI) residue hydrophobic sequences. The Fmoc-based chemical synthesis utilizes four lysine residues with ε-amine *t*-Boc protecting groups while the branching lysyl group employs Fmoc groups at both α- and ε-amine groups. The *t*-Boc at the ε-amine group allows for linear extension of the peptide while preventing any side reactions at the side-chain amino groups. The release of the two Fmoc protecting groups on the branching lysine allows for the simultaneous addition of identical amino acids to the bifurcated chain, thereby permitting the synthesis of the bis-N-terminal hydrophobic tails: FLIVIGSII (h_9) or FLIVI (h_5). Several variants of the peptides were prepared, which include the N-terminal phenylalanines unblocked or blocked by either acetylation or the covalent attachment of a fluorescent dye. The data presented here were obtained using N-termini acetylated peptides unless otherwise noted.

The stepwise addition of amino acids to both the α- and ε-amine of a lysine was previously described by Iwamoto *et al.* (1994)[37].

Based on the molecular architecture, we hypothesized that above certain concentrations, analogous to the critical micellar concentration (CMC) observed for phospholipids, the peptides would undergo supramolecular self-assembly. Most likely, the hydrophobic segments of these peptides initially drive the formation of ordered bilayer delimited, spherical water-filled structures with the positively charged lysines facing the aqueous phase, and the hydrophobic residues interacting in the center of the assembly. In addition to the weaker hydrophobic interactions that stabilize lipid bilayers, these assemblies could form hydrogen-bonding networks between adjacent β-sheets (see CD data) to maintain the peptide assemblies at much lower concentrations (low micromolar) where most phospholipid assemblies normally dissociate.

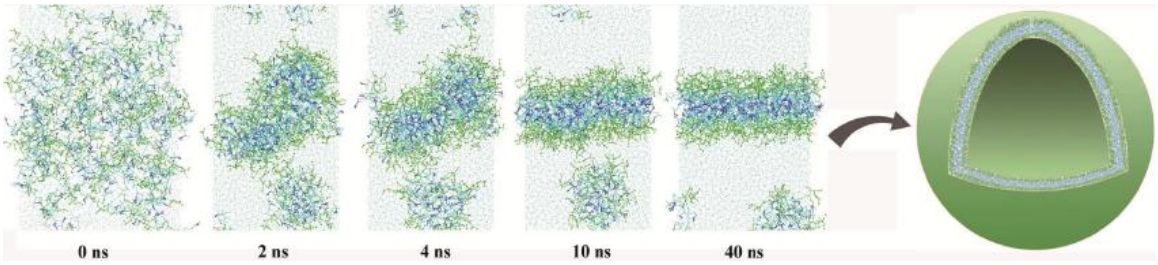

Figure 2.6. 2-dimensional coarse-grained simulation of bis(h_5)-K-K_4 bilayer self-assembly.

All lysine residues are plotted in green ball-and-stick representations, the aromatic sidechains of phenylalanine residues in blue sticks, and all other residues in cyan. The snapshots were taken at 0 ns, 2 ns, 4 ns, 10 ns and 40 ns, respectively. A hypothetical peptide vesicle model, based on available data is shown to the right.

Molecular dynamic simulations support the parallel between these peptides and phospholipids. Fig. 2.6 summarizes a coarse-grained simulation of the self-assembly process for the shorter peptide- bis(h_5)-K-K_4, which experimentally, leads to stable β-sheet assemblies in solution as measured by circular dichroism. Starting from a random distribution of the coarse

grained modeled peptides in water at time zero, the peptides rapidly begin to segregate and by 40 ns have formed a discernable bilayer structure. Interestingly, equilibrium simulations suggest that these branched peptides have similar lateral dimensions compared to phospholipids in the bilayers. The effect of temperature on the stability of the peptide bilayers appears to be similar to that of lipid-based ones.

2.3.2. Preparation and characterization of peptide assemblies

In water, these peptides initially form small spherical assemblies with diameters of 50-150 nm (Fig. 2.7A-D), a size on the order of adenovirus capsid particles (40-80 nm in diameter)[38].

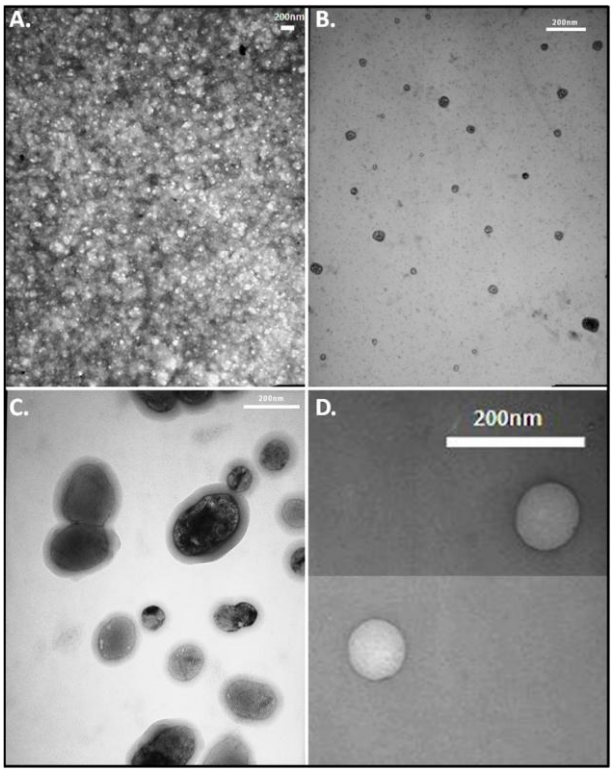

Figure 2.7. Transmission Electron Micrograph (TEM) of peptide assemblies bis(h_9:h_5)-K-K_4 (200 nm scale bar)

These peptides self-assemble into bilayer assemblies. TEM images of (A) a concentrated and (B, C and D) diluted samples of the peptide mixture, stained with 5 % Phosphotungstic Acid and Osmium tetroxide (OsO_4) vapors, respectively.

The peptide bilayer assemblies can be prepared from the bis(h_9)-K-K_4 and bis(h_5)-K-K_4 peptides by themselves or in combination. Mixing of the longer and shorter peptide chains is analogous to the preparation of lipid bicelles[39]. We generally used an equimolar mixture of the two peptides (N-termini blocked) to reduce potential strain due to high curvature. This ratio yields more homogeneous preparations based on sedimentation rates and a sharper distribution recorded using analytical ultracentrifugation velocity sedimentation protocols (see sedimentation velocity experiments). We observed that these preparations also resulted in better samples for collecting Transmission Electron Microscope (TEM) images.

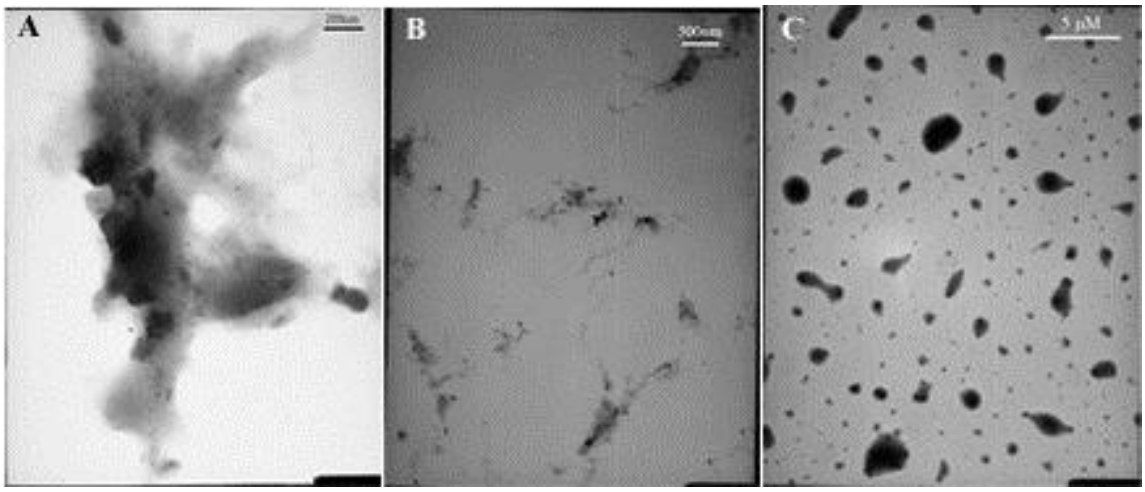

Figure 2.8. Transmission Electron Micrograph (TEM) of control peptides
(A) h_9 linear peptide, (B) bis(h_7)-K-K_4 and (C) bis(h_{5Y})-K-K_4. These peptides do not form nano sized spherical assemblies. Diluted samples stained with OsO_4 vapors.

Preparation of the peptide bilayer assemblies begins with the mixing of the two peptides, bis(h_9)-K-K_4 and bis(h_5)-K-K_4, individually dissolved in 40 % 2,2,2,-Trifluoroethanol (TFE). Under these conditions the peptides adopt a helical conformation, thereby forcing the peptides into a monomeric state, thus ensuring proper mixing. Once combined, the solution was briefly vortexed and allowed to stand for two hours before removing the solvent under vacuum. The dried samples were redissolved in water added dropwise. The rehydrated samples were vortexed

briefly, adjusted to pH 7 and allowed to stand at least two hours before using. Peptide concentrations were determined using the molar extinction coefficient (ε) of two Phe residues per sequence, at 257.5 nm (195 cm^{-1} M^{-1}). This equimolar ratio of the peptide mixture will henceforth be referred to as bis(h_9:h_5)-K-K4.

In Fig. 2.7, TEM images are shown for a 1.6 mM, (panel A) and diluted 25μM (panels B-D) of bis(h_9:h_5)-K-K_4 preparations. The TEM images revealed that the peptide mixtures adopt a spherical morphology with a fairly uniform size distribution between 50-150 nm. This size distribution range is in agreement with dynamic light scattering (DLS) data (see DLS data), using identically prepared samples. The DLS data yielded an average hydrodynamic radius value with a diameter of 160 nm. The concentrated sample (Fig. 2.7A) appears as a densely packed layer that resembles fish roe. In Fig 2.7C, under dilute conditions, individual liposome-like structures are visible with some appearing to be fusing and others, which are larger and more oblong, as though they have completed the fusing process. This property of fusion is commonly associated with lipid bilayers. Other sequences failed to show any spherical assemblies indicating that branching as well as the sequence plays an important role in the assembly of these vesicles. TEM images (Fig. 2.8) of (A) linear peptide which is similar to bis(h_9)-K-K_4 but lacks a branching point at the ε-amino group of the Lysine side chain. (B) a slightly modified shorter branched peptide, bis(h_7)-K-K_4 with the hydrophobic sequences VFFLIVI at the N-termini and (C) bis(h_{5Y})-K-K_5 where the phenylalanine residues have been replaced with tyrosine .

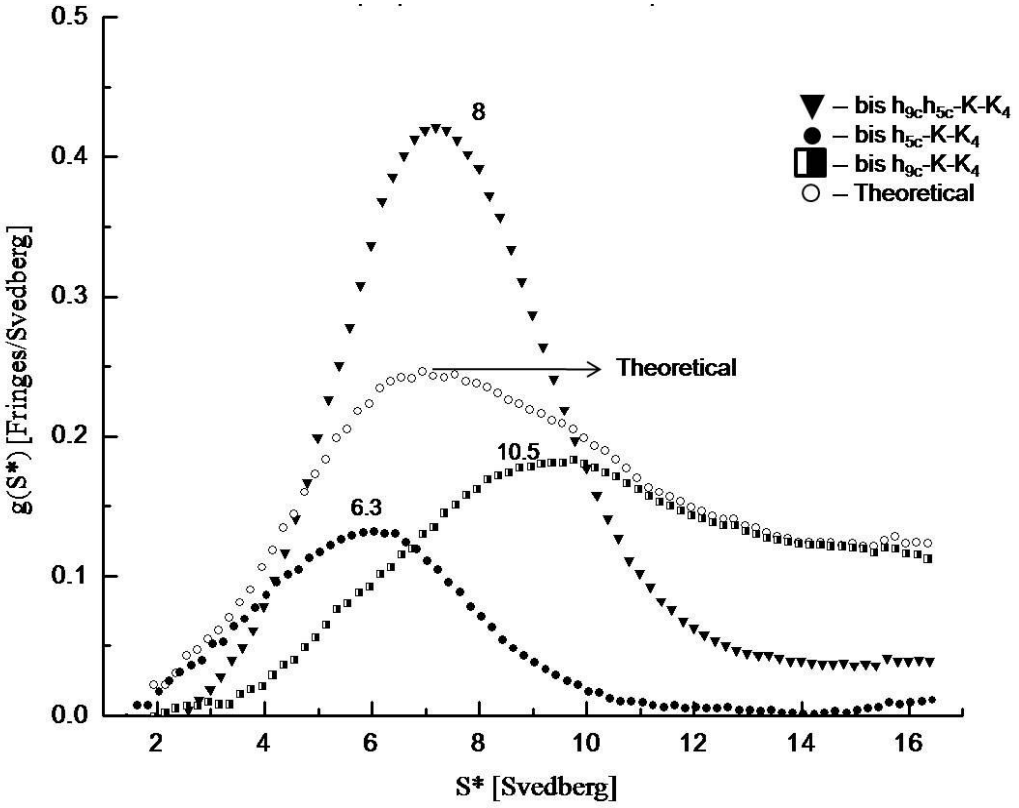

Figure 2.9. Sedimentation velocity analysis of peptides using analytical ultracentrifugation. Individual peptides, bis(h_5)-K-K_4 and bis(h_9)-K-K_4 show an apparent sedimentation coefficient of 6.3 S (solid circles) and 10.5 S (half-filled squares) respectively while the peptide mixture, bis(h_9:h_5)-K-K_4 (solid traingles) is centered around 8s. A theoretical (open circles) distribution refers to a hypothetical distribution which is a sum of peaks of the individual peptide distribution.

In the analytical ultracentrifuge experiments looking at the supramolecular assembly of individual bis(h_5)-K-K_4 and bis(h_9)-K-K_4, the two peptides yielded structures with different sedimentation rates (Fig. 2.9). The smaller peptide assembly sedimented at roughly 60 % that of the larger peptide's structure, indicating a substantial difference in size. This result suggests that ultimately structures with different sizes can be generated based on the chain length of the hydrophobic segments.

The S values are unusually low for a particle whose mean diameter is ~100 nm. Using SEDFIT ("a software for the analysis of analytical ultracentrifugation and other hydrodynamic data, written at the National Institutes of Health and distributed without charge for research use", https://sedfitsedphat.nibib.nih.gov), it was calculated that an s value of 8 corresponds to a spherical particle of roughly 10 nm in size (without hydration) while a spherical particle with a diameter of 100 nm, would have an s value in the hundreds. As a control experiment 2 mM POPC:POPS liposome samples of 1 μm and 100 nm mean diameter were tested and showed a sedimentation rate of close to 250 S and 200 S respectively.

In a separate bilayer assembly experiment employing mixed peptide sequences with free N-termini (no acetyl capping), larger structures were detected with confocal microscopy when the solutions stood for 2 or more days (Fig 2.10A, 2.10B), visualized by the addition of 5(6)-Carboxyfluorescein. On day three, the fused peptide bilayer assemblies formed a thin membrane-bounded enclosure that trapped micron sized peptide aggregates (Fig. 2.10B). The aggregated material likely comes from bridgehead peptides internalized during the many rounds of fusion. Capping the N-termini, to remove the positive charge, appears to hinder the fusion process, as we failed to observe larger, micron-sized structures. For this reason, we chose to use N-termini acetyl capped peptides, in order to work with assemblies that remain in the nanometer size range.

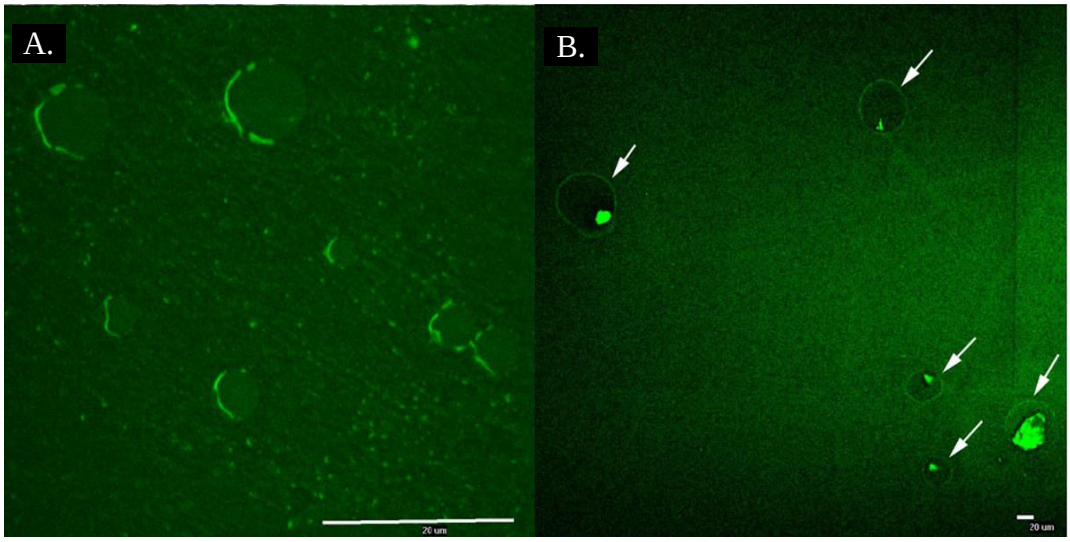

Figure 2.10. Confocal Images of peptide assemblies

bis(h_9:h_5)-K-K_4 assemblies prepared in a solution of 5(6)-Carboxyfluorescein. The samples were imaged 48 h (A) and 72 h (B) after preparation.

The CD spectra support the β-sheet conformation in the assembled branched-peptides structures (Fig. 2.11A, solid line), with a bisignate profile characteristic of a β-sheet secondary structure with a minimum at 218 nm and maximum at 198 nm. However, when dissolved in 40 % TFE, the peptides adopt helical-like conformations with the characteristic α-helix minima at 208 nm, 222 nm, and a maximum at 190 nm (Fig. 2.11A, dotted line). The linear sequence (h_9-K_5), lacking the branching point, appears to have a random structure (Fig. 2.11A, dashed line). It failed to show any type of assembly in either analytical ultracentrifugation studies or TEM images (Fig 2.8A). These data support the requirement for branched sequences for assembly and are able to undergo a transition from helix (monomer) to beta structure (assemblies) depending on solvent conditions.

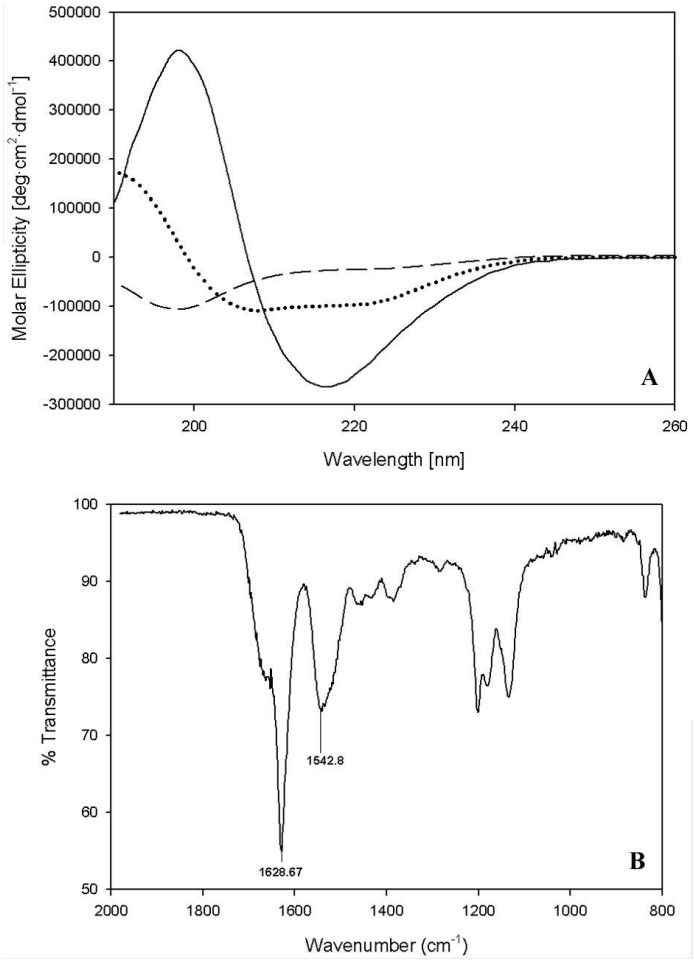

Figure 2.11. Circular dichroism (CD) and Infra-red (FTIR) spectroscopy to determine secondary structure of peptides.

(A). CD spectroscopy shows that the branched bis(h_9:h_5)-K-K_4 peptide mixture adopts a β-sheet secondary structure (solid line) at pH 7 in 5 mM $NaHCO_3$, a helical structure (dotted line) in 40 % TFE and remains unstructured (dashed line) when lacking the lysine branch point.. (B). FTIR spectroscopy of a lyophilized sample shows the characteristic 1629 cm^{-1} maximum corresponding to β-sheet secondary structure.

The peptide assemblies were very stable, withstanding the action of SDS, urea and trypsin, as determined by the absence of change in the CD spectra before and after treatment. Once assembled, the bis(h_9:h_5)-K-K_4 peptides can be switched from a pure aqueous solution to one

containing 40 % TFE thereby yielding a CD spectrum with the hallmark α-helical minima and maximum, indicating that a reversible inter-conversion between β-sheet and α-helical is possible.

ATR-FTIR was used to further confirm the peptide secondary structure in the assembled state. The spectra of a dry peptide mixture sample (Figure 2.11B) revealed a single amide-I stretch at 1629 cm^{-1}. Normally, antiparallel β-sheets possess principal β-sheet amide I stretching vibration at a maximum of 1630-1640 cm^{-1} [40,41] with a secondary absorption band at a frequency 50-70 cm^{-1} higher. The absence of the secondary absorption in Figure 4b is more consistent with the branched peptides adopting a parallel β-sheet orientation. This result is consistent with those observed from the self-assembly simulations (Figure 2.6).

Dynamic light scattering data of a concentrated sample of the peptide vesicles yielded an average hydrodynamic radius of 80 nm (Fig. 2.12). The hydrodynamic radius of the sample was obtained by performing curve fitting and analyzing the distribution, using Dynal (performed by Dr. Louis R. Nemzer) yielded a mean auto correlation time of 1.85 ms for the major distribution (Fig. 2.12A-C). This autocorrelation time was used to calculate the hydrodynamic radius from the Stokes-Einstein equation *(see material and methods section 2.2.10 for details)*.

$$\tau = \frac{6\pi\eta R_H.\lambda_o}{2kT[4\pi n_{liquid} \cdot \sin\left(\frac{\theta}{2}\right)]^2}$$

Where, **τ**: Correlation time; **η**: Viscocity (0.7978 x 10^{-3} P.s); $\mathbf{R_H}$: hydrodynamic radius (m); λ_0 = wavelength (cm^{-1}); **k**: Boltzman constant (1.38 x 10^{-23}J K^{-1}); **T**: Temperature (300°K); $\mathbf{n_{liquid}}$ is the refractive index of the solution (1.33); θ = the angle at which the detector was located with respect to the sample (30^o).

$$0.001852 = \frac{6 \times 3.14 \times 0.7978 \times 10^{-3}(Pa.S) \times R_H(488 \times 10^{-9})^2 cm^2}{2 \times 1.38 \times 10^{-23}(JK^{-1}) \times 300K[4 \times 3.14 \times 1.33 \times \sin(15)]^2}$$

$$R_H = 80nm$$

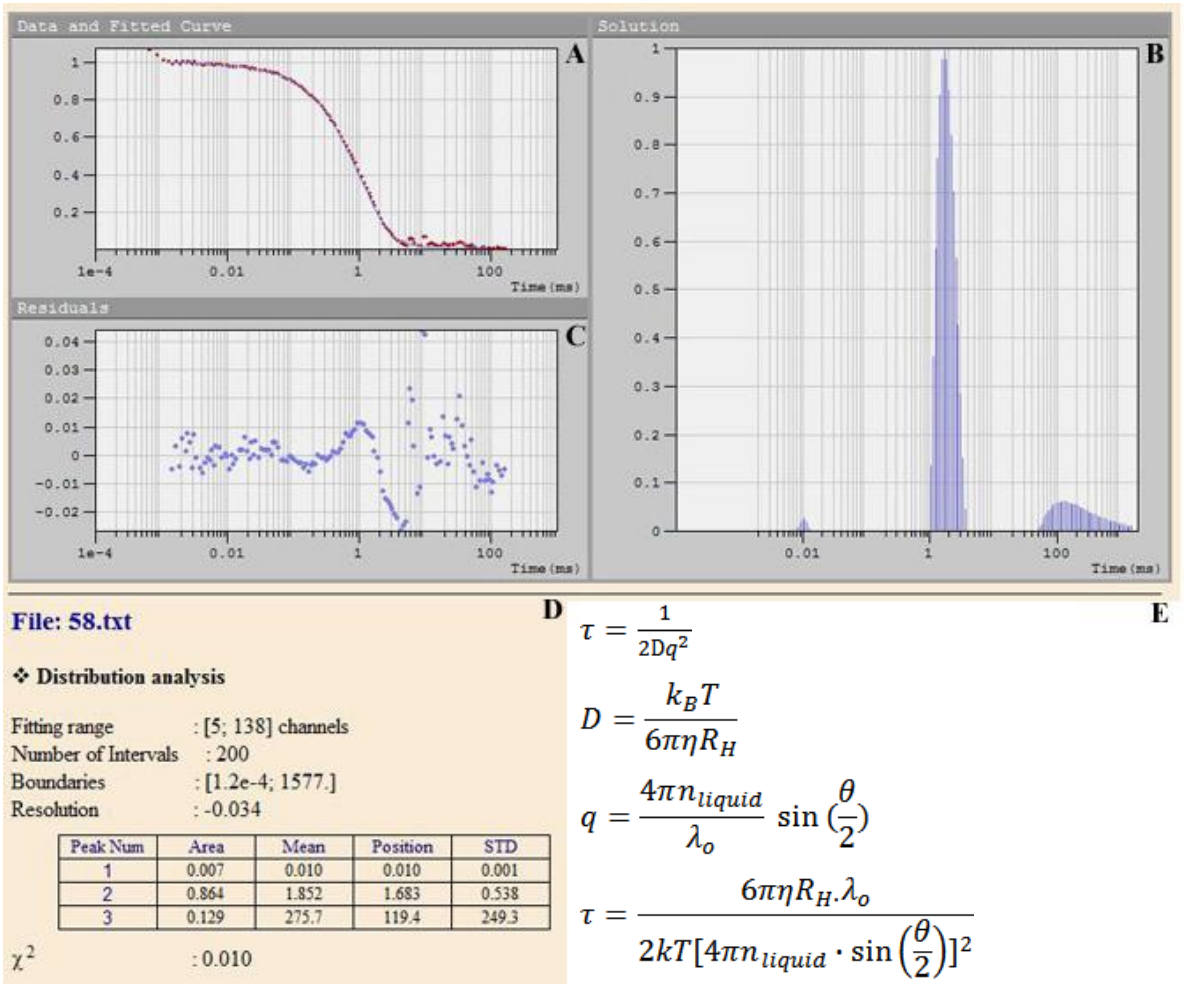

Figure 2.12. Dynamic Light Scattering.

(A). logarithmic plot of time vs. correlation function. (B). Distribution analysis of the data showing two major distributions centered around 1.68ms and 119.4 ms. (C). Residuals of the curve fitting of the data in panel (A). (D). Table of the results of the distribution analysis. (E). Equations used in calculating hydrodynamic radius.

2.3.3. Encapsulation studies with 5(6)-Carboxyfluorescein

In order to improve the encapsulation efficiency, we prepared the peptide assemblies in an organic solvent, ethanol, while simultaneously encapsulating the dye 5(6)-Carboxyfluorescein. The peptides and the dye were initially dissolved in 100 % ethanol and eventually diluted with water to achieve various solvent concentrations (70 %-10 %). After encapsulation, the samples were separated over a 30,000 MWCO filter and dried under vacuum. The dried samples were

brought up in 50 % ethanol concentrations and their fluorescence intensities recorded. The encapsulation efficiency initially showed an increase up to 10 % ethanol concentration but soon began to decrease with higher ethanol concentrations (Fig. 2.13A). A comparative study of the CD spectra of the individual peptides shows that peptides initially start off in a beta conformation and slowly change to a more helical conformation as the concentration of ethanol increases (Fig. 2.13 B and D).

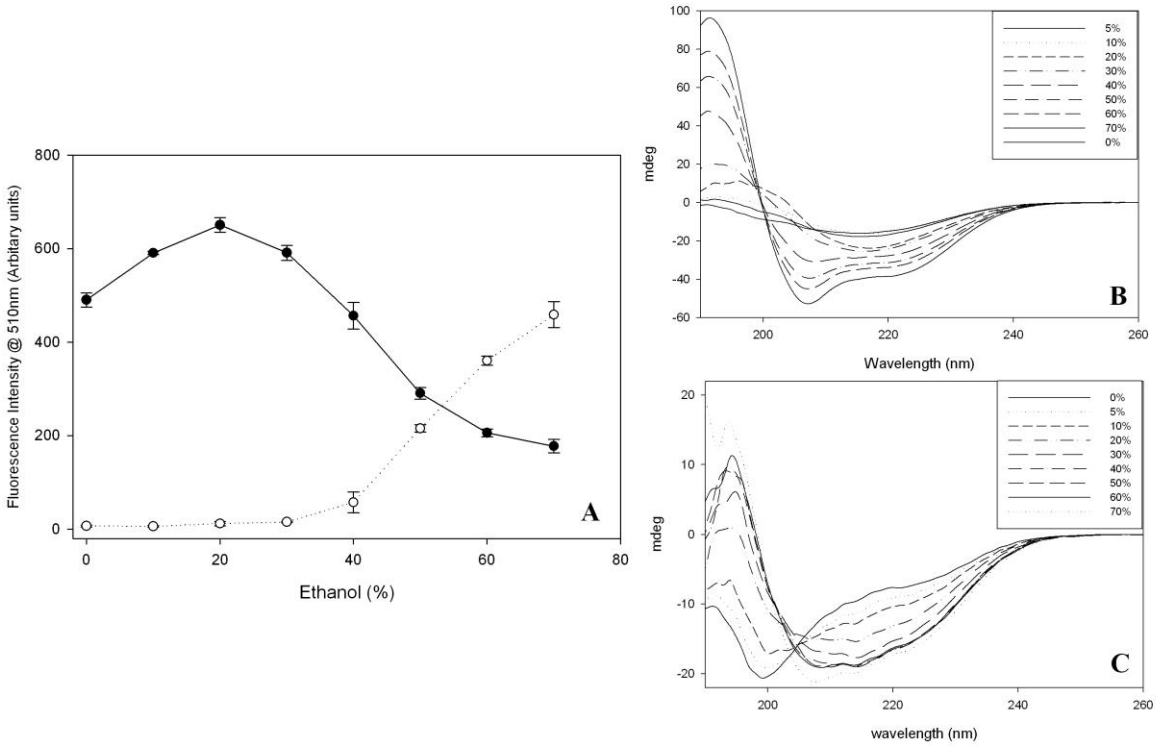

Figure 2.13. Encapsulation efficiency in increasing ethanol concentration.

(A) 5(6)-Carboxyfluorescein loaded peptide vesicles were prepared in different ethanol concentrations and separated over 30 kDa MWCO filters. Fluorescence intensities of the filtrate (open circles) and retentate (solid circles) were collected after separation and show that encapsulation efficiency decreases with increasing ethanol concentration. No curve fitting was done. Lines connect the midpoints of each data point. (B and C) CD spectra of the individual peptides obtained in different ethanol concentrations (corresponds to the ethanol concentrations used in A.

The helical conformation is an indicator of the monomeric state of the peptide. The amount of dye in each sample is kept the same. With increasing ethanol concentrations the peptides begin to adopt a helical conformation which leads to their dissociation and hence they are unable to retain the dye. The initial increase in encapsulation efficiency (from 0-10 % ethanol) is the result of increased solubility of the dye in ethanol over water. Three contributing factors to increased encapsulation are (1). increased solubility of the dye in ethanol, relative to water (2). higher initial concentration of the dye and (3). the shift from a purely hydrophobic environment, where the peptides are more dispersed and monomeric, to a more hydrophilic environment as the sample becomes diluted, thus giving the peptides a better chance of coming together and trapping the dye molecules.

To differentiate dye encapsulation from dye binding, 5(6)-Carboxyfluorescein was added at two different stages of vesicle formation. The first one involved preparing the vesicles in the presence of the dye and in the second, the dye was added after the vesicles were formed. The rationale involves saturating the binding sites on the outside of the vesicle with increasing dye concentration. The binding should increase until at a certain dye concentration no more dye will bind to the surface. On the other hand, if the dye is encapsulated (inside the vesicle), it will continue to show an increase in dye intensity until the dye reaches its solubility limit. At high dye concentrations, (a) fluorescence self-quenching, (b) fluorescence intensity changes due to dye-peptide interaction, (c) dye-solubility and (d) filter-membrane saturation are important factors that need to be addressed. To avoid self-quenching at high concentrations, the dried samples (after separation) were dissolved in large volumes of the solvent. TFE was chosen as a solvent for two primary reasons. (1) At concentrations above 40 % TFE the peptides adopt a completely helical secondary structure (see CD data Fig. 2.11) and exist as monomers. Hence in

100 % TFE, intact vesicles are absent. This is important because any dye still trapped inside the vesicles may exhibit self-quenching due to a locally high concentration of the dye. (2) In TFE there is no intensity change due to peptide-dye interaction (data shown or not shown). Stock solutions of the dye were filtered through 0.22 μm filters to remove any insoluble dye particles. Pre-wetting of the filter with organic solvent and multiple washes were performed during the separation step to avoid filter saturation and dead volume effects.

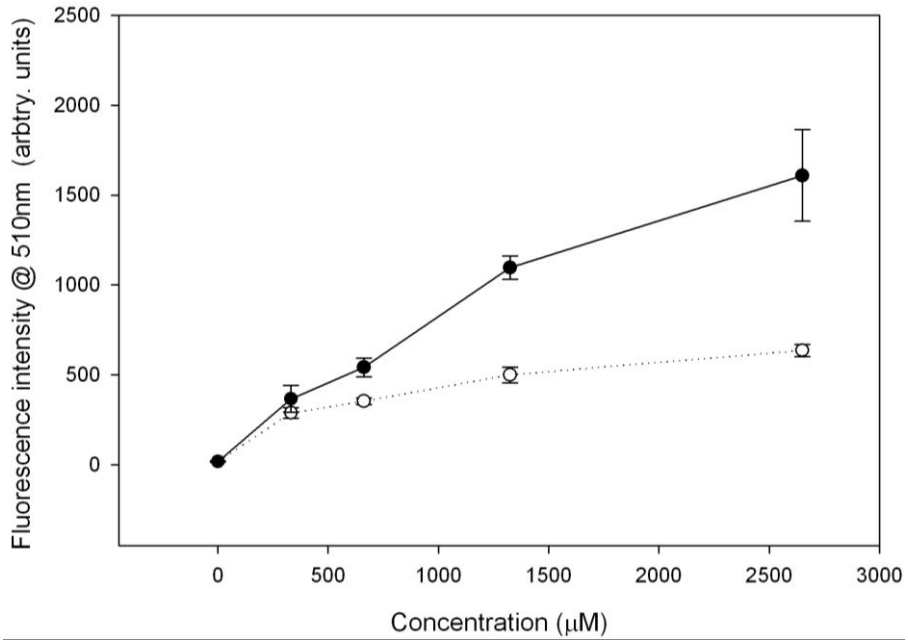

Figure 2.14. Encapsulation of increasing amounts of 5(6)-Carboxyfluorescein.
Peptide assemblies prepared with the dye present during vesicle formation **(**solid circles**)** or added after the vesicles are formed (open circles). Each data point represents an average of 3 separate experiments performed on different days. Data points are connect with straight lines through their midpoints. Trend is not a curve-fit.

Fig. 2.14 shows the results of increasing concentrations of the dye, 5(6)-Carboxyfluorescein, encapsulated into and bound to peptide vesicles that were prepared by the two different methods described above. The results indicate that more dye is incorporated (encapsulation + binding) when the vesicles form in the presence of the dye (Fig. 2.14, solid

circles) as compared to the dye added to preformed vesicles (Fig. 2.14, open circles). The concentration of the peptide in the two samples remained constant indicating that fluorescence intensity changes of the dye were due to dye binding or encapsulated and not due to peptide-dye interaction.

2.3.4. Peptide sequence modifications

Peptides with slight modifications to the original sequence were synthesized and their secondary structure studied using circular dichroism. The modifications included (1) replacing the C-terminal poly lysine chain with arginines or polyehtyleneglycol [these peptides were synthesized by Xiao Yao] (2) modifying the N-terminal sequence by either randomizing the sequence or making minor modifications to the original sequence. While we had difficulty obtaining the final product for some sequences (Table. 2.1), others yielded no spherical assemblies when viewed under TEM.

Table 2-1. Peptides Synthesized

Sequence	**Seq.ID**	**MW**	**Solubility**	**2° Structure**	
$(FLIVI)_2$-K-KKKK	bis(h_5)-K-K_4	1828.279	Soluble	Beta	
$(VFFLIVI)_2$-K-KKKK	bis(h_7)-K-K_4	2320.553	Soluble	Beta	
$(FLIVIGSII)_2$-K-KKKK	bis(h_9)-K-K_4	2568.723	Soluble	Beta	
FLIVIGSII-KKKKK	h_9-K_5	1655.123	Soluble	Unstructured	
Ac-$(IIVGSLIFI)_2$-K-K_4	bis(h_{9cs})-K-K_4	2652.743	Soluble	Beta	
Ac-$(FLIVI)_2$-K-KKKK	bis(h_{5c})-K-K_4	1912.3	Soluble	Beta	
Ac-$(FLIVIGSII)_2$-K-KKKK	bis(h_{9c})-K-K_4	2652.743	Soluble	Beta	
Ac-$(FLIVI)_2$-K-PEG	bis(h_{5c})-K-PEG	1604.9	Insoluble	---	**Synthesized by Xiao Yao**
Ac-$(FLIVIGSII)_2$-K-PEG	bis(h_{9c})-K-PEG	2363.3	Insoluble	---	
Ac-(FLIVI)-K-RRRRR	bis(h_{9c})-K-R_4	2764.75	Insoluble	---	
Ac-$(YLIVI)_2$-K-K_4	bis(h_{5cY})-K-K_4	1944.28	Soluble	Beta	

2.4. Conclusions

To the best of our knowledge, no other branching amphiphilic peptides have been successfully designed, simulated, synthesized and tested that behave similarly to phospholipids. By combining an oligolysine tail with two strong β-forming hydrophobic sequences we have identified such an ensemble. The linear version of the peptides failed to show any lipid- or detergent-like behavior. One might have expected the linear sequence to form micelles, however this was not the case. Clearly, the bis- arrangement of the hydrophobic sequences is essential for assembly.

Direct pictorial evidence (cryo-EM) visualizing the bilayer would have helped strengthen our hypothesis but currently we lack the resources to obtain such images. Taken together, the peptide architecture, the final assembly state, and results from the encapsulation studies, it is hard for me to imagine these vesicles forming anything other than a bilayer delineated vesicle. Based on the peptide architecture we expected the hydrophobic tails to adopt an anti-parallel beta conformation where the hydrophobic tails of the individual peptides interact so as to exclude water. FTIR data shows that the peptides adopt a parallel beta conformation. Together with the MD simulations, it is evident that the secondary structure could well be a mixture of hydrophobic chain entanglement and inter-molecular hydrogen bonding between adjacent tails. This helps explain the extremely strong cohesive nature of the assemblies and their resistance to treatments with SDS, Urea and trypsin.

An important question addressed at the latter part of this chapter is, do the self-assembled peptides form micelles, vesicles or a mixture of the two? While TEM images give a clue, the dye encapsulation assay proves beyond doubt that there is encapsulation of water solvated dye molecules in addition to binding (to the surface) indicating an interior space within the vesicles.

No specific experiments were carried out to address the question of mixtures of micelles and vesicles but TEM and AUC results indicate a slightly broad size distribution part of which could be a result of a mixture of final assemblies. Further studies related to encapsulation efficiency, leakage studies and stability would help in understanding how best to prepare these vesicles. Finally, while the encapsulation assay described here deals exclusively with a negatively charged dye (which is capable of binding to the positively charged lysine tails), a comparative encapsulation study involving a positively charged dye (Rhodamine B) was carried out (see Appendix A, Fig. A.3) and yielded a relatively low encapsulation efficiency. This encapsulation was done using the protocol described in section 2.2.1. and did not involve ethanol. One reason for this may involve the positive charges on the dye interfering with vesicular assembly. Neutral, uncharged dyes have problems with solubility in water and hence were not tried.

The branched peptides mimic the ability of phospholipids to form bilayer structures, trap solvent within the interior space, and under certain conditions, fuse to increase in size. This enclosed space was successfully used to trap small fluorescent molecules. We expect that since they are similar in size to viral particles, large molecules such as hydrophilic drugs, peptides, proteins and large plasmids could be encapsulated and taken up by cells.

Peptide nanoparticles, and more importantly peptide nanovesicles, are potential drug delivery systems that can be designed to achieve greater stability and specificity when compared to traditional delivery protocols. The peptides described here are relatively short, stable and easy to prepare. The ability of both short and longer peptides to associate, hints at possibilities of controlling the overall size of the assembly, which will be a useful property when delivering compounds of different sizes. Whereas lipid-based vesicles require additional steps, such as

extrusion through polycarbonate filters with defined pore sizes or sonication to achieve a homogeneous distribution, the peptide assemblies described here do not require such treatments.

2.5. References

[1] Allen, T. M., and Cullis, P. R. (2004). Drug delivery systems: Entering the mainstream. *Science (New York, N.Y.), 303*(5665), 1818-1822.

[2] Torchilin, V. P., Levchenko, T. S., Rammohan, R., Volodina, N., Papahadjopoulos-Sternberg, B., and D'Souza, G. G. (2003). Cell transfection in vitro and in vivo with nontoxic TAT peptide-liposome-DNA complexes. *Proceedings of the National Academy of Sciences of the United States of America, 100*(4), 1972-1977.

[3] Tanaka, T., Legat, A., Adam, E., Steuve, J., Gatot, J. S., Vandenbranden, M., et al. (2008). DiC14-amidine cationic liposomes stimulate myeloid dendritic cells through toll-like receptor 4. *European Journal of Immunology, 38*(5), 1351-1357.

[4] Ouali, M., Ruysschaert, J. M., Lonez, C., and Vandenbranden, M. (2007). Cationic lipids involved in gene transfer mobilize intracellular calcium. *Molecular Membrane Biology, 24*(3), 225-232.

[5] Koynova, R., Tarahovsky, Y. S., Wang, L., and MacDonald, R. C. (2007). Lipoplex formulation of superior efficacy exhibits high surface activity and fusogenicity, and readily releases DNA. *Biochimica Et Biophysica Acta, 1768*(2), 375-386.

[6] Kumar, V. V., Pichon, C., Refregiers, M., Guerin, B., Midoux, P., and Chaudhuri, A. (2003). Single histidine residue in head-group region is sufficient to impart remarkable gene transfection properties to cationic lipids: Evidence for histidine-mediated membrane fusion at acidic pH. *Gene Therapy, 10*(15), 1206-1215.

[7] Thomas, C. E., Schiedner, G., Kochanek, S., Castro, M. G., and Lowenstein, P. R. (2001). Preexisting antiadenoviral immunity is not a barrier to efficient and stable transduction of the brain, mediated by novel high-capacity adenovirus vectors. *Human Gene Therapy, 12*(7), 839-846.

[8] Kafri, T., Morgan, D., Krahl, T., Sarvetnick, N., Sherman, L., and Verma, I. (1998). Cellular immune response to adenoviral vector infected cells does not require de novo viral gene expression: Implications for gene therapy. *Proceedings of the National Academy of Sciences, 95*(19), 11377-11382.

[9] Thomas, C. E., Schiedner, G., Kochanek, S., Castro, M. G., and Lowenstein, P. R. (2000). Peripheral infection with adenovirus causes unexpected long-term brain inflammation in animals injected intracranially with first-generation, but not with high-capacity, adenovirus vectors: Toward realistic long-term neurological gene therapy for chronic diseases. *Proceedings of the National Academy of Sciences of the United States of America, 97*(13), 7482-7487.

[10] Assessment of adenoviral vector safety and toxicity: Report of the national institutes of health recombinant DNA advisory committee.(2002). *Human Gene Therapy, 13*(1), 3-13.

[11] Baum, C., Düllmann, J., Li, Z., Fehse, B., Meyer, J., Williams, D. A., von Kalle, C. (2003). Side effects of retroviral gene transfer into hematopoietic stem cells. *Blood, 101*(6), 2099-2113.

[12] Discher, D. E., and Ahmed, F. (2006). Polymersomes. *Annual Review of Biomedical Engineering, 8*, 323-341.

[13] Meng, F., Zhong, Z., and Feijen, J. (2009). Stimuli-responsive polymersomes for programmed drug delivery. *Biomacromolecules, 10*(2), 197-209.

[14] Aggeli, A., Bell, M., Boden, N., Keen, J. N., Knowles, P. F., McLeish, T. C., Pitkeathly, M., Radford, S. E. (1997). Responsive gels formed by the spontaneous self-assembly of peptides into polymeric beta-sheet tapes. *Nature, 386*(6622), 259-262.

[15] Nowak, A. P., Breedveld, V., Pakstis, L., Ozbas, B., Pine, D. J., Pochan, D., Deming, T. J. (2002). Rapidly recovering hydrogel scaffolds from self-assembling diblock copolypeptide amphiphiles. *Nature, 417*(6887), 424-428.

[16] Narmoneva, D. A., Oni, O., Sieminski, A. L., Zhang, S., Gertler, J. P., Kamm, R. D., Lee, R. T. (2005). Self-assembling short oligopeptides and the promotion of angiogenesis. *Biomaterials, 26*(23), 4837-4846.

[17] Vauthey, S., Santoso, S., Gong, H., Watson, N., and Zhang, S. (2002). Molecular self-assembly of surfactant-like peptides to form nanotubes and nanovesicles. *Proceedings of the National Academy of Sciences of the United States of America, 99*(8), 5355-5360.

[18] Santoso, S., Hwang, W., Hartman, H., and Zhang, S. (2002). Self-assembly of surfactant-like peptides with variable glycine tails to form nanotubes and nanovesicles. *Nano Letters, 2*(7), 687-691.

[19] Hartgerink, J. D., Beniash, E., and Stupp, S. I. (2002). Peptide-amphiphile nanofibers: A versatile scaffold for the preparation of self-assembling materials. *Proceedings of the National Academy of Sciences of the United States of America, 99*(8), 5133-5138.

[20] Aggeli, A., Nyrkova, I. A., Bell, M., Harding, R., Carrick, L., McLeish, T. C., Semenov, A. N., Boden, N. (2001). Hierarchical self-assembly of chiral rod-like molecules as a model for peptide beta -sheet tapes, ribbons, fibrils, and fibers. *Proceedings of the National Academy of Sciences of the United States of America, 98*(21), 11857-11862.

[21] Rodriguez-Hernandez, J., and Lecommandoux, S. (2005). Reversible inside-out micellization of pH-responsive and water-soluble vesicles based on polypeptide diblock copolymers. *Journal of the American Chemical Society, 127*(7), 2026-2027.

[22] Holowka, E. P., Pochan, D. J., and Deming, T. J. (2005). Charged polypeptide vesicles with controllable diameter. *Journal of the American Chemical Society, 127*(35), 12423-12428.

[23] Bellomo, E. G., Wyrsta, M. D., Pakstis, L., Pochan, D. J., and Deming, T. J. (2004). Stimuli-responsive polypeptide vesicles by conformation-specific assembly. *Nature Materials, 3*(4), 244-248.

[24] Tanisaka, H., Kizaka-Kondoh, S., Makino, A., Tanaka, S., Hiraoka, M., and Kimura, S. (2008). Near-infrared fluorescent labeled peptosome for application to cancer imaging. *Bioconjugate Chemistry, 19*(1), 109-117.

[25] Lim Soo, P., and Eisenberg, A. (2004). Preparation of block copolymer vesicles in solution. *Journal of Polymer Science Part B: Polymer Physics, 42*(6), 923-938.

[26] Discher, D. E., and Eisenberg, A. (2002). Polymer vesicles. *Science, 297*(5583), 967-973.

[27] Krebs, M. R., Bromley, E. H., Rogers, S. S., and Donald, A. M. (2005). The mechanism of amyloid spherulite formation by bovine insulin. *Biophysical Journal, 88*(3), 2013-2021.

[28] Hoshi, M., Sato, M., Matsumoto, S., Noguchi, A., Yasutake, K., Yoshida, N., Sato, K. (2003). Spherical aggregates of beta-amyloid (amylospheroid) show high neurotoxicity and activate tau protein kinase I/glycogen synthase kinase-3beta. *Proceedings of the National Academy of Sciences of the United States of America, 100*(11), 6370-6375.

[29] Brooks, B. R., Bruccoleri, R. E., Olafson, B. D., States, D. J., Swaminathan, S., and Karplus, M. (1983). CHARMM: A program for macromolecular energy, minimization, and dynamics calculations. *Journal of Computational Chemistry, 4*(2), 187-217.

[30] Brooks, B. R., Brooks, C. L.,3rd, Mackerell, A. D.,Jr, Nilsson, L., Petrella, R. J., Roux, B., Y. Won, Y., Archontis, G., Bartels, C., Boresch, S., Caflisch, A., Caves, L., Cui, Q., Dinner, A. R., Feig, M., Fischer, S., Gao, J., Hodoscek, M., Im, W., Kuczera, K., Lazaridis, T., Ma, J., Ovchinnikov, V., Paci, E., Pastor, R. W., Post, C. B., Pu, J. Z., Schaefer, M., Tidor, B., Venable, R. M., Woodcock, H. L., Wu, X., Yang, W., York, D. M., and Karplus, M. (2009). CHARMM: The biomolecular simulation program. *Journal of Computational Chemistry, 30*(10), 1545-1614.

[31] Marrink, S. J., Risselada, H. J., Yefimov, S., Tieleman, D. P., and de Vries, A. H. (2007). The MARTINI force field: Coarse grained model for biomolecular simulations. *The Journal of Physical Chemistry.B, 111*(27), 7812-7824.

[32] Monticelli, L., Kandasamy, S. K., Periole, X., Larson, R. G., Tieleman, D. P., and Marrink, S.-J. (2008). The MARTINI Coarse-Grained Force Field: Extension to Proteins. *Journal of Chemical Theory and Computation, 4*(5), 819-834.

[33] Shen, X., Mo, X., Moore, R., Frazier, S. J., Iwamoto, T., Tomich, J. M., et al. (2006). Adhesion and structure properties of protein nanomaterials containing hydrophobic and charged amino acids. *Journal of Nanoscience and Nanotechnology, 6*(3), 837-844.

[34] Mo, X., Hiromasa, Y., Warner, M., Al-Rawi, A. N., Iwamoto, T., Rahman, T. S., Sun, X., Tomich, J. M. (2008). Design of 11-residue peptides with unusual biophysical properties: Induced secondary structure in the absence of water. *Biophysical Journal, 94*(5), 1807-1817.

[35] Grove, A., Tomich, J. M., and Montal, M. (1991). A molecular blueprint for the pore-forming structure of voltage-gated calcium channels. *Proceedings of the National Academy of Sciences of the United States of America, 88*(15), 6418-6422.

[36] Grove, A., Tomich, J. M., Iwamoto, T., and Montal, M. (1993). Design of a functional calcium channel protein: Inferences about an ion channel-forming motif derived from the primary structure of voltage-gated calcium channels. *Protein Science : A Publication of the Protein Society, 2*(11), 1918-1930.

[37] Iwamoto, T., Grove, A., Montal, M. O., Montal, M., and Tomich, J. M. (1994). Chemical synthesis and characterization of peptides and oligomeric proteins designed to form transmembrane ion channels. *International Journal of Peptide and Protein Research, 43*(6), 597-607.

[38] Klyushnichenko, V., Bernier, A., Kamen, A., and Harmsen, E. (2001). Improved high-performance liquid chromatographic method in the analysis of adenovirus particles. *Journal of Chromatography.B, Biomedical Sciences and Applications, 755*(1-2), 27-36.

[39] Sanders, C. R., and Prosser, R. S. (1998). Bicelles: A model membrane system for all seasons? *Structure (London, England : 1993), 6*(10), 1227-1234.

[40] Jackson, M., and Mantsch, H. H. (1995). The use and misuse of FTIR spectroscopy in the determination of protein structure. *Critical Reviews in Biochemistry and Molecular Biology, 30*(2), 95-120.

[41] Arrondo, J. L., and Goni, F. M. (1999). Structure and dynamics of membrane proteins as studied by infrared spectroscopy. *Progress in Biophysics and Molecular Biology, 72*(4), 367-405.

Chapter 3 - Bis(h_9:h_5)-K-K_4 vesicles as *in vitro* delivery vehicles

3.1. Introduction

Polymeric vesicles and other nanoparticles show great promise as drug-delivery and gene-delivery systems. Using such systems, various molecules like hydrophobic and hydrophilic drugs, fluorescent dye markers, proteins and nucleic acids have been delivered *in vitro* and *in vivo.* The ability to deliver various molecules, small and large, is an ongoing research but of all the different molecules that polymeric vesicles can deliver, DNA is the one that is most studied[1,2]. This is understandable considering the emergence of alternative (to viruses) packaging and delivery systems that has resulted in a renewed interest in gene therapy. A wide variety of cationic liposomes, surfactants and peptide amphiphiles are being investigated for their usefulness in delivering genetic material. From these studies it is now known that DNA most readily binds to cationic lipids and surfactants. It is interesting to note that while we expect a DNA molecule binding to the outside of a cationic vesicle would do so in an extended conformation, research has shown that it in fact undergoes compaction when bound[3]. This DNA compaction can be reversed when anionic amphiphiles are added to the mixture, leading to de compaction of the DNA, where it is more likely to integrate into the host genome[4]. While it is tempting to dismiss all DNA interactions with cationic vesicles as simple electrostatic association, there are many reports of single stranded DNA associating more strongly than double stranded DNA to such cationic surfactants[5,6]. Double stranded DNA has a much larger linear charge density than single stranded DNA. Moreover, reports of small changes to the head group of the amphiphile lead to dramatic increases in transfection efficiencies[7]. Thus, there appear to be more factors than simple electrostatic association. Despite the numerous studies on the

interaction of DNA and cationic (and other polymeric) surfactant vesicles, the exact mechanism of DNA uptake still remains unclear[8]. In general, delivering DNA (using a vehicle) into a cell's nucleus has to overcome ~~certain~~ obstacles that include (but are not limited to) the DNA being taken up by the cells, released into the cytoplasm, entering the nucleus and finally, stably integrating into the host genome followed by its expression. Currently, in cell culture, most commercially available transfection agents are lipid-based. Very few, if any, are polymer based and to the best of our knowledge, none are peptide-based. A peptide based transfection agent has several advantages over lipid-based systems. It is relatively easy to modify peptides to attach cell specific recognition ligands. It is easier to synthesize them chemically and are more stable than lipids. The peptide vesicles described here are potential drug-delivery and gene-delivery vehicles that can be tuned to meet the requirements of targeted delivery.

3.2. Materials and Methods

3.2.1. Peptide synthesis (covalently labeled dye)

N-Hydroxy Succinimide ester of the 5/6-carboxy-tetramethyl rhodamine was used to couple the dye to the ε-amino site of a lysine residue (C-terminal) of bis(h_5)-K-K_4 in the presence of DIEA. Before the addition of the dye, the *t*-boc protected ε-amino group was deprotected using TFA. This labeled lysine was used as the first amino acid in the synthesis of the peptide using standard solid phase chemistry. The peptides were synthesized as described in *section 2.2.2.*

3.2.2. Cell Culture

Human lens epithelial (HLE), human breast cancer (MCF-7), rabbit lens epithelial (N/N 1003A) and mouse neuroblastoma (N2a) cells were obtained from Dr. Dolores Takemoto's lab (Biochemistry Department, Kansas State University).

HLE cells were grown in Minimum Essential Medium (MEM) with 10 % fetal bovine serum (FBS). MCF-7 cells were grown in Dulbecco's Modified Eagle Medium (DMEM) with 10 % FBS, 0.5 % antibiotics (streptomycin, penicillin and gentamycin) and 0.1 % insulin. N/N 1003A cells were grown in DMEM with 10 % fetal bovine serum (FBS) and 3.7 g/L $NaHCO_3$. N2A cells were grown in Eagle's Minimum Essential Medium with 10 % FBS. All cells were grown under normoxic condition (5 % CO_2, 21 % O_2) in T25 cell culture flasks (MIDSCI™, St. Louis, MO). Depending on the experiment, cells were grown in 6 well or 12 well culture plates by either seeding cells directly in wells or onto coverslips placed in the wells.

3.2.3. Loading peptide vesicles

Peptide vesicles were prepared with slight modifications to the protocol described previously (*section 2.2.1.*). DNase/RNase free water and DNase free pipette tips (MIDSCI™, St.Louis, MO) were used to prepare the samples. 1-3 µL of 1 µg/µL pEGFP-N3 was diluted to 100-600 µL using DNase/Rnase free water. Plasmid solution was added dropwise into the dried peptide mixture in autoclaved 1.5 mL Eppendorf tubes. These plasmid loaded peptide vesicle samples in the tubes were gently tapped, inverted a few times (instead of vortexing) and allowed to sit for 30 min at room temperature before adding them to the cell culture. When required, before addition of samples to the cell culture, loaded peptide vesicle samples were filtered through a 0.22 µm Costar spin-X centrifuge tube filter (Corning Incorporated, Corning, NY). The samples were spun at

10,000 rpm for 6 min in a benchtop centrifuge to drive the samples through the filter. Loaded peptide samples were added directly into the cell culture wells using micropipettes.

For 5(6)-Carboxyfluorescein encapsulation, bis(h_9:h_5)-K-K_4 assemblies were prepared using the protocol described in section 2.1.1 to achieve a final concentration of 25 µM of each peptide in a 600 µL final volume. The dried samples were rehydrated with a 0.5 mM solution of the fluorescent dye 5(6)-Carboxyfluorescein (MW = 376.3 Da) dissolved in DNase/RNase-free water.

3.2.4. Fluorescence microscopy

All fluorescent images were taken in Dr. Dolores Takemoto's lab (Biochemistry Department, Kansas State University), using a Nikon Eclipse E600 fluorescent microscope fitted with an Optronics Magnafire, CCD camera and appropriate filters (Blue, green and red). Images were acquired using the software, MagnaFire 2.1C (Olympus America Inc., Center Valley, PA).

3.2.5. 5(6)-Carboxyfluorescein uptake

HLE cells were seeded onto coverslips placed in 6 well plates containing 2 mL of the medium. When cells reached roughly 80-90 % confluence, 600 µL of the DMEM was replaced with the peptide vesicle solution loaded with 5(6)-Carboxyfluorescein. The cells were then allowed to grow at 37°C under normoxic conditions. At 4 h and 12 h after incubation with dye-loaded vesicles, the cells were washed twice with phosphate buffered saline (PBS) and fixed using 3.7 % paraformaldehyde (PFA). The fixed cells were then mounted on a glass slide and pictures were taken using the fluorescence microscope. Control cells were incubated with only the free fluorescent dye and no peptide vesicles. For peptide-dye co-localization experiments, rhodamine-labeled bis(h_5)-K-K_4 peptides were prepared separately and mixed with unlabeled bis(h_5)-K-K_4 in a 1:1 ratio. This mixture was

again mixed with unlabeled bis(h_9)-K-K_4 in 1:1 ratio and prepared as described in section 3.2.3.

MCF-7 cells were seeded onto coverslips placed in 12 well culture plates containing 1 mL of the medium. When cells reached roughly 80-90 % confluence, 100 µL of the medium was replaced with loaded peptide samples (25 µM each and 100 µL final volume) in each well. After 10 -12 h the medium was removed and washed three times with PBS. Cells were then fixed with 3.7 % PFA for 10 min. The PFA was subsequently removed and the cells washed three times with PBS. Fixed cells were incubated for 1 h with nuclear staining dye, DAPI. Excess DAPI was removed and the cells washed again with PBS. The coverslips containing the fixed and stained cells were mounted on to a glass slide containing a drop of ProLong® liquid mountant with antifade (Invitrogen, Carlsbad, CA). The coverslips were sealed using Sally Hansen (#01 invisible) nail polish.

3.2.6. Cytotoxicity assay

Cell toxicity assays were carried out to assess peptide toxicity in MCF-7, N/N 1003A and N2A cells. Cells were grown to roughly 60 % confluence in 12 well plates with 1 mL of media in conditions as described in section 3.2.1. 100 µL of the media was replaced with a solution of peptide assemblies prepared in nuclease free water. Peptide concentrations used were 10, 25, 50, 75, 100 and 200 µM each. Controls included, one well left undisturbed and the other contained 100 µL of nuclease free water. After a 6 h incubation with loaded peptide vesicle samples all media was removed and replaced with 1 mL of fresh media in each well. After 24 h, all medium was removed and cells were washed three times with PBS. Next, cells were treated for 5 min with 100 µL TrypLE™ Express (GIBCO [Life Technologies], Grand Island, NY) to release the cells from the surface of the well. Medium (900 µL) was added to each well and the contents transferred into a 1.5 mL Eppendorf

tube. The cells were centrifuged at 5000 rpm for 5 min in a benchtop centrifuge. The supernatant was discarded and the pellet was resuspended in 1 mL PBS. To check for cell viability, 10 µL of the resuspended cells were mixed with 10 µL of 2X trypan blue solutions and allowed to sit for 2 min before counting them in a Cellometer® AutoT4 automated cell counter (Nexcelom Bioscience LLC, Lawrence, MA). Assays were repeated three times and data were plotted using Sigmaplot (ver.9.01, Systat Software, Inc., Chicago, IL)

3.2.7. pEGFP-N3 plasmid transfection

Transfection experiments were carried out by encapsulating a ~4.7kb plasmid DNA (Fig. 12) that encodes for an enhanced green fluorescent protein (EGFP) and delivered to MCF-7 cells and N/N 1003A cells. The plasmid pEGFP-N3 was obtained from Dr. Dolores Takemoto lab (purchased from Clontech, Mountain View, CA). Controls for transfection were carried out using a commercial transfection agent, Lipofectamine™ 2000 (Invitrogen, Carlsbad, CA) (Fig. 3.1). Plasmid concentrations used for encapsulation varied from 0.36 µg – 3.6 µg, while peptide concentration were 50 µM each of bis(h_9)-K-K_4 and bis(h_5)-K-K_4 mixed in an equimolar ratio.

N/N 1003A cells (and in a separate experiment, MCF-7 cells) were grown to roughly 50-60 % confluence on coverslips placed in 6 well culture plates. Plasmid loaded peptide vesicle samples were prepared as described in section (3.2.3.). Prior to adding the loaded samples to the cells, all medium was removed from the wells and 1.8 mL of Opti-MEM® 1 reduced serum medium (Invitrogen, Carlsbad, CA) was added. Next, 200 µL of loaded samples were added to cells and allowed to grown in normoxic conditions. 6 h after incubation with loaded vesicles, the medium was removed and replaced with 2 mL of fresh DMEM (containing 10 % FBS and lacking loaded peptide samples) in each well. 48 h after

initial incubation, all medium was removed and the cells washed three times with PBS and fixed with freshly prepared 3.7 % PFA for 10 min. At the end of 10 min, the PFA was removed and cells washed three more times with PBS. Fixed cells (on coverslips) were removed and mounted on slides which had a drop of ProLong® Gold liquid mountant. This mountant contains a mixture of antifade and the nuclear stain, DAPI. The coverslips were sealed with nail polish. Slides were wrapped in aluminum foil and stored at 4°C overnight. The slides were imaged the next day using a fluorescence microscope.

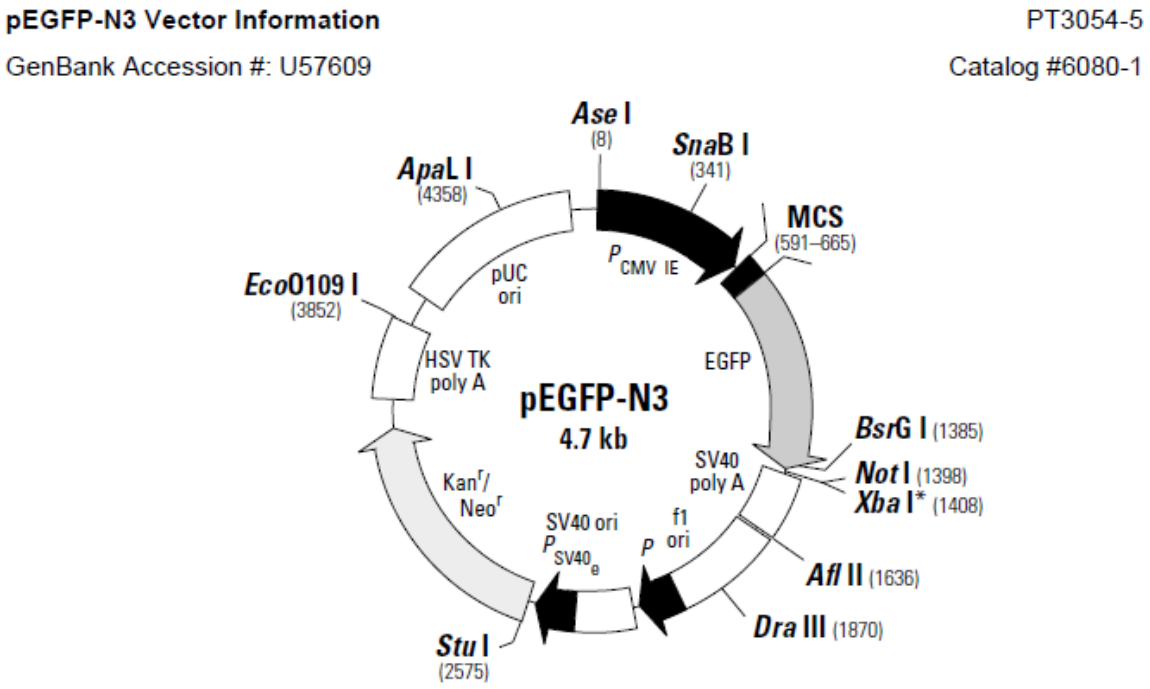

Figure 3.1. Restriction map and cloning sites of pEGFP-N3 (from bdbiosciences.com)

3.2.8. Plasmid digestion with nucleases and chemical method (Cu(II)-GSH)

Plasmid loaded peptide vesicles were prepared as described in section (3.2.3.). The nuclease, RQ-1 RNase-free Dnase-1 (Promega Corp., Madison, WI) treated samples were prepared according to the protocol supplied by the manufacturer. Briefly, to 100 µL of the loaded vesicle sample solution containing 1µg pEGFP-N3, 8 µL of the nuclease, followed by 10 µL of a 10x

reaction buffer (400 mM Tris-HCl (pH 8.0), 100 mM $MgSO_4$ and 10 mM $CaCl_2$, provided by manufacturer) was added. This sample was incubated for 30 min at 37°C. At the end of the reaction, 1 µL of the stop solution (20 mM EGTA (pH 8.0), provided by manufacturer) was added and the sample incubated for 10 min at 65°C, to inactivate the DNase.

Benzonase treated samples were prepared by mixing 0.5 µL of the enzyme (250 units/µL in 20 mM Tris, 0.2 mM $MgCl_2$ and 20 mM NaCl) with 200 µL of peptide sample containing 1µg pEGFP-N3. To this mixture, 10 µL of a 10x reaction buffer (supplied with RQ-1 RNase-free Dnase-1 kit, see above) was added and incubated at 37°C for 30 min. At the end of 30 min, 2 µL of stop solution (supplied with RQ-1 RNase-free Dnase-1 kit, see above) was added and the sample incubated at 65°C for 10 min. Concentration of the enzyme used was determined based on results obtained with treatment of the plasmid for different time intervals (see Appendix A, Fig A.1).

For chemical cleavage, stock solutions of glutathione (GSH) and copper sulphate ($CuSO_4$) were prepared at 1 M concentrations each and stored at 4°C until further use. All plasmid loaded vesicles were prepared with slight modification to the protocol described in section (3.2.3.). Instead of DNase/RNase free water, the dried peptides were rehydrated with 1µg pEGFP-N3 diluted in 50 mM sodium phosphate buffer with 50 mM NaCl and pH 8, to a final volume of 100 µL. The samples were treated with 400 µM each of GSH and $CuSO_4$ and incubated at 40°C for 90 min. 2 µL of the stop solution (20 mM EGTA (pH 8.0) from Promega RQ-1 RNase-free Dnase-1 kit) was added to stop the reaction. The concentrations of GSH and $CuSO_4$ used in the final experiment were determined after treating the plasmid with increasing concentrations of GSH and $CuSO_4$ (see Appendix A, Fig. A.2).

Gel experiments were carried out in Dr. Gerald Reeck's lab (Biochemistry Department, Kansas State University). All samples were run on a 0.5 % agarose gel containing 0.2 % ethidium bromide. 10 µL of each sample was mixed with loading buffer in a 1:5 ratio. 10 µL of this mixture was loaded into each well and the gel was allowed to run for 45 min (nuclease experiment) and 1 h (chemical cleavage experiment) at 100 V. At the end of the run, the gel was removed and placed on a UV scanner and images acquired using Kodak Digital Science 1D ver. 2.0. (Scientific Imaging Systems, New Haven, CT)

3.3. Results and Discussion

3.3.1. Peptide vesicles as delivery vehicles in vitro

The potential of these peptide assemblies to function *in vitro* as delivery vehicles was explored by preloading the assemblies with the fluorescent dye 5(6)-Carboxyfluorescein during the aqueous hydration/assembly step. This protocol is similar to that used to encapsulate compounds in lipid vesicles: the assemblies form around solutes dissolved in the aqueous systems. Non-encapsulated dye was removed by gel filtration over Sephadex G-10. Dye added to preformed vesicles did not adhere appreciably to the assemblies and was removed during the gel filtration step. The loading efficiency was checked with three different fluorescent compounds, 5(6)-Carboxyfluorescein, tryptophan and Rhodamine 6G (see Appendix A, Fig. A.3). The calculated trapping efficiency was approximately 5 to 8 % with the generation of 10^{10} to 10^{11} vesicles, using a 1.6 mM concentration of the bis(h_9:h_5)-K-K_4 peptides.

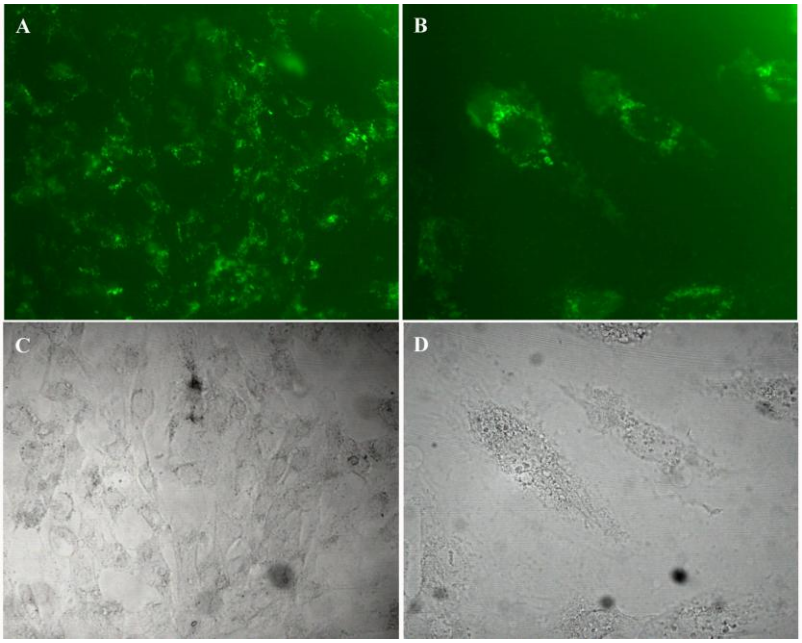

Figure 3.2. Cellular uptake of preloaded peptide assemblies by HLE cells.

Fluorescence microscope images of HLE cells grown on coverslips and incubated with peptide assemblies loaded with 5(6)-Carboxyfluorescein for 12 h. Images show that the dye is localized primarily at the peri-nuclear region. Cells were fixed with 3.7 % paraformaldehyde before imaging. (A) 20x magnification, (B) 40x magnification, (C and D) bright field images of A and B respectively.

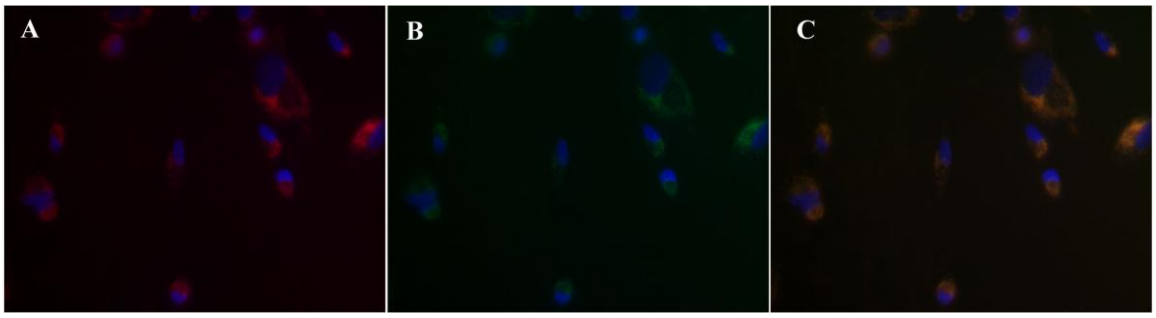

Figure 3.3. Peptide–dye co-localization in N/N 1003A cells.

(A-C) Bis(h_9:h_5)-K-K_4 assemblies with one of the peptides labeled (bis(h_5)-K-K_4 labeled with Carboxytetramethylrhodamine) and loaded with 5(6)-Carboxyfluorescein were delivered to N/N 1003A cells. Green and red filter settings were used for the detection of Rhodamine labeled peptide (A) and 5(6)-Carboxyfluorescein (B) respectively. (C) is a merge of a and b showing co-localization of dye and peptide assembly within the cell.

Vesicular uptake was followed in two different epithelial cell lines: HLE and N/N 1003A cells grown on cover slips (in six well cell culture plates). Both cell types showed uptake of soluble 5(6)-Carboxyfluorescein loaded bis(h_9:h_5)-K-K_4 peptide assemblies. Control cells, incubated with either free dye or dye mixed with the linear peptide (h_9-K_5) showed no incorporated fluorescence (image not shown). In Fig. 3.2, HLE cells show uptake of the dye after 12 h of incubation with peptide vesicles loaded with the dye and localize on the peri-nuclear region of the cell. In Fig. 3.3 a-c bis(h_9:h_5)-K-K_4 vesicles containing encapsulated 5(6)-Carboxyfluorescein were prepared with a portion of the (bis(h_5)-K-K_4) peptide covalently attached to the fluorescent dye Carboxytetramethylrhodamine (50 % label). These vesicles were then incubated with N/N 1003A cells. This experiment was designed to look for the co-localization of the trapped soluble dye with the peptide assemblies labeled with a different fluorescent dye (Rhodamine). The images shown are of the same cells visualized with different filter settings to check for co-localization of the two dyes. After a 10 h incubation period, encapsulated 5(6)-Carboxyfluorescein (Fig. 3.3.a) was visible when viewed with a green filter indicating that the cells had internalized the dye. In Fig. 14b the cells were imaged using a red filter also showing the cellular uptake of the covalently labeled peptide assemblies. Fig. 3.3.c shows the color merge of 3.3.a and 3.3.b, indicating co-localization of the soluble dye and the rhodamine-labeled peptide within the cell. Co-localization indicates that the intact loaded vesicles enter the cytoplasm rather than releasing their contents through a fusion-like mechanism at the plasma membrane. Due to the inert nature of the dyes, these experiments gave no indication that the dye was released from the vesicles within the cell. All we can claim with this line of investigation is that the soluble dye has been delivered. MCF-7 cells when incubated with free dye (Fig.

3.4..a) or when the dye was mixed with control peptides (Fig. 3.4. c-f) did not show appreciable uptake of the dye. The peptides used as controls were: Linear peptide (h9), sequence scrambled peptide (h_{9s}) and $K_2h_5K_2$.

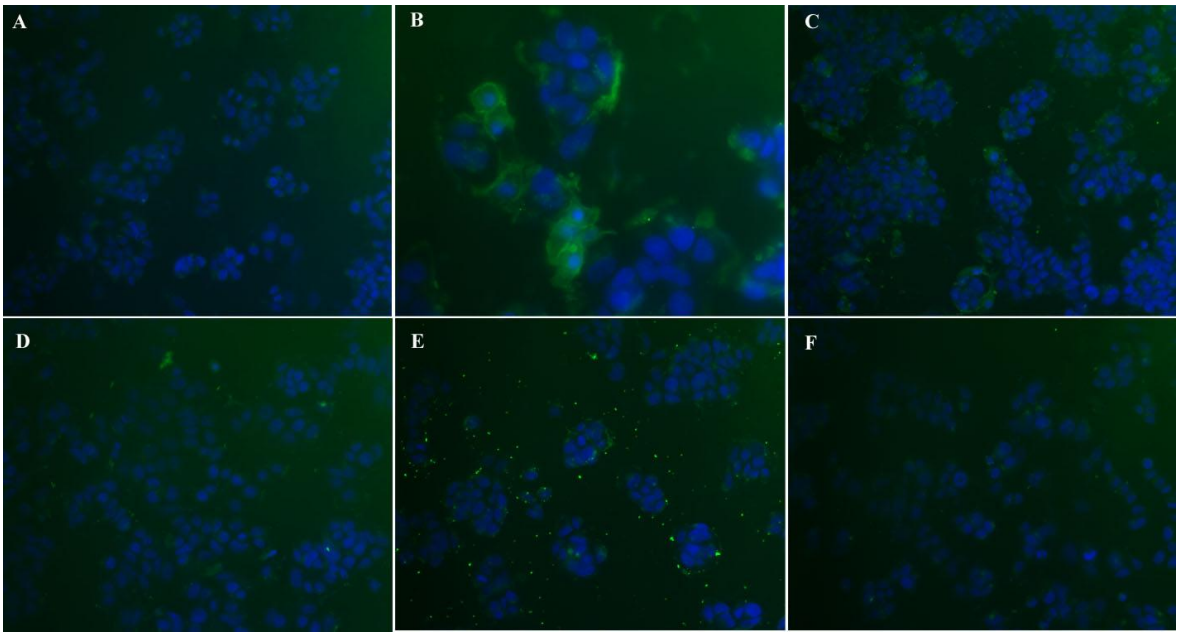

Figure 3.4. Comparing dye uptake in MCF-7 cells using various peptides.
MCF-7 cells incubated with (A) free 5(6)-Carboxyfluorescein, or mixed with peptides (B) bis(h_9)-K-K_4, (C) bis(h_5)-K-K_4, (D) scrambled, sequence of bis (h_{9cs})-K-K_4, (E) Linear peptide-h9 and (F) $K_2h_5K_2$. DAPI was used as nuclear stain.

Cellular uptake of lipid vesicles occurs via membrane fusion and the subsequent release of the vesicle contents directly into the cytoplasm. Cellular uptake of the peptide vesicles described here occurs non-specifically, most likely via endocytosis. However, the presence of multiple addressable functional groups could allow for the attachment of receptor targeting molecules, such as biotin, estradiol and TAT sequence thereby helping to target the vesicles to specific cell types. The peptide concentration used in these experiments was 50 µM. There was no apparent toxic effect on the cells at this concentration. Cell toxicity

assays carried out for the peptide assemblies in three different cell types showed no observable cell death at concentrations up to 50 μM (Fig. 3.5).

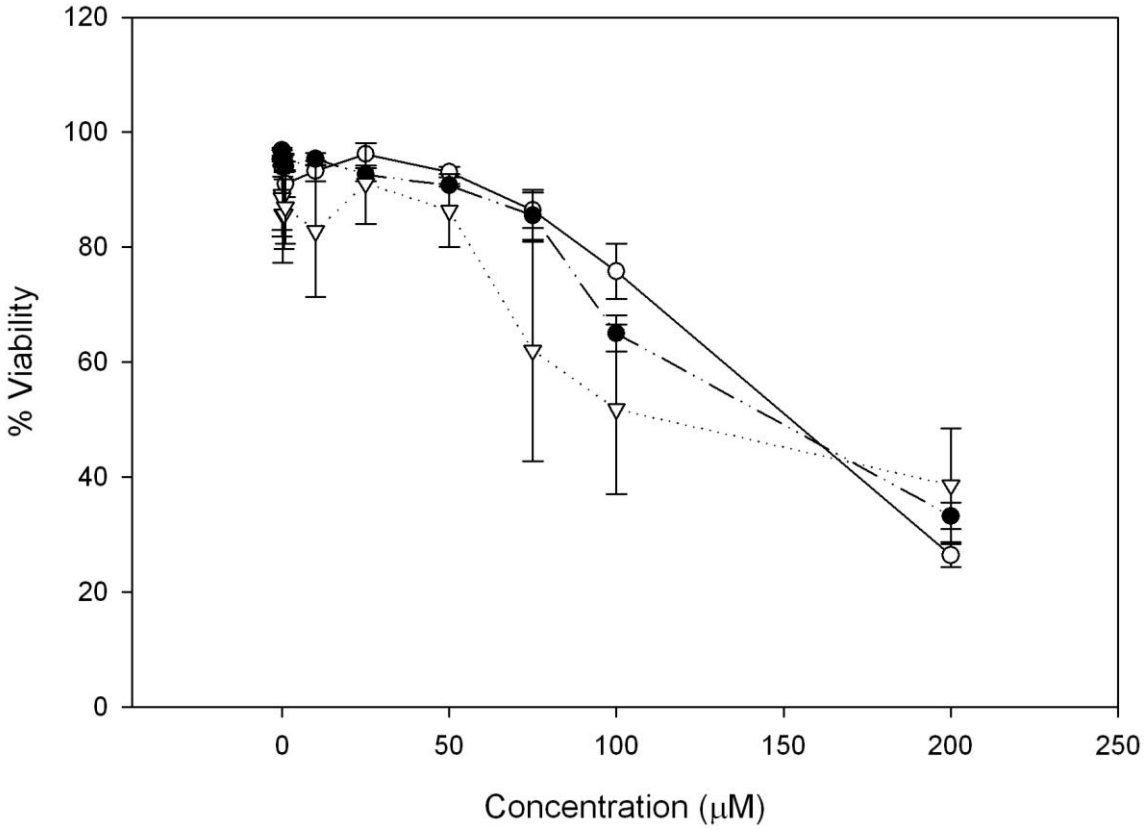

Figure 3.5. Cell Cytotoxicity assay.

Cell toxicity assays were performed for peptide assemblies in three different cell types, N2a (open circles), N/N 1003A (closed circles) and MCF-7(open triangles) cells. Each data point represents an average of 3 separate experiments performed on different days.Data points are connect with straightlines through their midpoints. Trend is not a curve-fit.

3.3.2. Delivery of plasmid DNA using peptide assemblies

To further investigate the ability of these peptide assemblies to deliver and release larger biologically relevant cargos, we encapsulated the ~4.7 kb DNA plasmid pEGFP-N3 that encodes the enhanced green fluorescent protein (EGFP) for transfection studies. The plasmid encapsulation was carried out using the protocols previously described. The encapsulated pEGFP-N3 was directly added to N/N 1003A rabbit lens epithelial cells (Fig.

3.6) or MCF-7 cells (Fig. 3.7) grown on coverslips. After 6 h incubation, fresh medium was added and the cells were allowed to grow for another 24 h. Cells were then fixed with 3.7 % PFA and stained with DAPI (nuclear stain) before imaging with a fluorescent microscope.

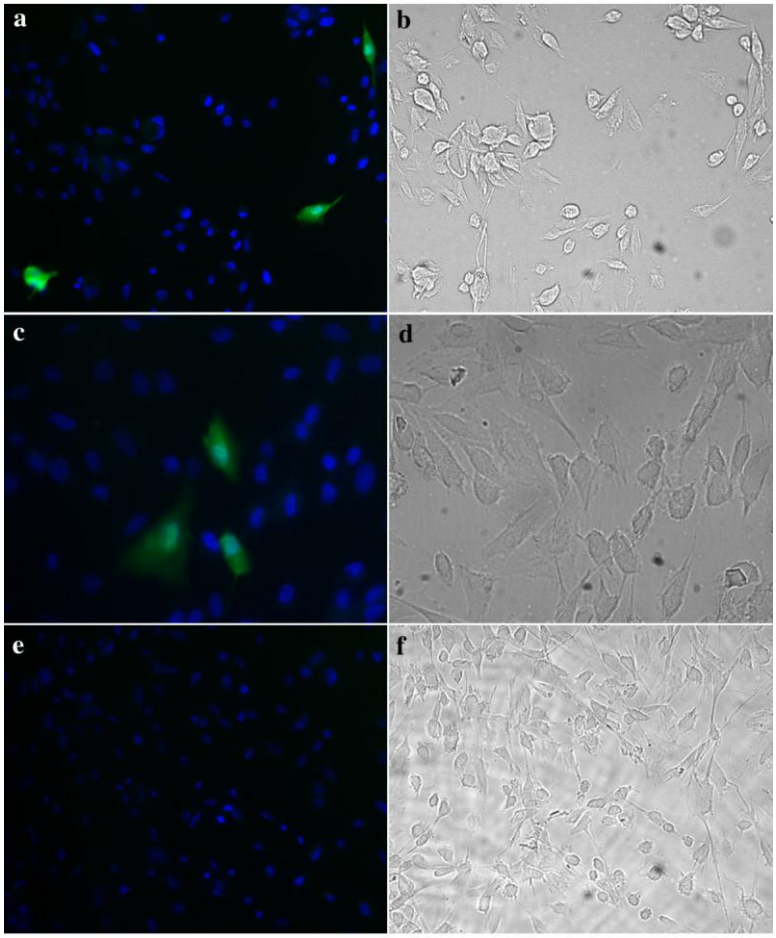

Figure 3.6. N/N 1003A cells transfected with pEGFP-N3 plasmid DNA encapsulated in peptide assemblies.

(a). Fluorescent microscopy images of N/N 1003A cells transfected with encapsulated plasmid, show EGFP expression. (c). Encapsulated plasmid, treated with DNase-1 prior to their addition to cells, showed EGFP expression. (e). Cells treated with naked pEGFP-N3 (unencapsulated), showed no EGFP expression. b, d and f are bright field images of a, c

and e respectively. DAPI was used as the nuclear stain. Cells were fixed with 3.7 % PFA and stained with nuclear dye DAPI.

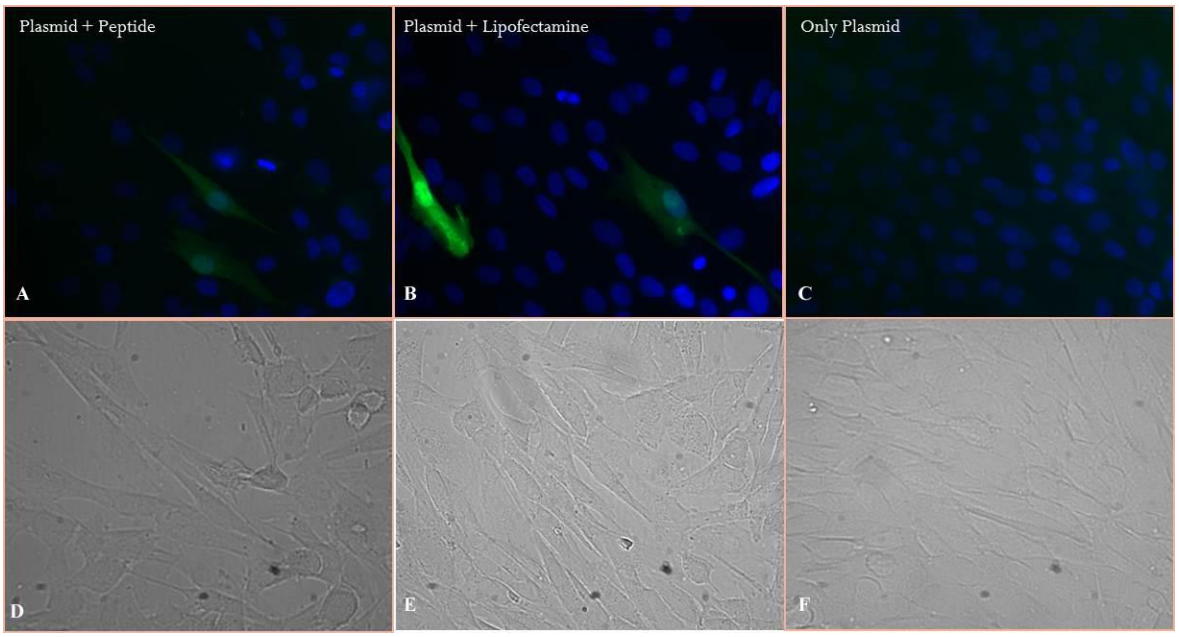

Figure 3.7. MCF-7 cells transfected with pEGFP-N3 plasmid DNA encapsulated in peptide assemblies.

Fluorescence microscope images of MCF-7 cells grown on coverslips and transfected with pEGFP-N3 using (A) peptide assemblies, (B) Lipofectamine™ and naked plasmid (C). Cells were stained with DAPI and fixed with 4 % PFA. D, E and F are bright field images of A, B and C respectively.

In the case of N/N 1003A cells, EGFP expression was observed only when the plasmid was delivered using the peptide assemblies (Fig. 3.6a). To test if the peptide assemblies could offer protection to the encapsulated plasmid during delivery, we treated the free and encapsulated plasmid with DNase-1 for 30 min at 37 °C before adding them directly to N/N 1003A cells grown on cover slips. Cells incubated with DNase-1 treated-encapsulated plasmid were able to express EGFP (Fig. 3.6c), confirming the protective role of the peptide assemblies during delivery of the encapsulated cargo. Control cells with either the free plasmid or plasmid treated with DNase-1 showed no expression (3.6e), most

likely due to the breakdown of the plasmid as a result of DNase-1 hydrolysis. Similar results were observed with MCF-7 cells when transfected with pEGFP-N3. EGFP expression was observed only when the plasmid was delivered using either the peptide bilayer assemblies (Fig. 3.7a) or when using a commercial transfection agent, Lipofectamine™ (Fig. 3.7b). Control cells with only the free plasmid did not show EGFP expression (Fig. 3.7c).

Under certain conditions, we observed that MCF-7 cells transfected with the pEGFP-N3 showed a faint green fluorescence which was absent in cells transfected with the free plasmid or in control cells that have only the peptide vesicles but no plasmid (see Apendix A, Fig. A.4). The fluorescence is not the usual bright green fluorescence associated with GFP expression. We suspect that this could be very low levels of EGFP expression. The most likely cause of such low intensity fluorescence would be that the cells take up the plasmid loaded peptide vesicles but are unable to release all of the plasmid from the peptide vesicles. The observed low intensity fluorescence could be the result of a very low number of plasmid(s) in the cell.

In most cases, transfection of plasmid DNA into most cell types leads to only a transient expression. Very few cells successfully integrate foreign DNA into their genome. To determine if the transfection using peptide assemblies resulted in any stable transfections, we transfected N/N 1003A cells grown in T-25 flasks (5 mL) with the peptide assemblies and after 48 h, added the drug G-418 disulfate (RPI Corp., Mount Prospect, IL) at a concentration of 1 mg/mL into the medium for selecting stable transfectants. This particular concentration (1 mg/mL) was chosen based on a cell cytotoxicity assay carried out in N/N 1003A cells treated with varying concentrations of G-

418 disulfate (0.1-2 mg/mL). This work was done by Ms. Adriana Avila as part of her research. The plasmid EGFP-N3 carries the neomycin gene (*neo*^{r}) as a selection marker and can be used to amplify cells that have stably integrated the plasmid (or portions of it) into their genome. After growing the cells in this selection medium for two weeks, we obtained four colonies that were allowed to grow for two more weeks before imaging them under a fluorescence microscope for GFP expression (Fig. 3.8). Fluorescence microscopy images revealed that only three out of the four colonies expressed GFP. Two sets of controls were used. In one, 100 μL of the medium was replaced with DNase/RNase free water and in the other, 100 μL of medium was replaced with DNase/RNase free water containing 1 μg of the plasmid. Both sets of control cells eventually died after a week.

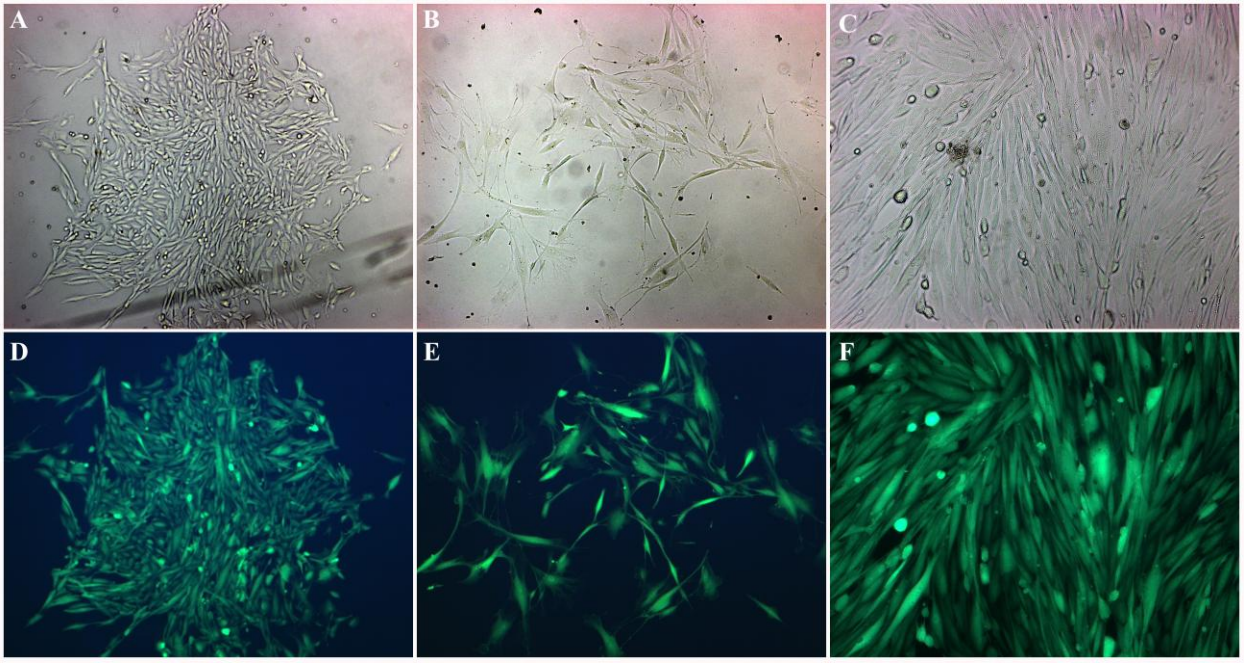

Figure 3.8. Stable transfection of N/N 1003A cells using peptide assemblies.
Fluorescence microscope images of N/N 1003A cells transfected with pEGFP-N3 using peptide assemblies and grown in selection medium containing 1mg/mL G-418 disulfate for four weeks. Three (D, E and F) separate colonies expressing GFP. A, B and C are bright field images of D, E and F respectively.

3.3.3. Location of plasmid within peptide assemblies (inside vs. Outside)

Given that two highly charged entities, peptide vesicles (positive) and plasmid DNA (negative), are coming together more than one type of association is possible. In addition to encapsulation these molecules will interact electrostatically. In order to determine the types of associations of the plasmid within the peptide vesicles, we treated the plasmid loaded vesicles with two different nucleases, DNase-1 and Benzonase. Both these nucleases are endonucleases that cleave DNA non-specifically. DNase-1 acts on single stranded, double stranded and chromatin DNA and preferentially cleaves at the 5' phosphodiester linkages adjacent to pyrimidine nucleotides[9]. Benzonase (genetically engineered nuclease from *Serratia marcescens*) cleaves all forms of DNA and RNA[10,11]. Benzonase is also a preferred nuclease for removal of nucleic acid contaminants from recombinant protein preparations (according to the manufacturer's website). We hypothesized that if the portion of the plasmid encapsulated inside the peptide vesicles will be protected from the action of the nucleases and remain intact. On the other hand, if the plasmid is bound on the outside of the vesicles it should be cleaved by the nucleases. Plasmid loaded peptide vesicle samples were prepared with the plasmid added to preformed vesicles or during vesicle formation. These preparations were treated with the nucleases and separated over an agarose gel containing ethidium bromide. The results (Fig. 3.9) indicate that while the major portion of the plasmid is cleaved by the nucleases, a small fraction of the plasmid, when prepared with the peptide assemblies, doesn't enter the gel and remains intact (Fig. 3.9 lanes 2, 4-6, 8 and 9). This small fraction remains in the well due to the charge neutralization of the plasmid (DNA is negatively charged and binds to the positively charged lysine tails of the peptide) but can also be the result of the plasmid being encapsulated within the peptide vesicles. It is known that nuclease activity may be inhibited by the binding of DNA to peptide/protein. Hence, we decided

to do away with nucleases and use a chemical method to cleave the plasmid DNA. To determine if this small fraction of plasmid (stuck in the well) is a result of nuclease-inactivity or encapsulation, we treated the plasmid loaded peptide samples with glutathione (GSH) in the presence of $CuSO_4$ (Fig. 21). GSH in the presence of Cu^{2+} forms hydroxyl radicals that attack the bases of DNA resulting in base damage and strand scission[12,13]. Results from this experiment indicate that most (if not all) DNA is cleaved under these conditions (Fig. 3.10 lanes - 4,5,7 and 8). We cannot be entirely certain if the GSH and copper ions are impermeable to the interior of the vesicles. Hence, from the experiments above, we can only conclude whether the plasmid is protected or unprotected. In the case of nucleases, the plasmid is protected and in the case of GSH-Cu complex, it is unprotected.

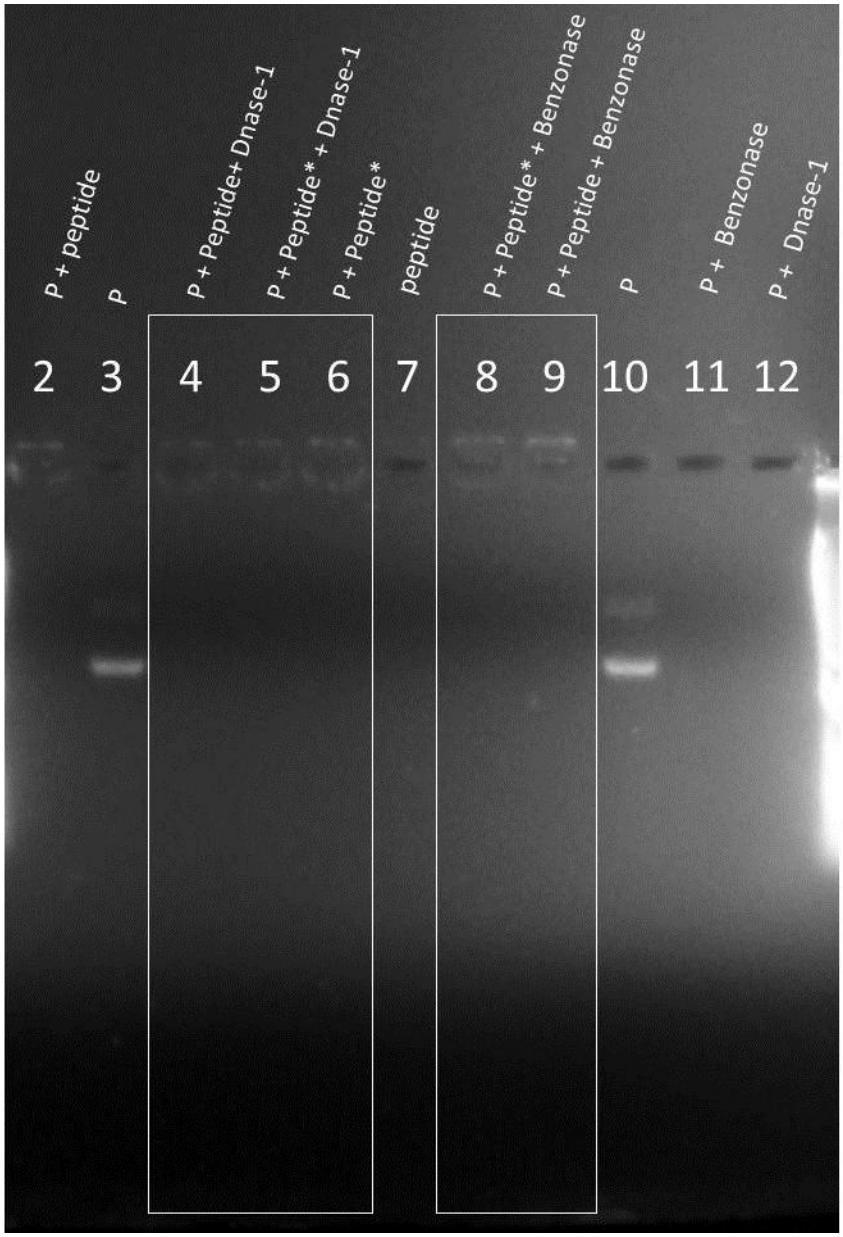

Figure 3.9. Treatment of plasmid loaded peptide samples with nucleases.

A 0.5 % agarose gel containing ethidium bromide shows the results of various samples treated with two different nucleases where, P refers to plasmid (pEGFP-N3) and Peptide* are samples where the plasmid is added to preformed peptide vesicles. Lanes 4-5 and 8-9 are plasmid loaded peptide samples treated with DNase-1 and Benzonase respectively and show complete degradation except for some plasmid DNA in the well. Lanes 11 and 12 are free plasmids treated with nucleases and show complete degradation of the plasmid. Lanes 3 and 10 are free plasmids that have not been treated with any nucleases. Lanes 2, 3 6 and 7 are controls.

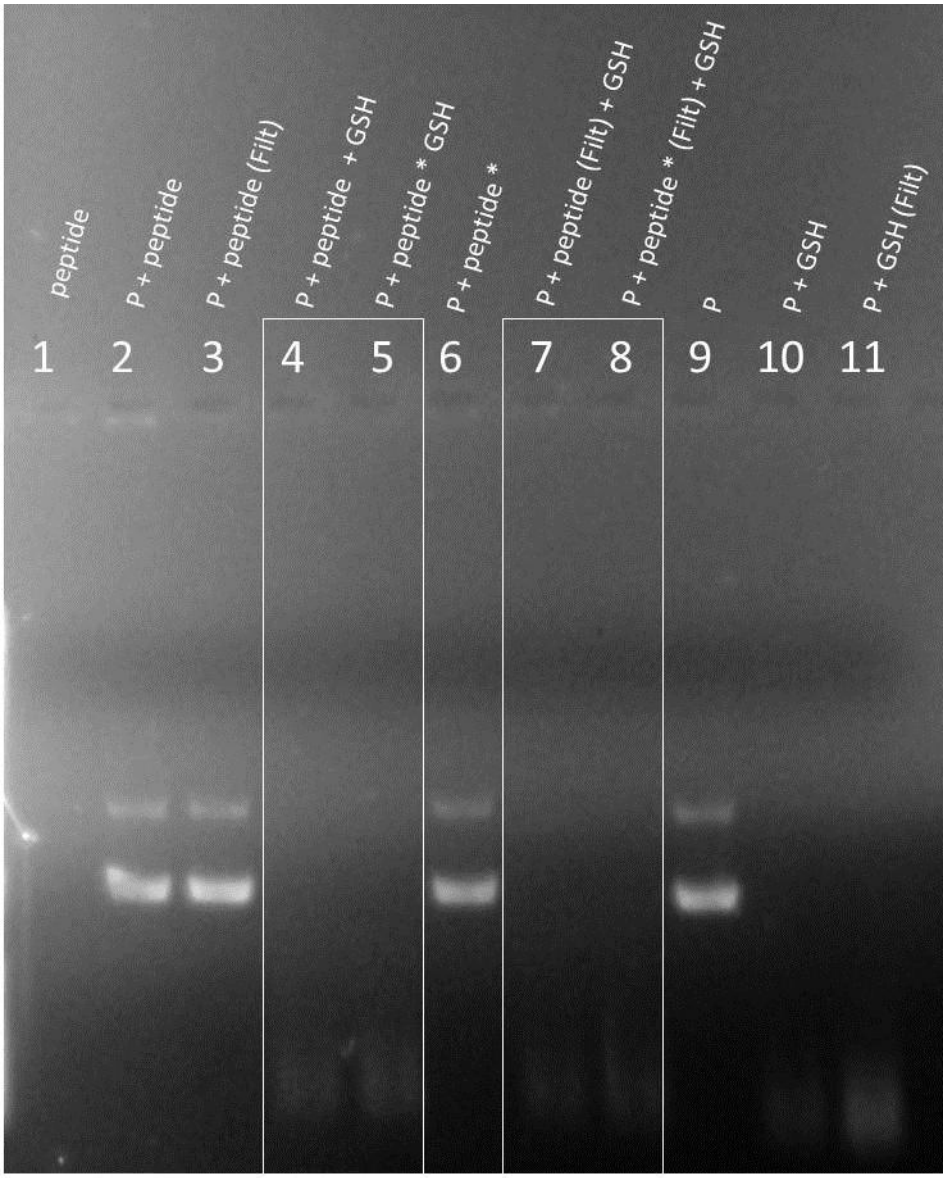

Figure 3.10. Treatment of plasmid loaded peptide samples with Cu(II)- GSH.

A 0.5 % agarose gel containing ethidium bromide show results of various samples treated with Cu(II)-GSH complex where, P refers to plasmid (pEGFP-N3) and Peptide* are samples where the plasmid is added to preformed peptide vesicles. Lanes 4-5 and 7-8 are plasmid loaded peptide samples treated with Cu(II)-GSH complex with or without filtering through a 30K MWCO filters respectively and show highly degraded plasmid DNA. Lanes 10 and 11 are free plasmids treated with Cu(II)-GSH complex. Lanes 1, 2, 3 and 9 are controls that are not treated with the complex and show intact plasmid.

3.4. Conclusions

The potential to deliver small fluorescent dye molecules (5(6)-Carboxyfluorescein and Rhodamine 6G) using the peptide bilayer assemblies described, were tested in a variety of cell types: Human lens epithelial cells, human breast adenocarcinoma cells and rabbit lens epithelial cells. These cell types showed significant uptake of the dye molecules when delivered through the peptide assemblies. Uptake of free dye (added directly to the medium) showed poor to no uptake of the negatively charged dye while the positively charged dye was taken up more readily.

While these peptide vesicles act as hollow nanocarriers for small molecules, in the case of large molecules like nucleic acids, they appear to act as nanoparticles. Using these peptide assemblies, we have shown that it is possible to transfect epithelial cells and obtain both transient and stable transfectants. We have also shown that these peptide assemblies offered plasmid DNA a modest level of protection from the action of nucleases like DNase-1 and Benzonase. Although we have not quantified the transfection efficiency by flow cytometry, from fluorescence images alone, it appears that the overall efficiency is low when compared to a commercial transfection agent, Lipofectamine™. The overall transfection efficiency could be improved by tagging the peptide with various cell specific ligand molecules (estrogens and other small sterol molecules, TAT sequence and other recognition sequences) or introduced to cells in conjunction with techniques like electroporation. Although we do not present the data here, we have observed over the course of the research that certain simple precautions like using reduced serum medium for initial peptide assembly delivery and using low concentration of the DNA (1-2μg) yielded more consistent transfections across different epithelial cell lines.

3.5. References

[1] Felgner, P. L., Gadek, T. R., Holm, M., Roman, R., Chan, H. W., Wenz, M., Northrop, J. P., Ringold, G. M., and Danielsen, M. (1987). Lipofection: A highly efficient, lipid-mediated DNA-transfection procedure. *Proceedings of the National Academy of Sciences of the United States of America, 84*(21), 7413-7417.

[2] El-Aneed, A. (2004). An overview of current delivery systems in cancer gene therapy. *Journal of Controlled Release : Official Journal of the Controlled Release Society, 94*(1), 1-14.

[3] Mel'nikov, S. M., Dias, R., Mel'nikova, Y. S., Marques, E. F., Miguel, M. G., and Lindman, B. (1999). DNA conformational dynamics in the presence of catanionic mixtures. *FEBS Letters, 453*(1-2), 113-118.

[4] Dias, R. S., Lindman, B., and Miguel, M. G. (2002). Compaction and decompaction of DNA in the presence of catanionic amphiphile mixtures. *The Journal of Physical Chemistry B, 106*(48), 12608-12612.

[5] Rosa, M., Dias, R., Miguel, M. D., and Lindman, B. (2005). *Biomacromolecules, 6*, 2164.

[6] Dias, R. S., Magno, L. M., Valente, A. J. M., Das, D., Das, P. K., Maiti, S., et al. (2008). Interaction between DNA and cationic surfactants: Effect of DNA conformation and surfactant headgroupâ€ . *The Journal of Physical Chemistry B, 112*(46), 14446-14452.

[7] Dias, R., and Lindman, B. (2008). *DNA interactions with polymers and surfactants* John Wiley.

[8] Safinya, C. R. (2001). Structures of lipid-DNA complexes: Supramolecular assembly and gene delivery. *Current Opinion in Structural Biology, 11*(4), 440-448.

[9] Moore, S. (1981) Pancreatic DNase. in *The Enzymes*, Vol. 14, Boyer, P. D. (ed.), pp. 281-296, Academic Press, New York, USA.

[10] Benzonase® Brochure (1999) Code No. W 220911, Merck KGaA, Darmstadt, Germany

[11] Janning, P., Schrader, W., and Linscheid, M. (1994). A new mass spectrometric approach to detect modifications in DNA. *Rapid Communications in Mass Spectrometry : RCM, 8*(12), 1035-1040.

[12] Reed, C. J., and Douglas, K. T. (1991). Chemical cleavage of plasmid DNA by glutathione in the presence of cu(II) ions. the cu(II)-thiol system for DNA strand scission. *The Biochemical Journal, 275 (Pt 3)*(Pt 3), 601-608.

[13] John, D., and Douglas, K. (1996). *A common chemical mechanism used for DNA cleavage by copper(II) activated by thiols and ascorbate is distinct from that for copper(II): Hydrogen peroxide cleavage* Springer Netherlands.

Chapter 4 - Conclusions and Future Directives

We have described here, a set of relatively short peptide sequences that are capable of self-assembling into nanovesicles (150-200 nm, using TEM and DLS). When placed in an aqueous environment, these peptide nanovesicles are capable of entrapping solutes within their interior, as shown by encapsulation studies performed with fluorescent dyes. While the individual peptides are capable of assembly and adopt a vesicular morphology (as observed with TEM), we chose to use an equimolar mixture of the long and short peptide since mixing the two peptides sequences resulted in better sample preparations (supported by sedimentation velocity experiments). Mixing the long and short peptides allows for release of curvature strain on the vesicles. Vesicle assembly appears to be driven by hydrophobic interactions and stabilized by a mix of inter-molecular hydrogen bonding and hydrophobic tail entanglement resulting in an overall secondary structure that is dominated by a beta-conformation.

The strong hydrogen bonding between adjacent peptides in the vesicular assembly results in assemblies that are very stable. Treatment with denaturing agents such as temperature, SDS, urea and trypsin did not affect the secondary structure of these peptides. Strong interactions between the peptides makes it possible for the peptides to have a very low critical assembly concentration (CAC) in sub μM range. This is an advantageous property when using them as delivery vehicles. With low CACs, the assembly can remain intact even upon dilution, which is the case in *in vivo* delivery. On the other hand, when delivering these vesicles to cells grown in culture, it might be useful to make them somewhat weaker so that once taken up by the cells, the vesicles fall apart and release their contents more readily. The peptides can be re-designed to weaken the interactions between the individual peptides. The isoleucines and valine in the FLIVIGSII sequence most likely contribute to chain entanglement and beta formation; replacing

them with alanines, will not only weaken the interacting forces but will also result in a more homogeneous assemblies. This latter claim is based on studies with other peptide amphiphiles where use of alanine and valine tails resulted in formation of more homogeneous nanostructures[1]. It is also possible to achieve different vesicular sizes by changing the overall chain length of the peptide sequences. One such way would be to vary the number of lysine residues at the C-termini and follow the size distribution by TEM and DLS. While this may result in different sizes, it may also result in loss of vesicular architecture or the possibility of the re-designed peptides to adopt morphologies other than vesicles. Fig. 1.13 and the work by Discher, D. E., and Ahmed, F. (2006)[2] is a useful guide for varying the overall chain length. We attempted to determine if the ratio of the two peptides could result in a difference in size distribution of the assemblies. AUC experiments of samples prepared in various ratios did not yield any meaningful results.

Attaching various recognition molecules to the peptide sequences could be used to make vesicles that can be targeted to specific cells. Common recognition molecules include TAT sequence, biotin and sterol molecules. Sterols (especially hormones) have specific cytoplasmic receptors that help with uptake and transport of the molecule into the nucleus. Certain breast cancer cells are known to over-express estradiol receptor (ER-α)[3] and are known to localize in the lipid rafts on cell surfaces[4,5]. ER-α is known to shuttle between the cytoplasm and nucleus[6] If these peptide vesicles could be prepared by decorating the outside of the vesicle with estradiol, they should be taken up with relative selectivity and can deliver anti-cancer drugs with more effectiveness. We are currently working on this line of research. We attempted attaching estradiol to the C-termini of these peptides but encountered solubility issues while activating the estradiol molecule (before tagging them onto the peptides). While performing such experiments,

one needs to make sure that the medium does not contain phenol red. Phenol red is a weak estrogen[7] and competes with estradiol for binding to the estrogen receptor[8].

We have shown that, using these peptide nanovesicles, it is possible to deliver both small (fluorescent dyes) and large molecules (plasmid) to cells grown in culture. In the case of small molecules, the peptide assemblies act as hollow nanocarriers with the molecules trapped inside the vesicle, for plasmids, they appear to act more as particles. We were able to deliver plasmids of different sizes, namely, a 732bp fragment excised from pCX-EGFP, EGFP-N3 (~4.7kbp) and pcDNA 3.1 with a 1.3kb insert (~6.8kb). [Mouse embryonic fibroblast cells transfected with the 732bp fragment excised from pCX-EGFP showed poor transfection efficiencies. This work was done in Dr. Mark Weiss's lab, Kansas State University and is unpublished data]. Using these peptide vesicles we were able to achieve transient and stable transfectants. From our results, it appears that most (if not all) of the plasmid is bound on the outside of the nanovesicle. One of the advantages of using these peptide vesicles to deliver DNA is the protection it offers against the action of nucleases like DNase-1 and Benzonase.

Method of delivery: The mechanism by which cells take up these vesicles or how they fall apart once inside the cell is still unknown. At this point, we believe that dilution aids in vesicle disassembly subsequently leading to release of cargo. Re-designing the peptides to achieve less stable vesicles, should help determine if the low transfection rates observed are due to the inability of the cells to break down the vesicles in order to release the DNA. At this point, no special technique or method of delivery is used. Loaded peptide vesicles are simply added to the media in which the cells are grown. It might be possible to improve vesicle uptake by using methods like electroporation (for cells grown in culture), where short bursts of current are applied to the cells (in solution). This current helps make the cell membranes temporarily leaky

and allows for uptake of DNA or other large molecules. Other options could include mixing the peptides with phospholipids to help the vesicles fuse to the cell membrane with more ease. It is known that even commercial transfections agents like Lipofectamine™ fails to show appreciable transfection in certain cell lines. Mixing these peptides with such commercial lipid transfection agents may help improve their transfection efficiencies.

Materials to deliver: A host of different compounds could be packaged and delivered using these vesicles. A simple way to determine the size/molecular weight range of compounds that can be encapsulated could be determined by preparing these vesicles in the presence of a mixture of proteins of a defined molecular weight range. This can be done by individually mixing selected proteins of different molecular weights or using commercially available pre-stained molecular weight markers (e.g. Rainbow™ molecular weight markers available from G.E Healthcare). Vesicles prepared in the presence of this protein mixture can be loaded onto a native gel and compared with free markers proteins. Encapsulated protein markers would show a difference in the position of their bands compared to the controls.

Anti-cancer drugs, antibiotics, vitamins and co-factors could be packaged and delivered to target cells. Cytochrome C is an attractive candidate for packaging and delivering. Cytochrome C is a small (~12kDa) but highly conserved protein which is best known for its function in the inner mitochondrial membrane where it shuttles electrons from one protein complex to another. Cytochrome C is also known to induce apoptosis (programmed cell death) by initiating the caspase cascade of proteins[9]. This caspase cascade initiation is triggered by many different signals, one of which is the release of cytochrome C. There are various approaches being researched to triggering apoptosis in cancerous cells as a way to limit their

growth and proliferation. While it is a plausible strategy to trigger apoptosis in cancerous cells, it is important that it must be done in a highly selective manner such that normal cells are not affected. Hence, targeted delivery and apoptotic triggering mechanism should go hand in hand in any sort of treatment that involves limiting the growth of cancerous cells via apoptosis.

Peptide bilayer: MD simulation suggests that the peptide assembly adopts a bilayer conformation. Though we do not have direct evidence for such a claim, observations from TEM, CD data and the peptide architecture strongly suggests that the most probable final structure for these vesicles have to be one that is bilayer lineated. The question of whether it is a bilayer or something else is very challenging at this point. While we attempted to address this question both directly and indirectly, we did not get any conclusive answers, mostly due to technical difficulties. An attempt to image these vesicles using a cryo-EM (samples were sent to Dr. Zhou's lab at UCLA) was unsuccessful. While they were able to observe vesicles using negative staining under a TEM, the same was not possible with CryoEM. According to Dr. Zhou's lab, this is not uncommon since many lipid samples show similar issues (visible under TEM but not so with cryoEM) as a result of blotting.

We tried using a classical biochemistry approach (an idea that came up during a committee meeting) by labeling the outside of the intact vesicles and later breaking them apart to determine if only half of the total peptides are labeled. We chose to label the ε-amino group of the lysine side chain on the C-terminal end of the peptide (which sticks out into the aqueous environment) with biotin. After this labeling, we broke the vesicles apart by diluting them into an organic solvent (50 % acetonitrile with 0.1 % TFA) and attempted to quantitate them using mass spectrometry (ESI-MS). Though we could observe trace amounts of the biotin labeled peptide,

the peptides in general, ionized poorly. Hence it was difficult to ascertain if the variation in the peak heights was due to poor ionization or difference in labeled and unlabeled peptides. This is only a technical difficulty and with the choice of right solvents and conditions, it is possible to achieve better results.

References

[1] Zhao, X., and Zhang, S. (2006). Molecular designer self-assembling peptides. *Chemical Society Reviews, 35*(11), 1105-1110.

[2] Discher, D. E., and Ahmed, F. (2006). Polymersomes. *Annual Review of Biomedical Engineering, 8*, 323-341.

[3] Schuur, E. R., & Weigel, R. J. (2000). Monoallelic amplification of estrogen receptor-alpha expression in breast cancer. *Cancer Research, 60*(10), 2598-2601.

[4] Hammes, S. R., & Levin, E. R. (2007). Extranuclear steroid receptors: Nature and actions. *Endocrine Reviews, 28*(7), 726-741.

[5] Marino, M., & Ascenzi, P. (2008). Membrane association of estrogen receptor alpha and beta influences 17beta-estradiol-mediated cancer cell proliferation. *Steroids, 73*(9-10), 853-858.

[6] Dauvois, S., White, R., & Parker, M. G. (1993). The antiestrogen ICI 182780 disrupts estrogen receptor nucleocytoplasmic shuttling. *Journal of Cell Science, 106 (Pt 4)*(Pt 4), 1377-1388.

[7] Berthois, Y., Katzenellenbogen, J. A., & Katzenellenbogen, B. S. (1986). Phenol red in tissue culture media is a weak estrogen: Implications concerning the study of estrogen-responsive cells in culture. *Proceedings of the National Academy of Sciences of the United States of America, 83*(8), 2496-2500.

[8] Welshons, W. V., Wolf, M. F., Murphy, C. S., & Jordan, V. C. (1988). Estrogenic activity of phenol red. *Molecular and Cellular Endocrinology, 57*(3), 169-178.

[9] Garland, J. M., & Rudin, C. (1998). Cytochrome c induces caspase-dependent apoptosis in intact hematopoietic cells and overrides apoptosis suppression mediated by bcl-2, growth factor signaling, MAP-kinase-kinase, and malignant change. *Blood, 92*(4), 1235-1246.

Appendix A - Supplemental figures

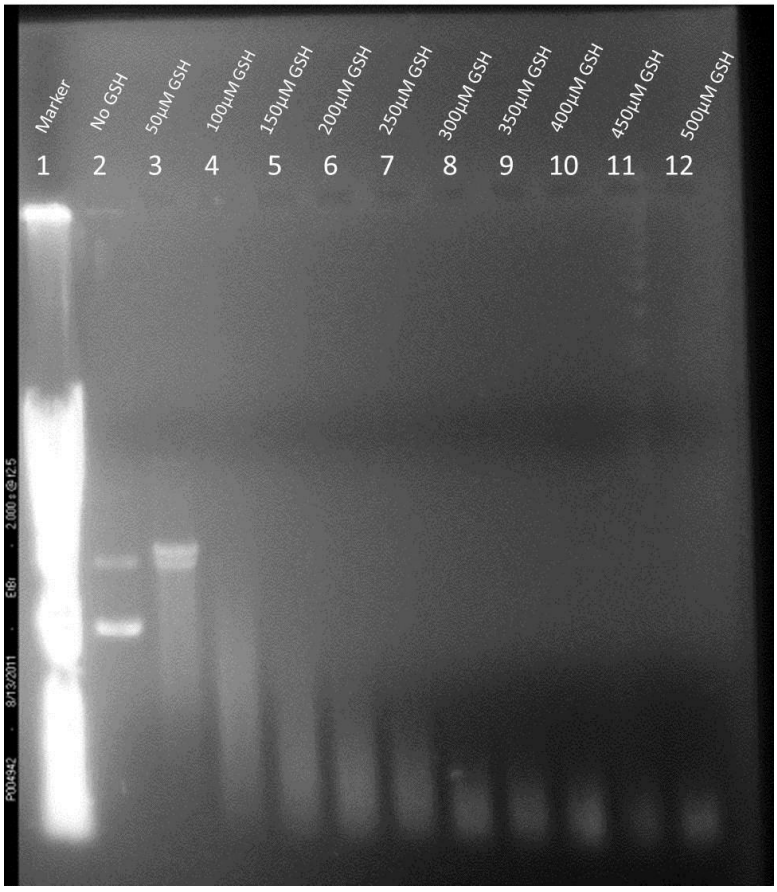

Figure A.1. Concentration dependence of Cu(II)-GSH cleavage of pEGFP-N3.

Chemical cleavage of pEGFP-N3 was carried out at increasing concentrations of Cu(II)-GSH to determine optimal concentration to be used. Lane 2-12 contains 1µg pEGFP-N3 with 0-500 µM GSH. Lane 1-6 contains 200 µM $CuSO_4$ while lane 7-12 contains 400 µM CuSO4. All samples were prepared in 10 mM sodium phosphate buffer with 50 mM NaCl and pH 8. Samples were incubated for 90 min at 40°C.

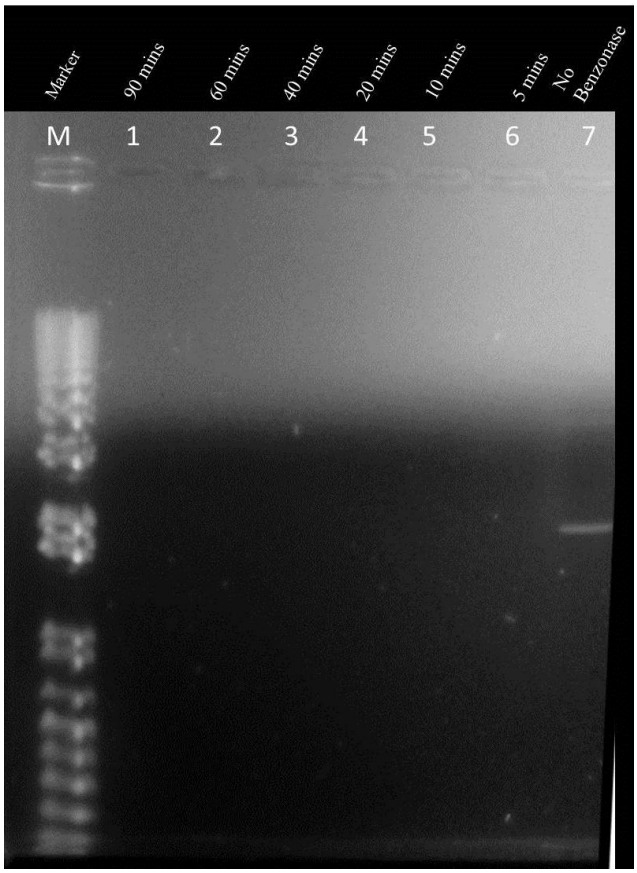

Figure A.2. Treatment of pEGFP-N3 with Benzonase for different time periods.

1μg pEGFP-N3 incubated with 0.5 μL benzonase (250 units/μL) and allowed to incubate at 37°C for different time periods. Lanes 1-6 contain the plasmid and nuclease and show no bands indicating that all DNA has been cleaved. Lane 7 is a control where no enzyme was added.

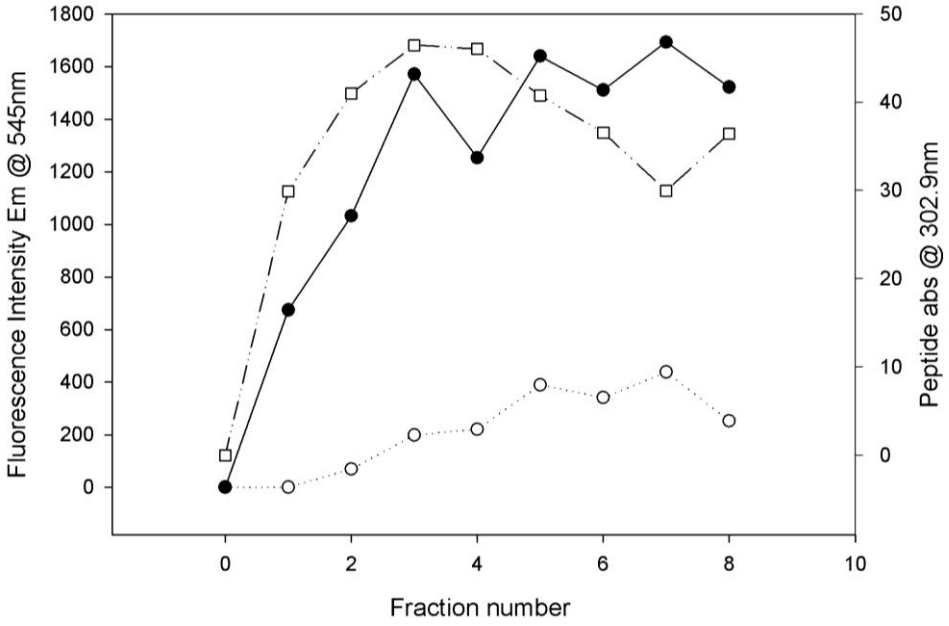

Figure A.3. Encapsulation of Rhodamine 6G by peptide vesicles.

Peptide vesicles were prepared in the presence of Rhodamine 6G and separated over a Sephadex G-10 spin column. Fluorescence intensity of Rhodamine 6G when prepared with peptide vesicles (closed circles) and without peptide vesicles (open circles). The peptide concentration in each of the eluted sample was determined by measuring its absorbance (closed squares).

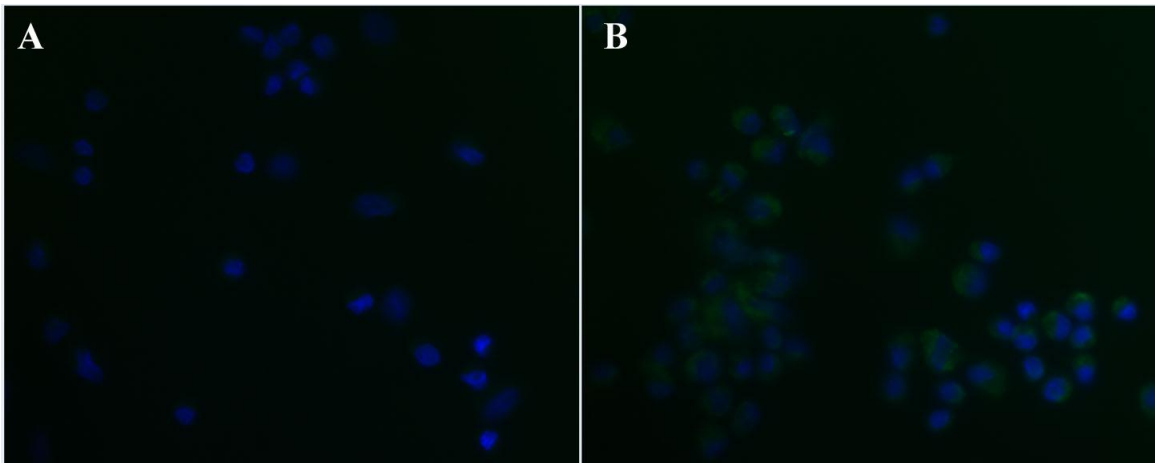

Figure A.4. MCF-7 cells transfected with pEGFP-N3 show a faint green fluorescence.

Fluorescence microscope images of MCF-7 cells transfected with (A) free pEGFP-N3 or (B) pEGFP-N3 loaded peptide vesicles.